Peter Fabian
Martin Dameris

# Ozone in the Atmosphere

## Basic Principles, Natural and Human Impacts

Springer

# Ozone in the Atmosphere

Peter Fabian • Martin Dameris

# Ozone in the Atmosphere

## Basic Principles, Natural and Human Impacts

Springer

Peter Fabian
Immission Research
Technical University of Munich (TUM)
Germany

Martin Dameris
Institute of Atmospheric Physics
German Aerospace Center (DLR)
Oberpfaffenhofen-Wessling
Germany

ISBN 978-3-642-54098-1 ISBN 978-3-642-54099-8 (eBook)
DOI 10.1007/978-3-642-54099-8
Springer Heidelberg New York Dordrecht London

Library of Congress Control Number: 2014936482



Printed on acid-free paper

Springer is part of Springer Science+Business Media (www.springer.com)

# Note from the Author

Because of severe health problems which even deteriorated by mid-2013, I had to stop working for this book with two subchapters still missing. Thus, its publication in 2014, 30 years after the discovery of the Antarctic Ozone Hole, was at risk.

Sections 5.1 and 5.4 had not been written, and therefore I asked Prof. Dr. Martin Dameris of DLR Oberpfaffenhofen to step in and write these two sections. Martin, a world-renowned atmospheric modeller and member of the WMO Ozone assessment team, just the right person for this job, readily agreed. That way the manuscript was completed, and the book can appear.

I am very grateful to Martin whose excellent articles fit very well. The authorships are stated under the respective chapter titles.

# Preface

In spring 2013, when Prof. Dr. Peter Fabian asked me to assist him during the final phase of writing this book about atmospheric ozone, only two sections were not finished at that time. Being asked by Peter Fabian has been a privilege for me. It was a real pleasure to work with him and to discuss the content of this book. We had several meetings in my office, and Peter Fabian, despite being seriously ill, was always full of energy and optimistic. We finished writing the manuscript for the book in December 2013. We received the galley proofs in mid-February 2014. Immediately, Peter and I started to check the proof. On 2 March I visited him for the last time in the hospital. We discussed the final changes of the manuscript, and we finally agreed on the subtitle of the book: "Basic principles, natural and human impacts". The final wish of Peter Fabian was to hold the printed book in his hands. Sadly enough, this wish was not fulfilled—Peter Fabian deceased on 11 March 2014, at the age of 76 years.

Peter Fabian studied Physics, Geophysics and Meteorology in Göttingen (Germany) and Innsbruck (Austria). For his thesis on atmospheric ozone, he was awarded the doctor's degree in 1966. As a postdoctoral research associate he worked at the University of California (UCLA), USA. From 1968 to 1988 he chaired the department "Trace substances in the atmosphere" at the Max-Planck-Institute in Katlenburg-Lindau (Germany). He received his habilitation in 1981 and became professor at the University of Göttingen. In 1988, Peter Fabian was appointed a full professor in München (chair of Bioclimatology and Immission Research). In 2003 he was conferred the emeritus status.

His numerous research papers were particularly devoted to the chemistry of the air and the transport of trace gases in the atmosphere. Peter Fabian was a pioneering scientist for investigations of aircraft emissions on the composition of the atmosphere. Among others, he studied the impact of nitrogen oxide emissions on the stratospheric ozone layer. Beyond that, his measurements of the vertical distribution of important halogen hydrocarbons were essential for the understanding of ozone depletion in the stratosphere. He was acknowledged as a worldwide recognised expert in ozone research. Therefore, in 1988 Peter Fabian received the honorary doctor (doctor honoris causa) of the Universidad de Mendoza (Argentina).

During his time in Munich, Peter Fabian was focusing on tropospheric photochemistry in congested urban areas. For example, he investigated the changes of ozone and related precursors in connection with aviation in the area of the Munich airport.

His enormous knowledge is documented in several books, for example in "Atmosphere and Environment" or "Living in a Greenhouse". He had the extraordinary competence to write complex scientific findings in a manner which is also understandable for non-experts. He inspired students in his lectures, seminars and scientific talks on conferences about atmospheric science. He mentored many diploma and PhD students, who successfully passed their exams and to whom Peter Fabian became a decisive supporter for their career. Peter Fabian's ideas and hints were always taken with pleasure.

Many of us have known and appreciated Peter Fabian as a leading scientist, colleague, advisor and friend. We will always remember his friendly and authentic manner.

Munich, Germany Martin Dameris

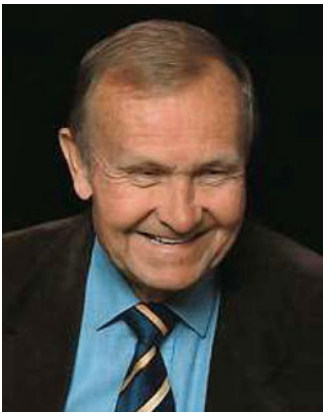

Prof. Dr. Peter Fabian

# Contents


**1 Introduction** . . . . . 1

**2 Discovery of Ozone in the Atmosphere** . . . . . 5
References . . . . . 10

**3 The Ozone Layer** . . . . . 13
3.1 Photochemistry of Atmospheric Ozone . . . . . 13
3.1.1 The Chapman Reaction Cycle . . . . . 13
3.1.2 Dynamical Processes . . . . . 16
3.1.3 Catalytic Reaction Cycles . . . . . 17
3.1.4 Heterogeneous Reactions . . . . . 22
3.2 Global Ozone Distribution . . . . . 25
3.3 UV Radiation and Ozone Layer Thickness . . . . . 26
3.4 Solar and Cosmic Effects . . . . . 30
3.5 Heavy Ozone and Isotope Effects . . . . . 35
3.6 Measurement Techniques . . . . . 36
3.6.1 Ground-Based Measurements . . . . . 36
References . . . . . 43

**4 Ozone in the Troposphere** . . . . . 49
4.1 The Natural Troposphere: Early Ozone Measurements . . . . . 49
4.2 Stratospheric–Tropospheric Exchange . . . . . 50
4.3 Photochemistry in the Troposphere . . . . . 54
4.3.1 Oxidation Capacity . . . . . 54
4.3.2 Methane Oxidation . . . . . 55
4.4 Natural Source Gases . . . . . 58
4.4.1 Biogenic Sources . . . . . 58
4.4.2 The Global Carbon Cycle . . . . . 60
4.4.3 The Global Nitrogen Cycle . . . . . 64
4.4.4 Nitrous Oxide ($N_2O$) . . . . . 66
4.4.5 Methane ($CH_4$) . . . . . 68
4.4.6 Carbon Monoxide (CO) . . . . . 71

4.4.7 Hydrogen ($H_2$) . . . 72
4.4.8 Methyl Chloride ($CH_3Cl$) . . . 75
4.4.9 Methyl Bromide ($CH_3Br$) . . . 76
4.4.10 Biogenic Hydrocarbons . . . 77
References . . . 79

**5 Human Impact** . . . 83
5.1 Stratospheric Ozone Depletion . . . 83
5.1.1 Ozone-Depleting Substances . . . 83
5.1.2 Global Ozone Loss . . . 86
5.1.3 Polar Ozone Loss . . . 89
5.1.4 Future Evolution of Stratospheric Ozone . . . 93
5.1.5 Impact of Aviation . . . 97
5.2 Tropospheric Ozone Increases . . . 97
5.2.1 Photochemical Smog . . . 98
5.2.2 Photosmog in Megacities . . . 102
5.2.3 Biomass Burning . . . 104
5.2.4 Global Impact: Present Tropospheric Ozone Distribution . . . 107
5.2.5 Impact on Vegetation, Humans, and Materials . . . 110
5.3 Surface UV and Ozone Layer Changes . . . 113
5.3.1 Long-Term Trends . . . 113
5.3.2 Effects of the Ozone Hole and Its Breakdown . . . 114
5.4 Ozone and Climate Change . . . 116
References . . . 119

**6 International Legislation: The Vienna Convention and the Montreal Protocol** . . . 125
References . . . 130

**7 Historical Highlights** . . . 131
7.1 The Discovery of the Antarctic Ozone Hole and Elucidation of Its Sources . . . 131
7.2 The 1995 Nobel Prize of Chemistry Awarded to Three Pioneers of Ozone Research . . . 133
7.3 Gordon M.B. Dobson, the International Ozone Commission and Its Quadrennial Ozone Symposia . . . 135
References . . . 137

# Chapter 1
# Introduction

Ozone ($O_3$), formed from three oxygen atoms, is a pungent smelling poisonous gas. Although it is a rare component of the Earth's atmosphere—in every ten million molecules of air, only about three are ozone—it is of fundamental importance for life on Earth.

Most of ozone, about 90 % of its total atmospheric abundance, is found in the stratosphere, between about 10 and 50 km altitude. In this higher part of the atmosphere, solar ultraviolet (UV) radiation can split (photolyze) oxygen ($O_2$) molecules, thereby producing oxygen atoms (O). These can react with $O_2$ molecules forming $O_3$. The stratospheric ozone belt, usually called the ozone layer, is maintained by a complex interplay of photochemistry and atmospheric dynamics.

In addition, the decomposition of long-lived trace gases mixed up from the surface provides a source of reactive substances which interfere with the ozone photochemistry. The most important of such natural "source gases" is nitrous oxide ($N_2O$) produced by soil bacteria. Its continuous flux into the atmosphere causes stratospheric ozone levels to be about 25 % lower than pure-oxygen photochemistry would predict. Man, by applying huge and increasing amounts of nitrogen fertilisers, has been increasing the flux of this natural "ozone depleter" $N_2O$. Moreover, the emission of halogenated hydrocarbons from spray cans, leaking refrigeration and air conditioning devices as well as solvents has lead to a significant global depletion of the ozone layer and severe seasonal ozone losses observed at high latitudes (polar ozone hole).

As most of these ozone depleting substances have atmospheric life times of hundreds of years, ozone losses still largely prevail, although production and thus further emission of such halogen compounds have been terminated by legislative measures.

The stratospheric ozone layer absorbs all but a small fraction of the solar ultraviolet (UV) radiation and thus prevents it from reaching the Earth's surface. High doses of UV radiation have potentially harmful effects on human health, animals, plants, microorganisms and materials. Thus, any reduction of the ozone layer thickness causing an increase of the UV flux bears important consequences for life. Further, the very existence of the stratosphere, an atmospheric layer with a

P. Fabian and M. Dameris, *Ozone in the Atmosphere*,
DOI 10.1007/978-3-642-54099-8_1, © Springer-Verlag Berlin Heidelberg 2014

positive temperature gradient that plays an important role in the atmospheric general circulation, depends on the ozone residing in this altitude region. It would not be an exaggeration to emphasise that life on the Earth's surface in its present form would not have evolved in the absence of the ozone layer. Thus, the ozone residing in the upper atmosphere is often called the "good ozone".

The remaining about 10 % of the atmospheric ozone is found in our direct environment, the lowest 10 km of the atmosphere called troposphere. In the natural troposphere free from anthropogenic influences, about 10–20 ozone molecules are found in every thousand million (one billion) molecules of air. At sea level these 10–20 parts per billion (ppb) correspond to about 20–40 micrograms per cubic metre ($\mu g/m^3$). These are mainly the result of downward transport from the stratosphere where ozone is produced photochemically. Human emissions from fires, automobile exhaust, and industry, however, provide substances from which ozone is produced in the troposphere as well. Such photosmog reactions can increase ozone levels up to several hundred ppb and more in polluted regions and, as a result of global mixing, to significantly elevated global ozone levels.

When ozone was discovered in the atmospheric environment, it was considered beneficial for human health. The good smell of forest air was thought to be due to ozone (it is rather hydrocarbons emitted by trees that cause that smell). City developers have often tried to lure settlers to ugly areas by creating street names such as "Ozone Avenue". On the contrary, ozone is poisonous and detrimental to human health at levels which are often exceeded in many areas of the world. Thus tropospheric ozone, the ozone in the air we breathe, is now often called the "bad ozone".

This is even more true since ozone is an efficient greenhouse gas as it absorbs thermal radiation around 9.6 μm wavelength. Thus, the increase of ozone in the troposphere directly enhances the Earth's greenhouse effect and contributes to global climate warming caused by $CO_2$ ond other man-made greenhouse gases.

The very existence of the ozone layer is due to the fact that the Earth's atmosphere contains oxygen. Unlike the other planets in the solar system whose atmospheres hold, if at all, traces of oxygen only, almost 21 % of the air we breathe is oxygen. This large fraction of oxygen is the result of life on Earth which evolved about 4 billion years ago under favourable conditions unique in the solar system: Earth orbits the Sun at a distance of about 150 million km where an average surface temperature of about 15 °C enables the existence of liquid water and thus oceans. It is well established that life evolved and flourished, before the atmosphere contained oxygen and thus an ozone shield against UV radiation, in the oceans. Myriads of microorganisms produced oxygen via photosynthesis, most of which was used up in the oxidation of iron and sulphur compounds. The remaining free oxgen gradually accumulated, and about 2 billion years ago atmospheric oxygen and the corresponding ozone layer were probably sufficient for the first organisms for settling on land. The biological activity and evolution of species accelerated leading to biodiversity and atmospheric conditions of the pre-industrial world.

The privileged conditions on Earth towards life can be realised by comparison with our neighbours in the solar system: Mars, orbiting the Sun further away than

Earth, at about 228 million km distance, has an average surface temperature of −50 °C, whereas Venus, with 108 million km distance closer to the Sun than Earth, exhibits deadly 460 °C.

Oxygen is not the only product of biological activity. The metabolism of microorganisms in the ocean and the continental soils liberates huge amounts of gaseous substances emitted into the atmosphere, such as nitrous oxide ($N_2O$), methane ($CH_4$) or methyl chloride ($CH_3Cl$). On the other hand, the biosphere takes up substances from the atmosphere, such as carbon dioxide ($CO_2$), water ($H_2O$) and nitrogen compounds. Actually, all atmospheric constituents, except the noble gases, circulate through the biosphere. Thus, our atmosphere largely is a product of biological activity and hence a consequence of life.

On the other hand, the atmosphere provides ideal climatic conditions for the biosphere. It constitutes a huge greenhouse which protects against harmful UV radiation but lets the visible radiation necessary for photosynthesis penetrate to the surface almost unattenuated. It also reduces the thermal emission from the surface: greenhouse gases such as $H_2O$, $CO_2$, $O_3$, $N_2O$ and $CH_4$ (in the order of their importance) absorb and re-emit parts of the Earth's thermal radiation, thus reducing the energy loss to space. Because of this (natural) greenhouse effect, the average surface temperature is 15 °C, about 33° higher compared to an Earth without such atmosphere. This natural greenhouse effect has continuously been increasing by anthropogenic emissions of greenhouse gases from burning of fossil fuels, destroying forests and various agricultural and industrial practices. Over the past 100 years, global average temperatures have risen by about 0.7°, and they are likely to increase further, by up to 5° until 2100, if greenhouse gas emissions continue to grow unabated. Global warming and related consequences are among the most severe problems for the well-being of our planet. This book dealing with the ozone layer will not explicitely address the issue of climate change. It will, however, touch upon it in as much as ozone is involved.

The Earth's atmosphere has evolved over more than 4 billion years, in close interaction with the biological evolution. Man, supposed to be the highest form of this evolution, is about to massively alter this greenhouse, by misusing the atmosphere as a waste dump. Severe ozone losses in the stratosphere, large ozone increases in the troposphere and climate changes are manifestations of human impact.

# Chapter 2
# Discovery of Ozone in the Atmosphere

The 1770s stand out as an epoch making period in the research of the atmospheric composition. During this decade, several of the most important constituents were identified and named. In 1774, J. Priestley and C.W. Scheele independently discovered oxygen. In the same year, Scheele identified chlorine and in 1777 nitrogen. Priestley discovered nitrous oxide ($N_2O$) in 1773, hydrogen chloride (HCl) and ammonia ($NH_3$) in 1774, sulphur dioxide ($SO_2$) in 1775 and carbon monoxide (CO) in 1779.

Although in 1785 van Marum noticed the characteristic smell of ozone in a gas discharge, and a little later J.W. Ritter observed its solar absorption, its discovery is credited to C.F. Schönbein (Fig. 2.1).

In 1839, while working in the laboratory, he detected a gas with a characteristic pungent smell which he called ozone (a greek word for smell) [1]. Schönbein was also the first to develop its monitoring technique, which later was adopted for ozone measurements at many meteorological observatories in the world. In 1858 Houzou and Levy initiated its first absolute measurements by a chemical method [2].

Paris was one of the first cities in the world to have initiated air quality monitoring in general and ozone measurements in particular, as early as 1865, with a network of 20 stations. Daily observations were coordinated by A. Levy, a chemist at the Montsouris observatory, and published in the Bulletin de la Statistique Municipale de la ville de Paris. The network was operated for 10 years and provided valuable information of ground level ozone levels at a time when air pollution was almost negligible, even in Paris. A modern evaluation of the Montsouris series of ozone measurements by Volz and Kley [3] indicates ozone levels of about 10 ppb, with spring values slightly higher than autumn values.

It is interesting to note that ozone was first discovered in the troposphere where ozone mixing ratios are very low compared to the stratosphere where the bulk of ozone resides. It was in 1878 that Cornu discovered, when he performed spectroscopic studies in the visible and UV regions, a sudden break off in the solar spectrum at wavelengths shorter than 300 nm. He also observed this to shift towards longer wavelengths when the solar elevation decreased and concluded this absorption to have been caused by atmospheric constituents [4]. Two years later,

P. Fabian and M. Dameris, *Ozone in the Atmosphere*,
DOI 10.1007/978-3-642-54099-8_2, © Springer-Verlag Berlin Heidelberg 2014

**Fig. 2.1** Christian Friedrich Schönbein (18 October 1799–29 August 1868)

W.N. Hartley discovered, in the laboratory as well as in the solar spectrum, a strong absorption band system in the wavelength region of 200–320 nm (Hartley bands) which he identified to have been caused by ozone. He also inferred that the break off in the solar spectrum observed by Cornu is due to ozone and that ozone concentrations in the stratosphere are much higher than near the ground. This was the discovery of the stratospheric ozone layer [5, 6].

In 1890 W. Huggins observed UV absorption bands in the region of 320–360 nm, adjacent to the Hartley bands, in the spectrum of Sirius. Fowler and Strutt in 1917 identified these, which were later referred to as Huggins bands, to be due to ozone [7].

The first quantitative measurement of the thickness of the ozone layer was achieved in 1920 by Fabry and Buisson. Based on measurements of the solar UV spectrum, they estimated the thickness of this layer to be equal to 3 mm of ozone at standard temperature and pressure (STP) [8]. This means, when all ozone molecules in a vertical column are thought to be concentrated in a homogeneous layer at sea level, this layer would be 3 mm thick.

In the 1920s, G.M.B. Dobson (Fig. 2.2) carried out systematic measurements of the ozone layer thickness, its seasonal and latitudinal variations, by employing a UV spectrograph he had developed in 1924. He also discovered, by investigating meteor trails, the existence of a warm layer in the stratosphere, with a temperature maximum around 50 km. He correctly presumed this to be due to the absorption of solar UV by ozone [9, 10]. In fact, this temperature maximum marks what is called

**Fig. 2.2** Gordon Miller Bourne Dobson (25 February 1889–11 March 1976)

the stratopause, the upper limit of the stratosphere. Above it temperatures decrease with height in the mesosphere (see Fig. 2.3). The region of the warm layer, which comprises both the stratosphere and the mesosphere, is called the "middle atmosphere". This warm layer is unique among the planetary atmospheres of the solar system: Only the Earth's atmosphere contains oxygen and thus ozone giving rise to a warm middle atmosphere (see Fig. 2.3).

In 1926 Dobson initiated a network of six stations, the first of its kind, for monitoring total ozone (as the ozone layer thickness was named) at Oxford, Valentia, Lerwick, Abisko, Lindenberg and Arosa. In 1928/1929 he extended this European network by installing UV spectrographs at Table Mountain (USA), Heluan (Egypt), Kodaikanal (India) and Christchurch (New Zealand) [11]. This early network was the beginning of systematic total ozone monitoring in a global network, which has been operating under the guidance of the International Ozone Commission (IOC) of the International Union of Geophysics and Geodesy (IUGG) supported by the World Meteorological Organization (WMO), until today. A later half-commercial version of Dobson's UV spectrophotometer (see Sect. 3.6) has been the backbone of this global network whose precision is still indispensable even decades after the availability of satellite borne sensors for global ozone observation and mapping. By the end of the 1960s the main features of total ozone as a function of season and latitude, for both hemispheres, had been derived already from the ground-based Dobson network ([12], see Fig. 2.4).

It is interesting to note that the discovery of the Antarctic ozone hole in 1984 is not credited to observations by satellite borne sensors operational at that time, but rather to ground based monitoring with Dobson spectrophotometers at Syowa station and Halley Bay, Antarctica (see Chaps. 5 and 7).

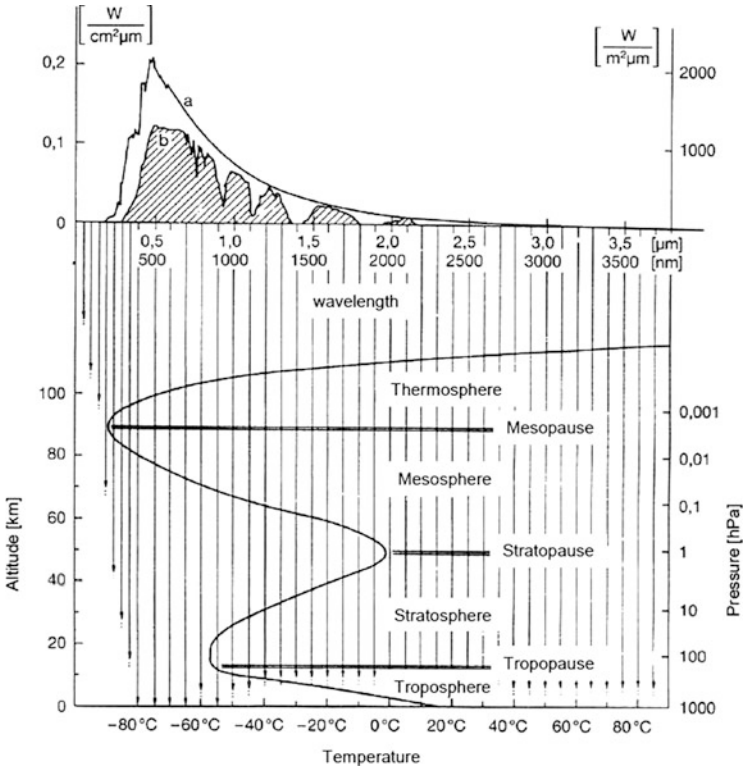


**Fig. 2.3** Vertical structure of the Earth's atmosphere

The ozone layer thickness (or total ozone) is nowadays given in Dobson Units (DU), with 100 DU being equivalent to 1 mm STP. Thus, the first total ozone value of 3 mm STP obtained in 1920 by Fabry and Buisson is equivalent to 300 DU and, compared with later values, quite realistic.

In 1924, F.W.P. Götz who was operating the Dobson station Arosa, at the altitude of 1,800 m asl, investigated the seasonal variation of the ozone layer. He found the ozone maximum around 25 km altitude and the largest variations occurring between 10 and 25 km.

More importantly, during an expedition to Spitsbergen in 1929, he discovered what was later named the Götz- or umkehr effect. He observed that the intensity ratio of the UV wavelength pair used for total ozone measurement in the direct sun (see Sect. 3.6) which decreases with increasing zenith angle (decreasing solar elevation) showed, when he used sky radiation from the zenith as light source, a surprising reversal (German: Umkehr) of this decrease when the Sun was close to the horizon. At very low solar elevations this ratio passed through a minimum and increased with solar elevation decreasing further (during sunset). At low elevations during sunrise the situation is reversed. He concluded this effect resulting from the layered structure of the ozone distribution and that these "umkehr" curves can be

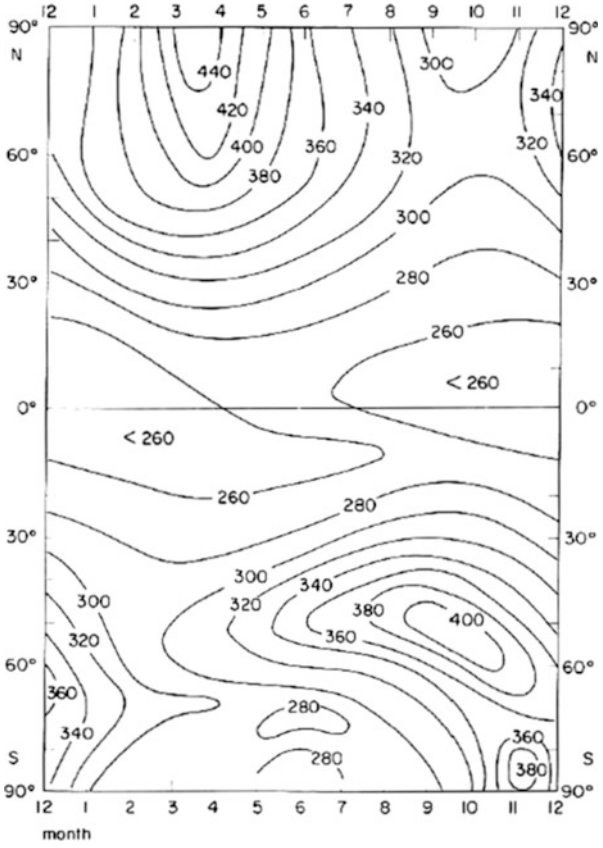


**Fig. 2.4** Total ozone (Dobson Units, DU) as a function of season and latitude in both hemispheres, based on ground-based measurements of the Global Dobson Network [12]

used for analytically deriving the vertical ozone profile. In collaboration with Meetham and Dobson, he developed a method for solving the integrals involved in the estimation of the vertical ozone distribution [13]. Of course this method can be applied under suitable meteorological conditions only, as a large fraction of the sky needs to be cloudfree. As the evaluation of ozone profiles from umkehr curves is a very elaborous method, only few profiles were derived during these early years. It was not before in the 1950s Dütsch and Mateer had developed a standardised routine method that the wealth of 20 years' umkehr data within the Dobson network could be exploited [14]. The umkehr method is still in use providing vertical ozone profiles, along with total ozone values, at many stations of the global Dobson network.

The first direct measurement of the vertical ozone distribution up to 31 km altitude was carried out in 1934 by E. and V. Regener by launching a balloon borne UV spectrograph whose spectrum was depicted every minute on a revolving photographic disc [15]. In the following years, sensors for in situ measurements of ozone and its vertical distribution were developed and widely applied in radiosonde networks (see Sect. 3.6).

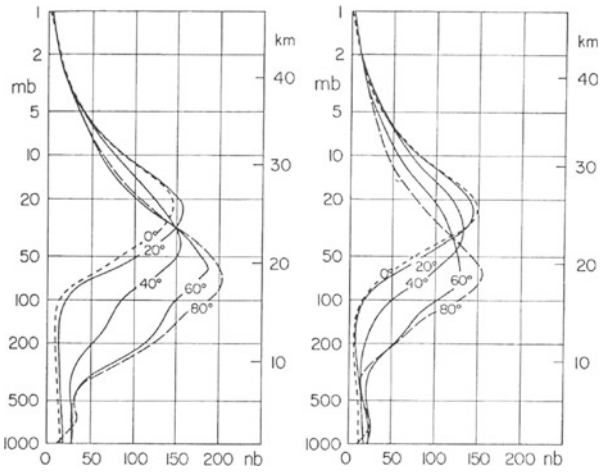


**Fig. 2.5** Average vertical distribution of ozone for different latitudes on the Northern Hemisphere, *left part*: February, *right part*: August. The ozone partial pressure in nb can be converted into ozone volume mixing ratio by dividing through the respective total pressure shown on the ordinate, after Dütsch [12]

Figure 2.5 shows a summary plot of average vertical ozone profiles based on radiosonde and umkehr data for the Northern Hemisphere [12], for February (left) and August (right). The ozone partial pressure is plotted in nanobar (nb) and allows the direct conversion to volume mixing ratios by dividing through the respective total pressure shown on the ordinate scale. This figure shows the typical features of the northern hemisphere ozone layer, its seasonal and latitudinal variations: the ozone maximum is highest over the tropics and decreases towards high latitudes, while the lower stratosphere below about 20 km shows ozone values increasing with latitude, this effect being strongest in late winter/spring. The ozone layer thickness (total ozone), the integral over the respective ozone profiles, increases from about 2.5 mm STP (250 DU) over low latitudes, where almost no seasonal variations are observed, to about 5.0 mm STP (500 DU) and 3.5 mm STP (350 DU) in February and August, respectively. These features largely agree with those shown in Fig. 2.4 based on the Dobson network.

While ground-based ozone observations have largely been limited to land stations, with strong bias towards the northern hemisphere, satellite borne sensors operational since the 1970s, with increasing data quality and resolution (see [6]), have provided a detailed global picture of the ozone layer and its variations with time, latitude and longitude (see Figs. 2.4 and 2.5).

## References

1. Schönbein CF (1840) Recherche sur la nature de l'odeur qui se manifeste dans certaines actions chimiques. Comptes Redus des Seances Paris 10:706–710
2. Houzeau A (1858) Preuve de la présence dans l'atmosphére d'un nouveau principe gazeux, l'oxygéne naissant. C R Acad Sci 46:89
3. Volz A, Kley D (1988) Evaluation of the Montsouris series of ozone measurements made in the nineteenth century. Nature 332:240–242, and the references given therein

4. Cornu A (1879) Observation de la limite ultraviolette du spectre solaire en diverses altitudes. C R Hebd Seances Acad Sci 89:808
5. Hartley WN (1880) On the probable absorption of solar radiation by atmospheric ozone. Chem News 42:268
6. Hartley WN (1881) On the absorption spectrum of ozone. J Chem Soc 39:57–61, and 111–128
7. Fowler A, Strutt RJ (1917) Atmospheric bands of atmospheric ozone in the spectra of sun and stars. Proc R Soc Lond A 93:577–583
8. Fabry C, Buisson H (1921) Etude de l'extrememité ultraviolette du spectre solaire. J Phys Radiat VI 2:197–226
9. Dobson GMB (1930) Observations of the amount of ozone in the Earth's atmosphere and its relations to other geophysical conditions. Proc R Soc Lond A 129:413
10. Dobson GMB (1931) A photoelectric spectrometer for measuring the amount of atmospheric ozone. Proc Roy Soc London 43:324–339
11. Dobson GMB (1968) Forty years' of research on atmospheric ozone at Oxford: a history. Appl Opt 7:37–405
12. Dütsch HU (1971) Photochemistry of atmospheric ozone. Adv Geophys 15:219–322
13. Götz FWP, Meetham AR, Dobson GMB (1934) The vertical distribution of ozone in the atmosphere. Proc R Soc Lond A 145:416–446
14. Dütsch HU (1959) Vertical ozone distribution from Umkehr observations. Arch Meteor Geophys Bioklim A 11:240–251
15. Regener E, Regener V (1938) Aufnahme des ultravioletten Sonnenspektrums in der Stratosphäre und vertikale Ozonverteilung. Phys Z 109:642–670

# Chapter 3
# The Ozone Layer

## 3.1 Photochemistry of Atmospheric Ozone

Ozone ($O_3$) is formed in the atmosphere when oxygen atoms (O) react with oxygen molecules ($O_2$). In the upper atmosphere solar UV radiation of wavelengths shorter than 242 nm can photolyze $O_2$ molecules and thereby produce O atoms. Since oxygen strongly absorbs solar UV, $O_2$ photolysis is restricted to the upper atmosphere. Figure 3.1, displaying absorption features of oxygen and ozone as a function of wavelength, shows that UV of wavelengths shorter than 242 nm is completely absorbed in the middle atmosphere and definitely does not reach the troposphere. Thus the resulting ozone layer is confined to the middle atmosphere, i.e. the stratosphere and mesosphere.

As will be shown in Chap. 4, ozone production occurs in the polluted troposphere as well. $NO_2$ molecules photolyze at longer wavelengths, up to 420 nm reaching the troposphere, thus liberating NO and O. As the unpolluted atmosphere contains very little $NO_2$ only, almost all ozone found in the natural troposphere is of stratospheric origin. In the polluted troposphere, however, when $NO_2$ is present, significant increases of the natural background ozone are observed as a result of tropospheric ozone production (see Chap. 4).

### *3.1.1 The Chapman Reaction Cycle*

The main reaction cycle of ozone formation in the middle atmosphere was developed 80 years ago by Chapman [1]. It is initiated by the photolysis of $O_2$

$$O_2 + h\nu\,(\lambda < 242\,\text{nm}) \rightarrow O + O \quad J_2 \tag{3.1}$$

followed by the three body reaction

P. Fabian and M. Dameris, *Ozone in the Atmosphere*,
DOI 10.1007/978-3-642-54099-8_3, © Springer-Verlag Berlin Heidelberg 2014

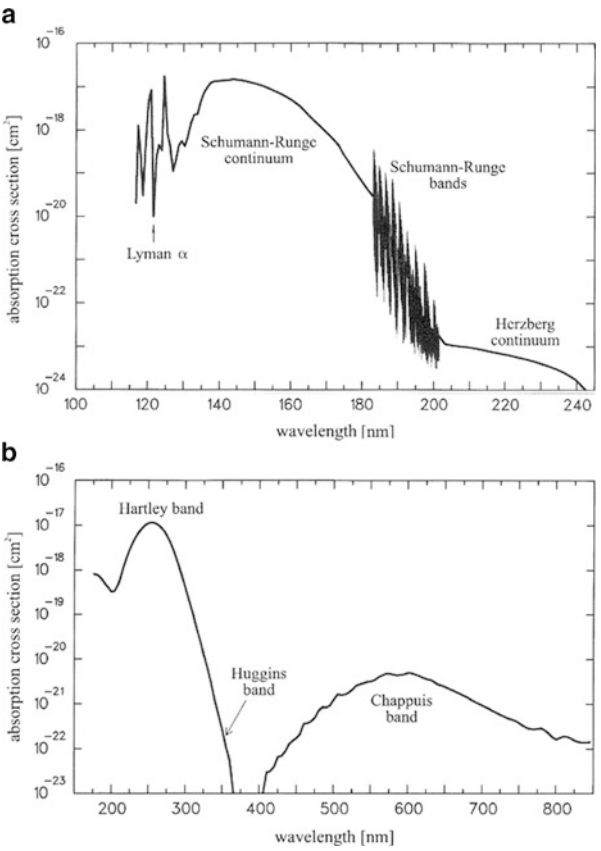


**Fig. 3.1** Absorption spectra of oxygen and ozone

$$O + O_2 + M \rightarrow O_3 + M \quad k_1 \tag{3.2}$$

Herein $h\nu$ denotes the quantum energy defined by Planck's constant $h = 6.225 \times 10^{-34}$ Js and the respective radiation frequency. $M$ is a neutral collision partner, any air molecule, necessary for the conservation of momentum.

Ozone is decomposed by photolysis

$$O_3 + h\nu(\lambda < 1,200\,\text{nm}) \rightarrow O + O_2 \quad J_3 \tag{3.3}$$

and the collision reaction

$$O + O_3 \rightarrow 2O_2 \quad k_3 \tag{3.4}$$

A fifth reaction

$$O + O + M \rightarrow O_2 + M$$

which is important above 60 km only [2] is disregarded here.

Herein $k_1$ and $k_3$ are the rate constants for the collision reactions (3.1) and (3.4) and $J_2$ and $J_3$ are the photolysis rates defined as

$$J = \int_0^\infty \eta(\lambda)\sigma(\lambda)I(\lambda)\mathrm{d}\lambda$$

with $\eta$ = quantum yield, $\sigma$ = absorption cross section and $I$ = radiation intensity as a function of the wavelength $\lambda$, for $O_2$ and $O_3$, respectively.

When [O], [$O_2$] and [$O_3$] denote the concentrations of O, $O_2$ and $O_3$, respectively, the rates of change of "odd oxygen" can be derived from (3.1)–(3.4) as

$$\mathrm{d}[O]/\mathrm{d}t = 2J_2[O_2] - k_1[O][O_2][M] + J_3[O_3] - k_3[O][O_3] \tag{3.5}$$

and

$$\mathrm{d}[O_3]/\mathrm{d}t = k_1[O][O_2][M] - J_3[O_3] - k_3[O][O_3] \tag{3.6}$$

Numerical estimates show that the reactions (3.2) and (3.3) converting odd oxygen species into each other are much faster than reactions (3.1) and (3.4) which produce or destroy odd oxygen.

Thus an equilibrium between O and $O_3$ is established very rapidly, which is practically independent of the formation and destruction of odd oxygen species [3]:

$$J_3[O_3] = k_1[O_2][O][M] \tag{3.7}$$

Because of the slower reactions (3.1) and (3.4) considerably more time is required for the system of odd oxygen species to reach equilibrium with the rest of the atmosphere, so that formation and destruction of such species balance. With these assumptions Eqs. (3.5)–(3.7) yield the equilibrium ozone concentration as

$$[O_3]_{\mathrm{equ.}} = (J_2k_2[M][O_2]/J_3k_3)^{1/2} \tag{3.8}$$

As [M] and [$O_2$] are decreasing and $J_2$ is increasing with height, it is obvious from (3.8) that the vertical ozone distribution must have a maximum, with [$O_3$] decreasing both below and above that altitude. This is the ozone layer resulting from pure oxygen photochemistry first established by Chapman.

This "Chapman layer", however, looks quite different from the real ozone layer shown in Fig. 2.4 [3]. Its maximum $O_3$ partial pressure lies around 30 km altitude, whereas it varies between 25 km at low and about 18 km at high latitudes in the real atmosphere.

The reason for this is the fact that photochemical reactions at different time scales occur in a highly dynamical atmosphere. Thus the distribution of a species

like ozone, which is not uniformly mixed with the main atmospheric constituents, is influenced by air motions such as winds and turbulence. Hence photochemical equilibrium cannot be assumed when dynamical processes are faster than photochemistry, which is the case throughout the lower stratosphere.

### 3.1.2 Dynamical Processes

In order to evaluate the relative importance of photochemical and dynamical processes, it is important to know the relaxation time of any disturbance of the photochemical equilibrium (called "time of half restoration" by Wulf and Deming [4]). According to Dütsch [3] this relaxation time is approximately given by the ratio of total content of odd oxygen species divided by their rate of formation.

Under stratospheric conditions ($[O] \ll [O_3]$), using Eq. (3.8) and the ratio $s = [M]/[O_2] = 4.75$, he obtains the following approximation:

$$\tau = 1/4(k_2[O_2]s/J_2J_3)^{1/2} \tag{3.9}$$

$\tau$ is found to be of the order of 1 hour at the stratopause (about 50 km) and increases rapidly with decreasing altitude, to values of 1 year and more below the level of the ozone maximum. The ozone distribution below 30 km is therefore largely determined by air motions, and the dependence of the ozone concentration on season and latitude at these levels is governed by the general circulation of the atmosphere. Above 50 km the relaxation time is so short that air motions play only a minor role and photochemistry dominates. Between 30 and 50 km both photochemistry and dynamics have to be considered.

A first conceptual model for the interplay of photochemistry and dynamics was presented by Dütsch (Ref. [12] of Chap. 2) based on studies by Brewer [5, 6] and Dobson [7]. According to this "Brewer–Dobson Cycle" the main ozone source region is the tropical stratosphere between about 20 and 35 km altitude. From there poleward and downward eddy mixing occurs, which is strongest over the winter hemisphere, with predominant westerly winds in the stratosphere. This downward motion carries ozone to lower altitudes, while its photochemical relaxation time increases rapidly. Thus ozone can accumulate maintaining non-equilibrium. That way the lower stratosphere is filled with excess ozone. This effect increasing with latitude, which is reflected by the vertical profiles shown in Fig. 2.4: below about 25 km ozone increases towards high latitudes. This effect is strongest during late winter and less pronounced during late summer. That way total ozone over high latitudes is about twice that over the tropics.

Above about 25 km, ozone is highest over the tropics and decreases towards higher latitudes, in accordance with photochemistry.

Compared to the troposphere where vertical mixing is fairly rapid, the stratosphere behaves, due to increasing temperatures with altitude, like a huge inversion

layer. Vertical mixing is suppressed and confined to quasi-horizontal motion along sloped, predominantly isentropic, surfaces.

Radioactive substances injected into the stratosphere by high-energy nuclear weapon tests have been used as tracers for investigating stratospheric mixing. Newell [8] could show by using tungsten-185 as tracer that meridional mixing from a tropical source largely occurs along isentropic surfaces that are generally oriented downwards towards higher latitudes. Similar findings were reported from using zirconium-95 as tracer [9]. The meridional mixing resulting from the three-dimensional interplay of waves and eddies, a poleward transport over thousands of km connected to sinking motion by a few km, is therefore called quasi-horizontal mixing.

The role of planetary waves in the maintenance of the upper stratospheric ozone distribution was investigated by Garcia and Hartmann [10], by modelling the effect of defined perturbations. Waves and eddies are the drivers of a global-scale circulation, by which air is withdrawn upward and poleward from the tropical lower stratosphere and pushed poleward and downward in the extratropical stratosphere. This wave-induced dynamics and its relation to stratospheric–tropospheric exchange have been evaluated by Holton et al. [11, 12], see Sect. 4.2.

Present models coupling a three-dimensional circulation model with photochemistry are capable of computing realistic global ozone distributions, with good resolution in time and space (see [13]).

By using the mere oxygen reactions, however, ozone is overestimated by about 30 %. Thus further ozone depleting reactions need to be considered which are discussed in the following chapter.

### *3.1.3 Catalytic Reaction Cycles*

The mere oxygen reactions maintain an interplay of source reactions [conversion of $3O_2$ to $2O_3$, reactions (3.1) + (3.2)] and sink reactions [conversion of $2O_3$ to $3O_2$, reactions (3.3) and (3.4)], with solar radiation providing the energy for the dissociation of $O_2$ and $O_3$.

In 1950 Bates and Nicolet [14] demonstrated that radicals (H, OH, $HO_2$) produced from water vapour influence the atmospheric distribution of odd oxygen species. However, as they assumed the direct photodissociation of $H_2O$ to be the only source of these $HO_x$ radicals ($x = 0$–2), this mechanism turned out to be important for mesospheric photochemistry only. It was not before Hampson [15] suggested, on the basis of laboratory measurements, that the water molecule might also be split by the reaction with excited ($^1$D)-oxygen atoms. These are produced by ozone photolysis at wavelengths shorter than 310 nm which are available throughout the atmosphere (even at ground level, see Sect. 3.3). The main reaction is

$$H_2O + O^* \rightarrow 2OH \tag{3.10}$$

with O* denoting the excited ($^1$D)-O produced by

$$O_3 + h\nu \rightarrow O^* + O_2(\lambda < 310\,\text{nm}) \tag{3.11}$$

The interesting fact is that the radicals act like catalysts in cycles in which odd oxygen is converted to $O_2$ molecules. The main $HO_x$ cycles are

$$\begin{array}{l} OH+O \rightarrow H+O_2 \\ \underline{H+O_3 \rightarrow OH+O_2} \\ O+O_3 \rightarrow 2O_2 \end{array} \qquad \text{(net reaction, HO}_\text{x}\text{ cycle 1)}$$

$$\begin{array}{l} OH+O_3 \rightarrow HO_2+O_2 \\ \underline{HO_2+O \rightarrow OH+O_2} \\ O_3+O \rightarrow 2O_2 \end{array} \qquad \text{(net reaction, HO}_\text{x}\text{ cycle 2)}$$

$$\begin{array}{l} OH+O_3 \rightarrow HO_2+O_2 \\ \underline{HO_2+O_3 \rightarrow OH+2O_2} \\ O_3+O_3 \rightarrow 3O_2 \end{array} \qquad \text{(net reaction, HO}_\text{x}\text{ cycle 2 a)}$$

$$\begin{array}{l} OH+O \rightarrow H+O_2 \\ H+O_2+M \rightarrow HO_2+M \\ \underline{HO_2+O \rightarrow OH+O_2} \\ O+O_2+O \rightarrow 2O_2 \end{array} \qquad \text{(net reaction, HO}_\text{x}\text{ cycle 3)}$$

with cycles 2a and 3 being important above 30 km and 40 km, respectively (Ref. [12] of Chap. 2), [16].

It turned out, however, that the incorporation of these $HO_x$ reactions, although most effective in the mesosphere, could reconcile less than 5 % of the aforementioned 30 % discrepancy between modelled and observed ozone in the stratosphere. The breakthrough came with the introduction of $NO_x$ reactions by Crutzen [17] and Johnston [18] based on ideas of Bates and Hays [19].

$NO_x$ radicals formed from nitrous oxide, a natural constituent (see Sect. 4.4.4), via

$$N_2O + O^* \rightarrow 2NO \tag{3.12}$$

catalytically destroy odd oxygen species through

$$\begin{array}{r} NO{+}O_3 \rightarrow NO_2{+}O_2 \\ \underline{NO_2{+}O \rightarrow NO{+}O_2} \\ O_3{+}O \rightarrow 2O_2 \end{array} \qquad \text{(net reaction, } NO_x \text{ cycle 1)}$$

$$\begin{array}{r} NO{+}O_3 \rightarrow NO_2{+}O_2 \\ NO_2{+}O_3 \rightarrow NO_3{+}O_2 \\ \underline{NO_3{+}h\nu \rightarrow NO{+}O_2} \\ O_3{+}O_3{+}h\nu \rightarrow 3O_2 \end{array} \qquad \text{(net reaction, } NO_x \text{ cycle 1 a)}$$

By including these $NO_x$ cycles, cycle 1a being most efficient in the lower stratosphere, most discrepancies between modelled and observed ozone distributions disappeared.

Finally, catalytic cycles involving chlorine [20, 21] and bromine [22] were identified in the 1970s, when the increasing anthropogenic emission of chlorine and bromine bearing substances, such as chloro-fluoro-carbons (CFCs), halons and methyl bromide, was beginning to cause concern. In the unpolluted atmosphere, with methyl chloride ($CH_3Cl$) and methyl bromide ($CH_3Br$) from natural sources being the main substances releasing Cl and Br in the stratosphere, the halogen impact on ozone was very small. However, from about 0.5 ppb and 8 ppt, of total Cl and Br, respectively, in the natural atmosphere, anthropogenic emissions have caused increases to more than 3.5 ppb and 16 ppt, respectively, until 2000. The resulting ozone depletions are discussed in Chap. 5. The basic Cl and Br cycles are given as follows:

$$\begin{array}{r} Cl{+}O_3 \rightarrow ClO{+}O_2 \\ \underline{ClO{+}O \rightarrow Cl{+}O_2} \\ O_3{+}O \rightarrow 2O_2 \end{array} \qquad \text{(net reaction } ClO_x \text{ cycle)}$$

$$\begin{array}{r} Br{+}O_3 \rightarrow BrO{+}O_2 \\ \underline{BrO{+}O \rightarrow Br{+}O_2} \\ O_3{+}O \rightarrow 2O_2 \end{array} \qquad \text{(net reaction } BrO_x \text{ cycle)}$$

The main production reactions of Cl and Br in the unpolluted atmosphere are

$$\begin{aligned} CH_3Cl + OH &\rightarrow Cl + \text{products} \quad \text{and} \quad CH_3Cl + h\nu(\lambda < 220\,\text{nm}) \\ &\rightarrow Cl + \text{products} \end{aligned} \tag{3.13}$$

$$\begin{aligned} CH_3Br + OH &\rightarrow Br + \text{products} \quad \text{and} \quad CH_3Br + h\nu(\lambda < 330\,\text{nm}) \\ &\rightarrow Br + \text{products} \end{aligned} \tag{3.14}$$

A detailed discussion of the halogen species and reactions is given in Chap. 5.

The catalytic cycles are coupled in various ways. Typical examples are the reactions

$$NO_2 + OH + M \rightarrow HNO_3 + M$$
$$NO_2 + ClO + M \rightarrow ClONO_2 + M$$
$$Cl + HO_2 \rightarrow HCl + O_2$$

through which active radicals of different groups are converted to stable substances such as $HNO_3$, $ClONO_2$ and HCl, so-called reservoir species that sequester radicals for some time. Reservoir species are formed in other reactions involving source gases such as $H_2$ and $CH_4$ (see Sect. 4.4):

$$Cl + H_2 \rightarrow HCl + H$$
$$Cl + CH_4 \rightarrow HCl + CH_3$$

Water vapour has a double function: it is both source gas for $HO_x$ radicals and also reservoir species formed in reactions such as

$$OH + HO_2 \rightarrow H_2O + O_2$$
$$OH + OH \rightarrow H_2O + O$$
$$OH + CH_4 \rightarrow H_2O + CH_3$$

There are coupling reactions such as

$$NO + ClO \rightarrow NO_2 + Cl \quad \text{and} \quad NO + HO_2 \rightarrow NO_2 + OH$$

in which radicals of different groups react such that the ozone depleting path of the respective cycles is bypassed.

Reservoir substances are reconverted to radicals by photolysis and reactions with OH, which can occur under daylight conditions only. Thus both groups reveal typical diurnal variations: radicals are formed at daylight, their maximum occurs at noon, while reservoir species are decomposed during daytime, their maximum occurs at night. Figure 3.2, based on model calculations [23], illustrates this behaviour.

In the unpolluted atmosphere the main sources for $HO_x$; $NO_x$; and $ClO_x$ radicals are $H_2O$, $H_2$, $CH_4$; $N_2O$; and $CH_3Cl$, respectively. Sources and budgets of these source gases are discussed in Sect. 4.4. Their decomposition largely occurring via photolysis or reactions with excited ($^1D$)-O and OH leads to the formation of radicals which, in catalytic cycles, convert odd oxygen species to $O_2$. Thus the ozone layer is regulated by substances originating from the Earth's surface. In the natural atmosphere, this flux of source gases must be balanced by a corresponding sink mechanism: reservoir substances act as sink substances whenever they are mixed to the troposphere, where they are dissolved in cloud water droplets and rained out. Depending on the stability of source gases towards decomposition, their atmospheric life cycles range about 1 year for $CH_3Cl$, 8 years for $CH_4$, 100 years for $N_2O$, up to several hundred years for man-made halocarbons (see Chap. 5).

In Fig. 3.3 the interplay of the most important reactions relevant to the ozone layer is shown schematically. The source gases shown in the boxes at the bottom are decomposed feeding radicals to the $NO_x$, $ClO_x$ and $HO_x$ catalytic cycles shown in the centre. Coupling reactions and the formation of reservoir or sink gases

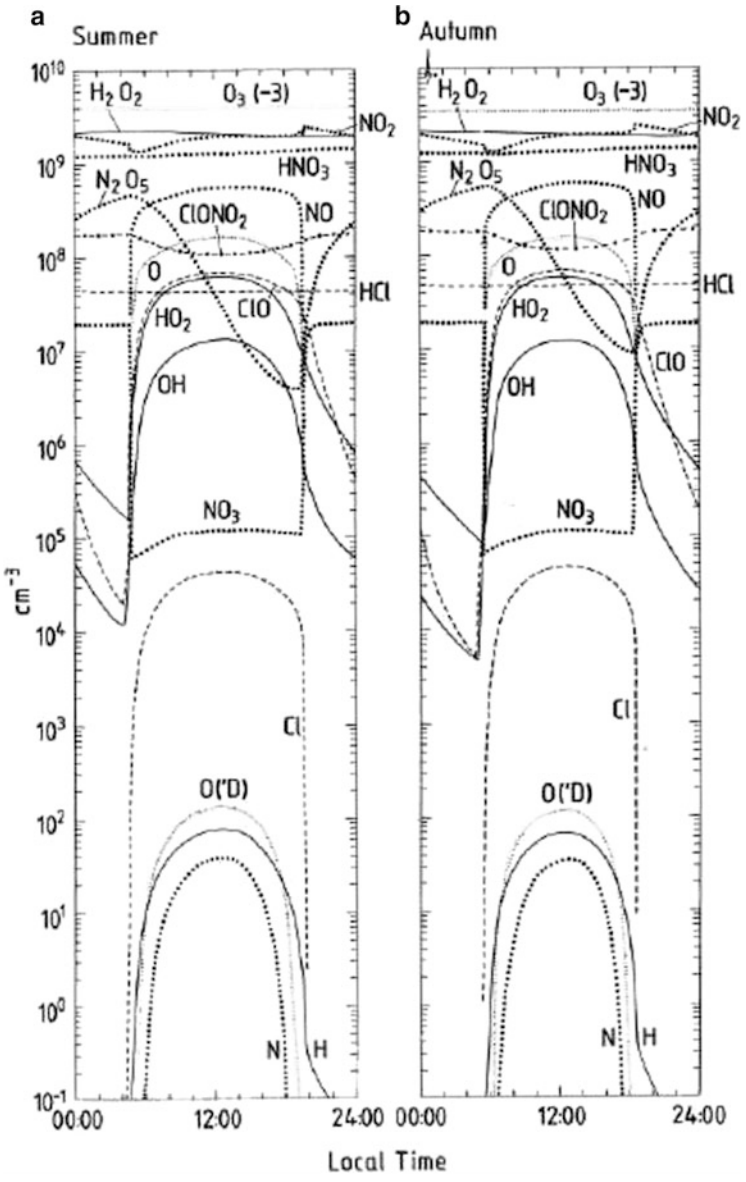


**Fig. 3.2** Diurnal variation of short lived species' concentrations, calculated for 47°N and 32 km altitude, for June (**a**) and September (**b**). For $O_3$ the scale was reduced by three orders of magnitude [23]

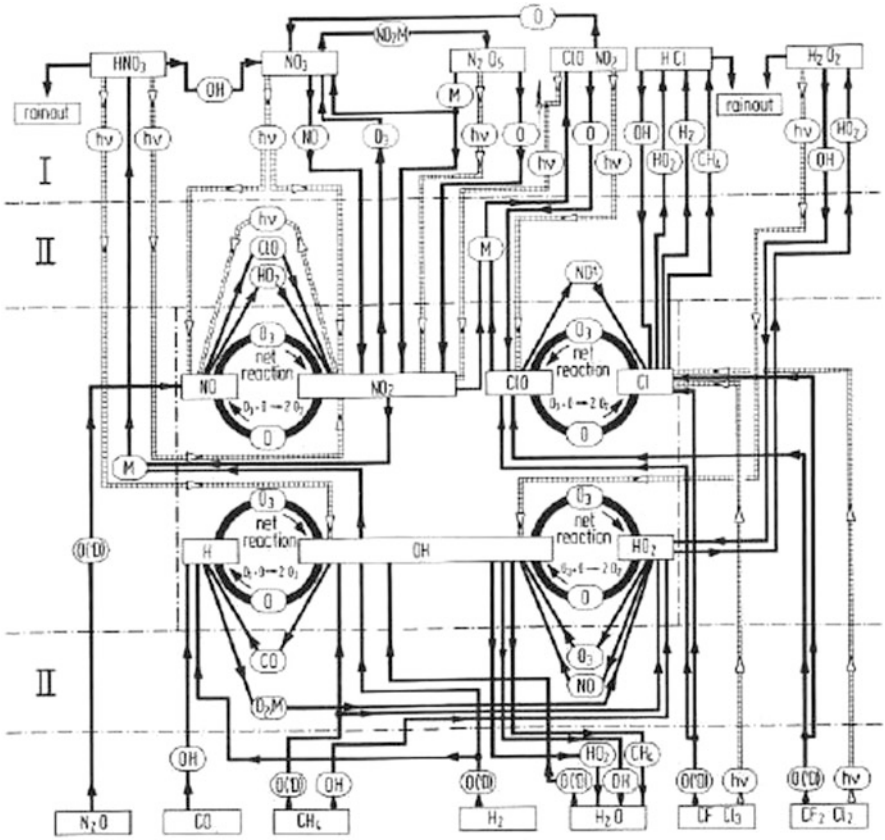


**Fig. 3.3** Schematics of important reactions related to the middle atmosphere ozone layer. Collision and photolytic reaction paths are shown by *solid lines* and *shaded double lines*, respectively. Pure oxygen reactions are omitted [24]

displayed in the boxes at the top are shown as well. It should be noted that, instead of $CH_3Cl$, $CFCl_3$ and $CF_2Cl_2$, two man-made substances not existing in the natural atmosphere, are shown here as source gases for $ClO_x$ radicals. As discussed in Chap. 5, these and other man-made halocarbons cause significant ozone depletions.

### *3.1.4 Heterogeneous Reactions*

Catalytic ozone destruction cycles based on homogeneous gas phase photochemistry largely operate in the higher layers of the stratosphere, above about 25–30 km altitude, where enough oxygen atoms are available for closing the catalytic cycles (see Sect. 3.1.3).

Heterogeneous reactions were discovered soon after the discovery of massive seasonal ozone depletions in polar regions, at altitude ranges between about 10 and 25 km. In fact, the "Antarctic Ozone Hole" was totally unforeseen as it could not be predicted based on homogeneous photochemistry (see Sects. 5.1 and 7.1). It is well known today that heterogeneous reactions on the surface of polar stratospheric clouds (PSCs) are the key for understanding this phenomenon.

In the very cold polar stratosphere clouds are common, especially during polar night conditions. On the surface of these PSCs halogen reservoir substances, such as HCl and $ClONO_2$ (see Sect. 3.1.3), are processed such that active chlorine is liberated. The most important of such heterogeneous reactions are

1. $ClONO_2 + HCl \rightarrow HNO_3 + Cl_2$
2. $ClONO_2 + H_2O \rightarrow HNO_3 + HOCl$
3. $HCl + HOCl \rightarrow H_2O + Cl_2$
4. $N_2O_5 + HCl \rightarrow HNO_3 + ClONO$
5. $N_2O_5 + H_2O \rightarrow 2HNO_3$

Reaction 2 can proceed directly on water or ice surfaces, while for reaction 1 HCl needs to be solved in the cloud particles. In both cases $HNO_3$ is formed which may remain solved in the liquid or solid phase. Thereby, $NO_x$ components are removed from the gas phase and remain sequestered as long as the cloud particles exist.

The products $Cl_2$, HOCl and ClONO photolyze as soon as solar radiation is available, for instance at the end of the polar night. Thereby Cl atoms are liberated which destroy ozone.

$NO_x$ components are converted to $N_2O_5$ through the reaction chain

6. $NO + O_3 \rightarrow NO_2 + O_2$
7. $NO_2 + O_3 \rightarrow NO_3 + O_2$
8. $NO_3 + NO_2 + M \rightarrow N_2O_5 + M$

Through reactions 4 and 5 $N_2O_5$ is converted to $HNO_3$, which remains sequestered in the cloud particles. By this "denitrification" of the lower stratosphere the equilibrium of the chlorine compounds is shifted towards the active Cl radicals.

As atomic oxygen is practically nonexistent below 25 km altitude, where most of the polar ozone losses are observed, significant ozone depletion can occur only when ClO formed in the reaction $Cl + O_3 \rightarrow ClO + O_2$

is reconverted to Cl by other reactions. These are illustrated in Fig. 3.4 according to

9. $ClO + ClO + M \rightarrow (ClO)2 + M$
   $(ClO)2 + \text{radiation} \rightarrow Cl + ClO_2$
   $ClO_2 + M \rightarrow Cl + O_2 + M$
10. $ClO + BrO \rightarrow Cl + Br + O_2$
11. $ClO + HO_2 \rightarrow HOCl + O_2$
    $HOCl + \text{radiation} \rightarrow OH + Cl$

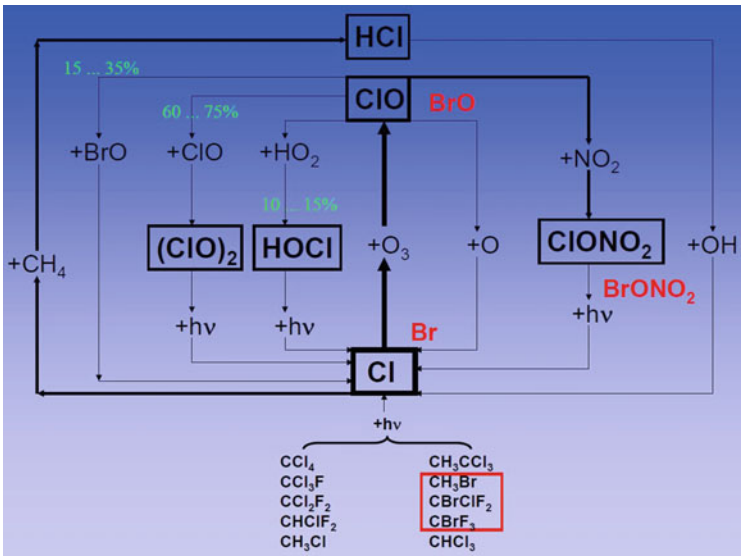


**Fig. 3.4** Scheme of photochemical reactions of the Ozone Hole

Bromine radicals liberated from bromine bearing source gases circulate in analogeous ways as shown in Fig. 3.4. (For the sake of clarity they are not shown directly. As shown by the red marking, Cl has to be replaced by Br.) Accordingly, bromine reservoir substances HBr and $BrONO_2$ are formed, which, different from their chlorine counterparts, are less stable. Photolysis and reactions with OH feed active bromine back to the catalytic cycles.

The extrapolar stratosphere is normally clear and free from clouds. Aerosol particles, however, can also provide surfaces for heterogeneous processes to occur. This particularly holds for times after strong volcanic eruptions injecting sulphur compounds into the stratosphere, where they are oxidised forming sulphate aerosol particles [25]. These reside for about 1–2 years and have been observed after the strong eruptions of El Chichon in Mexico (1982) and Pinatubo/Philippines (1991). Both eruptions occurred at a time when the atmospheric halogen level, due to anthropogenic emissions, was high already, and significant ozone depletion had been observed [26].

It has been speculated whether the extremely low ozone values observed over central Europe during the winter 1991/1992 leading to the Copenhagen amendment of the Montreal Protocol (see Chap. 6) were at least partly caused by the stratospheric aerosol cloud of the June 1991 eruption of Pinatubo, which had reached Europe by December 1991. This shows that natural processes such as volcanic eruptions can lead, via heterogeneous reactions in the lower stratosphere, to significant temporary ozone losses when the atmosphere is polluted with halogens.

## 3.2 Global Ozone Distribution

By the end of the 1960s, the main features of the ozone layer, its vertical and latitudinal distribution and seasonal variations, were fairly well established already, from ground-based measurements within the Dobson network. The layer thickness is smallest at tropical latitudes and increases towards higher latitudes (Fig. 2.4). The asymmetry of the hemispheres is obvious: while in the Northern Hemisphere total ozone increases well up to the pole, the maximum ozone layer thickness in the Southern hemisphere is reached at about 60° already and decreases beyond to lower values over the South Pole.

The undisturbed Southern polar region is characterised by low total ozone, during the polar winter months May–July even as low as the minimum values over the tropics, long before any anthropogenic ozone depletion (see Sect. 5.1) played a role. The vertical profiles displayed in Fig. 2.5 show, for Northern latitudes, that seasonal and latitudinal variations mainly affect the "dynamic" height region, the lower stratosphere below about 30 km, where ozone increases with latitude, while at altitudes above, where photochemistry dominates, the latitudinal gradient follows solar radiation, with highest values over the tropics (see Sect. 3.1.2).

Present numerical models, with full photochemical and dynamical schemes, are capable of reproducing the ozone layer quite well. By combining such models calculating the ozone distribution as a function of latitude, longitude, altitude and time with real measurements of total ozone in the ground-based network, global maps of total ozone can be achieved to a surprising degree of information, despite the fact that the stations are clustered on the continents and vast areas such as the oceans are practically void of measuring devices.

Since the 1970s, satellite borne instruments have revealed a wealth of details which cannot be expected to be achieved from a limited ground-based network. Since satellites orbit the Earth they produce detailed partial maps following the orbit, according to the swath geometry. At a given time, ozone fields are available for the respective swath only. In order to produce global maps, these partial maps have to be put together taking into account the time variation along the orbits. Present-day models, with detailed photochemical and dynamic codes, allow the construction of global maps, even when gaps in time and space occur in the data material.

The total ozone contour plots shown in Fig. 3.5 give a comparison between ground-based (left) and satellite data (right), for the periods 1964–1976 and 1970–1972, respectively (upper panels, "pre-ozone hole period"), and 1985–1993 and 1996–1997, respectively (lower level, with clear ozone hole signature). It is impressive how well the results achieved with both techniques agree. The "Antarctic ozone hole", a strong seasonal ozone depletion (see Sect. 5.1), is well pronounced in the lower panels between September and November, both in the ground-based as well as the satellite data.

In Fig. 3.6 total ozone layer thickness from satellite data is plotted as a function of latitude and time, from 1995 to 2008. The low values over low latitudes, high

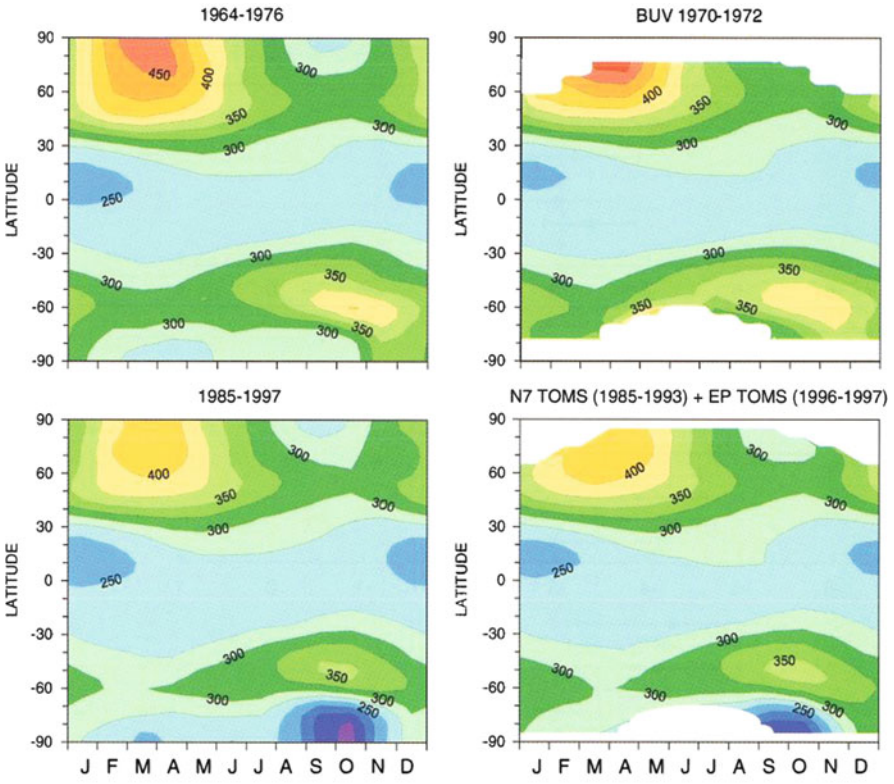


**Fig. 3.5** Total ozone measured by ground-based Dobsons and satellite-based instruments, from [27] contour plots of total ozone (Dobson unit, Du) by latitude and month. *Left plots*: Ground-based data for the period 1964–1976 (*upper panel*) and 1985–1997 (*lower panel*). *Right plots*: Satellite data for the periods 1970–1972 (*upper panel*) and 1985–1997. Nimbus 7 and Earth Probe TOMS (*lower panel*)

values over North polar regions, medium high values at about 60°S and the layer thickness decrease towards Antarctica can be seen, with interannual variations as well, along with the development of the Antarctic ozone hole.

## 3.3 UV Radiation and Ozone Layer Thickness

The solar UV radiation spectrum is divided into three wavelength ranges, UV-A (315–400 nm), UV-B (280–315 nm) and UV-C (200–280 nm). Due to strong absorption of oxygen and ozone (see Fig. 3.1) the very shortwave UV-C range does not reach the ground. The UV-A region is, like the visible solar radiation, almost unaffected by ozone. The UV-B region is of special interest as, mainly

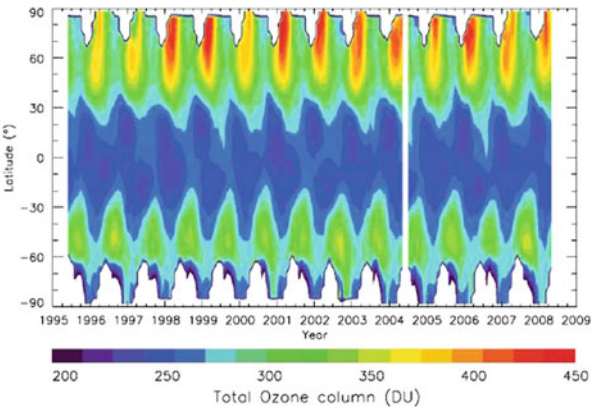


**Fig. 3.6** Latitudinal evolution of total ozone from June 1995 to May 2008. European satellite data from April 2004 are not available, from [13]

because of ozone absorption, it is the wavelength region where the shortwave cutoff of solar radiation occurs. It is illustrated in Fig. 3.7 (left part) for three ozone layer thicknesses, 360, 270 and 180 Dobson Units (DU).

The UV-B region is of particular interest because biological effects are dominant in this spectral range. Here, the action spectra of plant damage, DNA damage and plant growth show their major variations. This is illustrated in the right part of Fig. 3.7 by the corresponding action spectra "Plant", "DNA" and "Plant growth". The action spectra increases with decreasing UV wavelength, but, since the effect on plant damage increases almost exponentially, it dominates over the "positive" effect of plant growth which increases linearly towards shorter UV wavelengths. Thus, although a shift of solar UV fluxes towards shorter UV wavelengths has positive effects on plant growth, the negative biological effects dominate.

For humans, UV-B radiation in moderate doses is important, as it stimulates the formation of Vitamin D for instance. Increases of solar UV-B radiation expected from ozone depletion (see Sect. 5.3) can be harmful as they may cause sunburn and the formation of melanoma.

The UV-B radiation flux penetrating to the Earth's surface largely depends on the ozone layer thickness (see left part of Fig. 3.7). Thus any depletion of the protecting ozone layer tends to result in negative biological effects. For humans this means that sunburn and melanoma occur within shorter exposition times than under greater ozone layer thicknesses.

Besides the ozone layer thickness, other factors determining the UV flux at the surface are the latitude, time of day, season, altitude, weather conditions and ground reflection (albedo).

The time of day and the season determine the solar zenith angle and thus the absorption of a given ozone amount in the vertical column which in turn strongly depends on latitude (see Sect. 3.2). Of course, at night and during polar night when no solar radiation is available, there is no UV radiation at the ground, independent of any other factor.

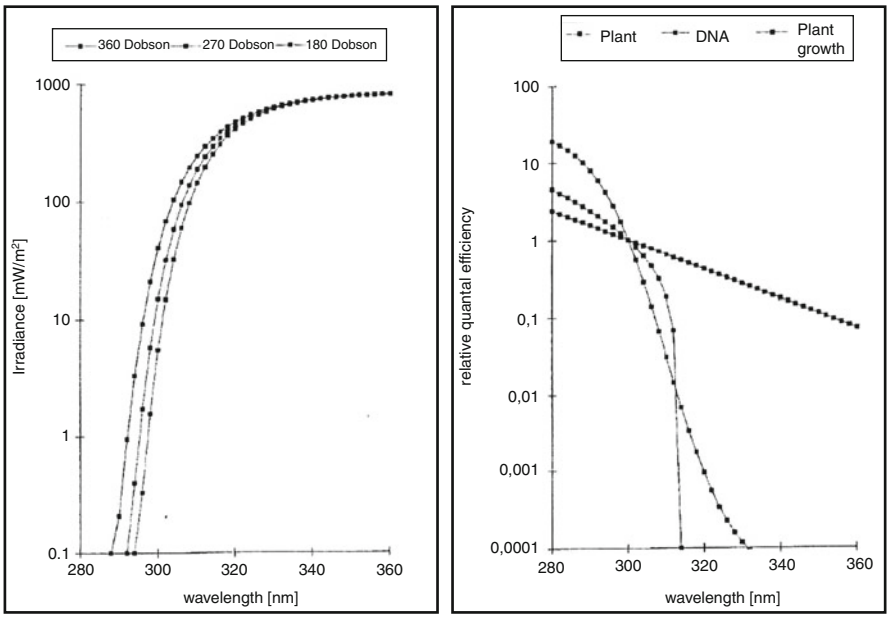


**Fig. 3.7** *Left panel*: Solar UV-B at ground level for different total ozone situations (highest sun on June 21 at 49°N). *Right panel*: Action spectra for DNA damage, plant damage (PLANT) and plant growth, after [28]

The altitude is important, because for increasing altitude the absorbing atmosphere gets reduced, in particular for situations of high levels of surface ozone (see Sect. 5.2). Weather conditions influence the radiation field in various ways: clouds tend to absorb depending on their thickness. Thin clouds may just partly convert the direct solar beam to diffuse radiation, while thick clouds can absorb a large percentage of all the incoming solar radiation.

Aerosols tend to scatter and thus convert part of the direct solar beam to diffuse radiation. Volcanic eruptions add aerosols to the atmosphere, and their impact on the UV radiation field is confirmed [29].

And ground surfaces of high reflectivity by snow, sand or pavement can intensify the surface UV radiation field [30].

All these parameters need to be properly addressed in radiation models used for computing UV fluxes at ground level. There is an agreement within the scientific community that this can be achieved to a reasonable but not perfect degree (see Chap. 7 of [11]).

The variability of surface UV irradiance in time and space is investigated by using measurements from ground-based instruments, as well as from estimates derived from a combination of satellite radiance measurements and radiative transfer modelling. Significant advancements have been achieved in recent years in measurement and calibration procedures of instruments and algorithms used both in ground-based and satellite-borne instruments.

Spectroradiometers are of the most reliable type of instruments to measure solar UV radiation at the ground surface [31]. Empirical or semi-empirical methods have been derived to determine actinic flux and photolysis frequencies from irradiance measurements. For clear-sky conditions the conversion with empirical models agrees better than 10 % with measurements, for cloudy conditions the agreement is within about 15 % [30]. The use of model calculations yields a similar agreement under clear and overcast conditions, but is less accurate under broken clouds [32]. A semi-empirical approach by combining measured actinic flux and irradiance spectra with model calculations results in similarly good agreement for all sky conditions [33].

Instruments on board of satellites provide global maps of surface UV irradiance by combining backscattered radiance measurements with radiation transfer models. The accuracy of the models is limited mostly by uncertainties in input parameters representing the atmosphere and the Earth's surface. In addition, long-term calibration drifts and the establishment of interpolation methods when combining different satellite datasets may introduce errors. As a matter of fact, satellite sensors for measuring ozone from backscattered UV radiation (see Sect. 3.6) are used for deriving the UV radiation field outside the atmosphere as well. Surface UV retrievals from the measurements of the Total Ozone Mapping Spectroradiometer (TOMS) instruments on board of different satellites (1978–2002) are probably the only dataset that has been extensively compared with ground-based measurements. Recently, the TOMS UV irradiance database has been expanded to include new products in addition of noon erythemally weighted irradiance and erythemal daily exposure, allowing for direct comparisons with ground-based measurements from UV spectroradiometers [34]. The erythemally weighted irradiance $E_{\mathrm{ery}}$ ($\lambda$) is one important example for biologically active UV radiation (human sunburn). It is calculated as a product of available UV $E(\lambda)$ and the erythemal action spectrum $s$ ($\lambda$). Its integration over the entire wavelength region leads to the so-called erythemal index $E_{\mathrm{ery}}$.

A biologically weighted radiation quantity is adequate to describe actual UV irradiance with a simple value for information of the public. A few years ago an international expert group decided to use the erythemal weighted irradiance in W $\mathrm{m}^{-2}$ multiplied with 40.1/W $\mathrm{m}^{-2}$ as so-called UV index, UVI [35].

The TOMS UV algorithm was successfully applied to the new Ozone Monitoring Instrument (OMI) on board the Aura satellite for continued monitoring of ozone, other trace gases and surface UV irradiance [36, 37]. OMI provided global maps of surface UV irradiance, an example is shown in Fig. 3.8. The upper panel is from Northern Hemisphere (NH) summer, the lower panel from NH winter. Besides the typical latitude dependence of surface UV from the global ozone distribution (see Sect. 3.2), with highest values over the tropics, the other dependencies of surface UV from solar zenith angle (no radiation at all during polar night), altitude (enhanced UV over the Himalayas and Andes) and meteorology (cloud bands) as discussed earlier in this chapter are clearly visible.

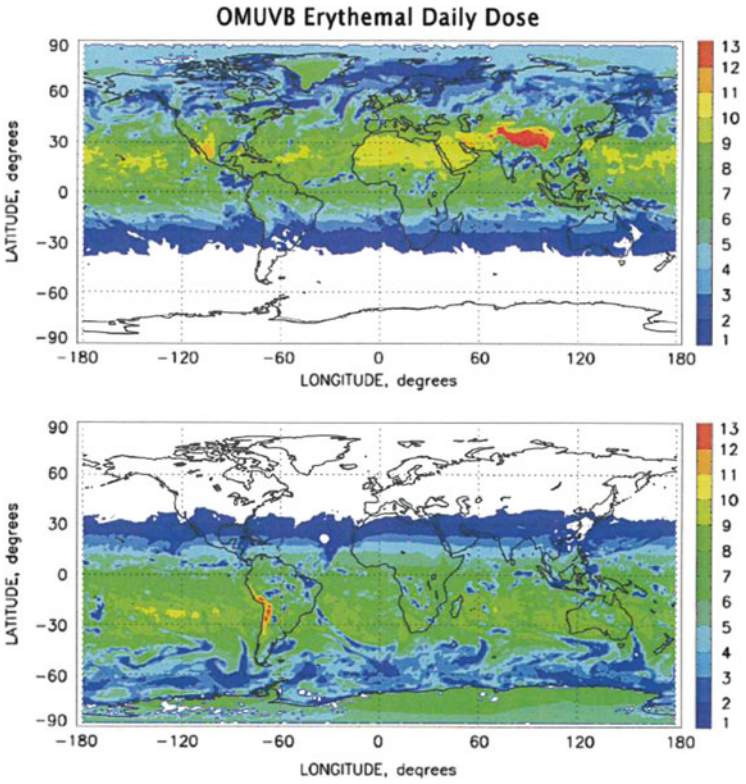


**Fig. 3.8** Global distribution of the cloud-corrected daily integral of erythemal radiation in kJ $m^{-2}$ for 28 June 2005 (*upper panel*) and 28 December 2005 (*lower panel*) derived from OMI measurements from [30]

## 3.4 Solar and Cosmic Effects

The influx of energetic charged particles leads in the atmosphere to the formation of $NO_x$ and $HO_x$ radicals which, via photochemical reactions, may influence the distribution of trace gases and in particular the ozone layer. Thereby charged particles of the galactic cosmic radiation as well as solar protons and electrons and relativistic electrons in connection with magnetospheric substorm activity play a role [38]. In the mesosphere, these predominantly lead to $HO_x$ radicals, while in the stratosphere mainly $NO_x$ radicals are formed. The production of $HO_x$ and $NO_x$ runs by ion reaction chains, whereby every ion/electron pair can produce 2 $HO_x$ and 1.5 $NO_x$ particles, respectively [38, 39].

Since $HO_x$ and $NO_x$ radicals can deplete ozone via catalytic reaction chains, ozone measurements at times of strong influx of charged particles, for instance during solar proton events, allow for testing models and thus the reality of the photochemical reactions involved. Fortunately the sun provided such test event, an

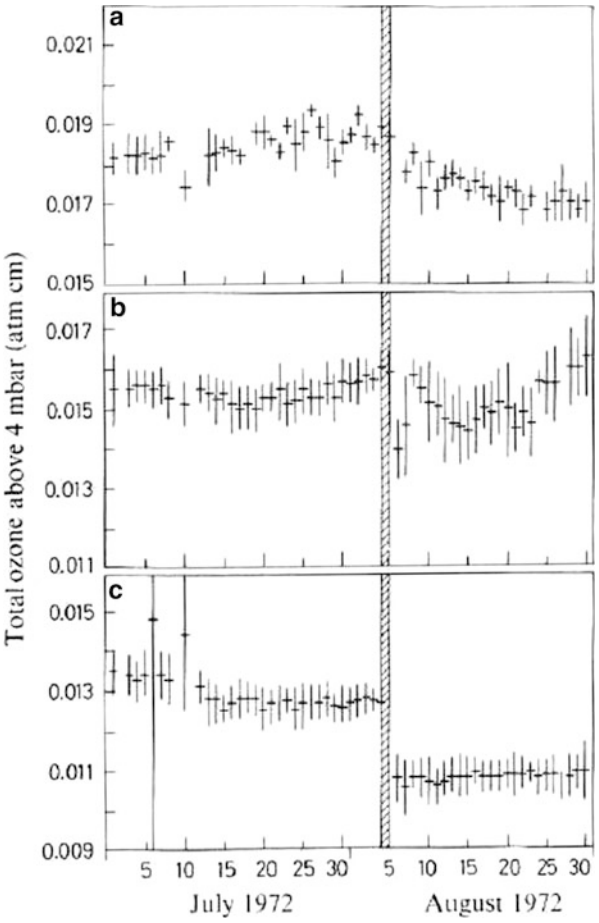


**Fig. 3.9** (**a**–**c**): Zonal means of total ozone above 4 mb for equatorial (**a**), middle (**b**) and high northern latitudes (**c**). The solar proton eruption occurred on 4 August 1972. The ozone data shown here were measured by the BUV—experiment aboard the NIMBUS-4 satellite. 1 atm-cm = 1,000 Dobson Units (DU), after [40]

extremely intensive proton eruption. This eruption of 4 August 1972 is among the most intensive ever observed. During this time the ozone layer was controlled by a UV sensor aboard the NIMBUS-4 satellite; from measurements of backscattered UV radiation total ozone above 4 mb (about 38 km altitude) was continuously derived [40]. Zonal means of these, for July and August and three different latitude zones, are plotted in Fig. 3.9 with their uncertainty ranges. In high northern latitudes, where the charged particles could penetrate almost unaffected by the Earth's magnetic field, the solar proton event caused an almost abrupt decrease of the ozone layer above the 4 mb level of almost 20 %.

In middle latitudes a slow decrease with final recovery, despite of two low values 2 and 3 days after the event, was measured, while in the tropics a slow decrease of 0.019 atm-cm in July up to 0.017 atm-cm at the end of August was found, which, however, does not appear to coincide with the solar event as its onset is before August 4 already. The slight ozone increase in July followed by the decrease

observed in the tropics, obviously is due to an abnormal temperature fall in July related to a stratospheric warming on the Southern Hemisphere, which vanishes again in August [40]. This example of the tropics, where, because of the shielding effect of the Earth's magnetic field, definitely no charged particles could penetrate, shows that natural fluctuations occur in the ozone layer, even at these high altitudes.

Figure 3.10 shows the results of a model simulation of this event by means of a two-dimensional model [41] along with satellite data for high latitudes. The model results based on two datasets of the $NO_x$ production rates of the event. The satellite data are related to the left ordinate scale. The model results show the relative ozone layer decrease above 7 mbar (about 34 km altitude), related to the undisturbed level on August 4, before the event (right ordinate scale). The comparison in Fig. 3.10 shows that the model reproduces this solar event basically correctly. Both model results qualitatively show a correct course of the event, although based on these computations alone it cannot be decided which of the two datasets of $NO_x$ production is the correct one. This solar event is of special importance, as the catalytic ozone depletion can be proved based on measured data.

In the mesosphere, the influx of charged particles produces mainly $HO_x$ radicals, H, OH and $HO_2$, from the water vapour there, which thus gets reduced. These $HO_x$ radicals lead to an immediate ozone depletion, but within a few hours depending on whether day or night conditions prevail, to the formation of molecular hydrogen ($H_2$) and back to water vapour. Crutzen and Solomon [39] have calculated that the solar proton eruption of August 4, 1972 must have lead to a drastic water vapour depletion, by two orders of magnitude around 80 km altitude, where permanent daytime conditions prevailed. $HO_x$ radicals hereby formed in the first place lead to an ozone depletion to about one-third of the level before the event. After the conversion of $HO_x$ to $H_2$, the ozone level increased again, not only to the original level but also to threefold of it, as practically all water vapour had been converted to $H_2$. Thus at 80 km altitude an ozone sensor would have measured a considerable ozone increase caused by this solar proton event, which only slowly would have been compensated by the slow backflow of water vapour from lower altitudes.

Secondary electrons leading to $NO_x$ radical formation originate from the influx of galactic cosmic radiation as well. This cosmic particle flux from space is controlled by the activity of the sun. Its intensity is in counterphase to solar activity: during solar activity maximum when solar plasma fluxes are largest, the galactic cosmic radiation is at its minimum, during solar activity minimum at its maximum. Thus the $NO_x$ production by the galactic cosmic radiation influx should vary in counterphase with the solar activity cycle. Above 30 km altitude where significant $NO_x$ amounts are formed through this process, a variation of ozone over the 11-year activity cycle of the sun can be expected. During solar activity maximum this $NO_x$ production is lowest. As the atmospheric residence time of $NO_x$ is about 2–3 years at this altitude, the ozone maximum of this solar cycle variation can be expected about 2–3 years after the solar activity maximum.

Before we continue with solar cycle ozone variations more important work related to solar proton events is discussed.

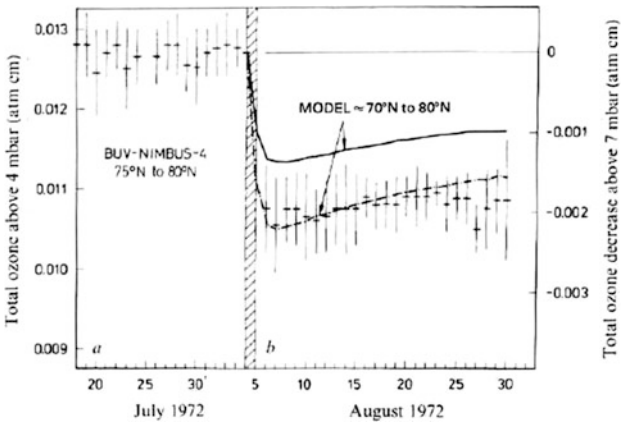


**Fig. 3.10** (**a**, **b**): Comparison of the BUV-NIMBUS-4 ozone data for high northern latitudes (Fig. 3.9c) with results of a two-dimensional model [41]. The model results are displayed as relative decrease of total ozone above 7 mbar compared to the "undisturbed" level on August 4, immediately before the onset of the proton eruption. The model computation bases on two datasets for the $NO_x$ production due to the influx of charged particles (*solid and dashed lines*)

The effect of the August 1972 solar proton effect is discussed by Reagan et al. [42], and the production of odd nitrogen and an intercomparison of source strength are presented by Jackman et al. [43]. Solomon and Crutzen [44] discuss chlorine chemistry related to the August 1972 event. McPeters et al. [45] deal with ozone depletion during all solar proton events in history. The effects on the entire middle atmosphere and other chemical constituents are presented in [38, 46, 47]. Nitrate formed from proton event-produced $NO_x$ radicals is removed by precipitation. A precision-dated ice-core nitrate record from Law Dome, East Antarctica, is compared to the timing of known solar proton events over the period 1888–1995. For most events a significant nitrate concentration peak could be identified [48].

Correlations of sunspot numbers and total ozone have often been found, but the results differ considerably from each other. This is partly due to the fact that this solar effect plays a role above 30 km altitude only encompassing 10 % of the ozone layer. The correlation of total ozone variations can be masked by dynamic variations affecting the 90 % below 30 km.

Nevertheless Angell and Korshover [49] could derive 11-year periods from the long ground-based total ozone measurements at Tromsö (70°N) and Arosa (47°N), from 1930 until 1970, whose amplitudes are related 2:1, and their phases are delayed by 32 and 38 months, respectively, against the 11-year solar activity cycle. This result is in agreement with a NO-modulation caused by the galactic cosmic radiation.

Paetzold et al. [50], however, found from ozone data measured by optical balloon-born sensors between 1951 and 1971, an 11-year period exactly in phase with the solar activity cycle. This result points to ozone variations over the solar

activity cycle not due to $NO_x$ modulation but rather due to variations of solar UV radiation between 180 and 340 nm wavelength. After results of several satellite experiments, the UV flux emitted by the sun, especially its short wave part with wavelengths below 242 nm which is responsible for ozone formation, varies with the 11-year solar cycle. At 175 nm the solar UV flux at sunspot maximum is about 50 % larger than at sunspot minimum. The amplitude decreases towards longer wavelengths, at 200 nm it is about 20 %, and it disappears in the visible spectral range. By means of model computations, Penner and Chang [51] could show that these UV variations lead to changes of ozone and temperature distributions and thus, because of the temperature dependence of reaction rates, to measurable variations of several other trace constituents as well. Thus at 30 km altitude, the concentration of the source gas $N_2O$ decreases by about 10 % from solar activity minimum to maximum, that of the source gas $CH_4$ by 5 %. At 50 km altitude these changes amount to 40 % and 24 %, respectively.

The relationship of short-term variations of ozone and solar activity most likely results from solar ultraviolet variability near 0.2 nm wavelength [52]. Based on NIMBUS-4 satellite measurements it has been thoroughly investigated [53]. The effects on other trace gases are documented in [54]. Angell [55] used long data series 1960–1990 to update his earlier paper [49] still containing a lot of uncertainties. Solar cycle variations of upper stratospheric ozone and temperature and their latitude and seasonal dependencies have been investigated by McCormack and Hood [56]. The temperature effect is very important in climate issues [57]. It has been shown that the Maunder Minimum (1645–1715), a time of extremely low temperatures on Earth, is due to solar cycle variations [58].

It should finally be mentioned that by the incredibly high energies of the order of $10^{40}$ to $10^{41}$ Joules, liberated as Gamma Radiation from nearby Supernova explosions, the ozone layer can, via the $NO_x$ mechanism, be heavily depleted, when these explosions happen to occur near the Earth [59]. As a consequence the heavily enhanced solar UV can cause mutations and lead to cell damages. Ruderman [60] argues that during the Earth's history several living beings may have been extinguished because of supernova explosions. Biological effects can have been caused by climatic variations as a consequence of massive $NO_x$ enhancements in the atmosphere, because enhanced $NO_2$ absorption of visible solar radiation leads to a global cooling [61].

Reid et al. [62] discuss the possibility that the extinction of certain plant species may be related to multiple reversals of the Earth's geomagnetic field. They argue that at times of magnetic field reversals solar proton explosions can lead to extremely massive reductions of the ozone layer because then the protecting magnetic field is weakened.

## 3.5 Heavy Ozone and Isotope Effects

Besides the bulk oxygen $^{16}O$ there exist two heavier isotopes $^{17}O$ and $^{18}O$ in the environment. Their abundances in ocean water are

| | |
|---|---|
| $^{16}O$ | 0.99757 |
| $^{17}O$ | 0.00038 |
| $^{18}O$ | 0.00205 |

This represents an important standard, the "Standard Mean Ocean Water" (SMOW).

For any sample the isotopic ratios are reported in the conventional delta notation, which for oxygen isotopes is given by

$$\delta^{18}O\ (‰) = \left(R^{18}{}_{sample}/R^{18}{}_{STD} - 1\right) \times 1,000$$
$$\delta^{17}O\ (‰) = \left(R^{17}{}_{sample}/R^{17}{}_{STD} - 1\right) \times 1,000$$

with $R^{17} = {}^{17}O/{}^{16}O$, $R^{18} = {}^{18}O/{}^{16}O$ and "STD" refers to standard mean ocean water (SMOW).

It is well known that the variation of these isotope ratios produces a highly correlated array, with $\delta\ {}^{17}O = 0.52\ \delta\ {}^{18}O$. This arises from the mass dependency of conventional isotope effects such as isotope exchange from the mass dependence of vibrational frequencies, kinetics, evaporation, condensation and velocity. A plot of isotopic measurements of a broad range of terrestrial samples displays the coherence of this $\delta\ {}^{17}O = 0.52\ \delta\ {}^{18}O$ relation shown in Fig. 3.11 [63]. Note that $\Delta\ {}^{17}O$ expresses the deviation in permille from the mass fractionation line.

The first exception to this observation was reported by Thiemens and Heidenreich [64]. It had been observed that, in the production of ozone by molecular oxygen, ozone was equally enriched in the isotopes $^{17}O$ and $^{18}O$, or $\delta\ {}^{17}O = \delta\ {}^{18}O$, instead of $\delta\ {}^{17}O = 0.52\ \delta\ {}^{18}O$. Mauersberger [65] observed that ozone possesses a high $^{18}O$ enrichment which can be used to make ozone an efficient diagnostic tracer for resolving photochemistry and atmospheric mixing [66]. From ozone isotopic data for $^{49}O_3$ and $^{50}O_3$ and from 28 stratospheric samples obtained over a 10-year period by balloon payloads, it could be shown that the enrichments of the heavy isotopes agree well with laboratory measurements [67]. In the mid-stratosphere, for $\delta\ {}^{17}O$ the range is 70–90 ‰, and for $\delta\ {}^{18}O$ 70–110 ‰.

Atmospheric constituents connected with ozone photochemistry processes show mass-independent isotope ratios as well. This holds for nitrous oxide ($N_2O$), sulphur compounds, carbon monoxide (CO), carbon dioxide ($CO_2$) and molecular oxygen ($O_2$) [68]. Thus atmospheric sulphate and sulphates in terrestrial sediments show oxygen isotopic anomalies as well [64, 69].

An interesting mass-independent fractionation was observed in nitrate of rain and fogwater samples collected in an Ecuadorian mountain forest. It could be

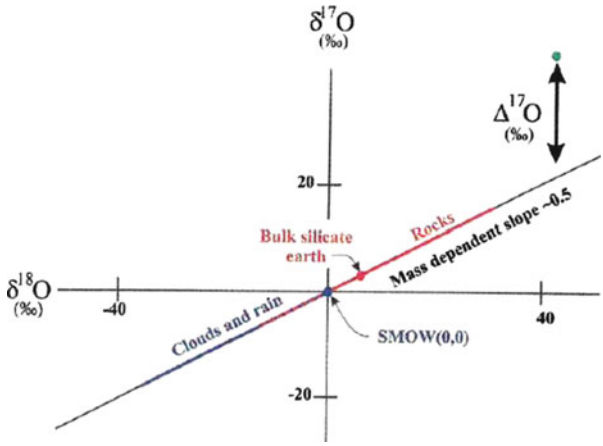


**Fig. 3.11** Three isotope plots for oxygen, illustrating the mass-depending slope and $\Delta\ ^{17}O$ [63]

shown that this nitrate had been produced in the atmosphere from precursor substances, with ozone photochemistry involved [70].

## 3.6 Measurement Techniques

Ozone in the atmosphere is measured by making use of its chemical and optical properties, some of which have been touched in Chap. 2 where highlights of the discovery of ozone in the atmosphere are briefly described. Here a systematic insight into presently used techniques and instrumentations is given.

### *3.6.1 Ground-Based Measurements*

#### Chemistry

Ozone in ambient air has successfully been measured by the following techniques:

The Montsouris Series

This method exploits the following iodine catalysed oxidation of arsenite ($AsO_3^{3-}$) to arsenate ($AsO_4^{3-}$):

$$(O_3)\ aq + I \rightarrow I\ O^- + O_2$$
$$AsO_3^{3-} + IO \rightarrow As\ O_4^{3-} + I$$
$$\text{Net: } O_3 + AsO_3^{3-} \rightarrow O_2 + AsO_4^{3-}$$

The main experimental equipment is a wash bottle filled with 20 ml of $5 \times 10^{-4}$ molar $K_3\ AsO_3$ and 2 ml of 3 % KI solution. After about 2–3 $m^3$ of ambient air are sucked through this solution, the arsenate that still remained is titrated with iodine. This method was applied successfully for 34 years, Volz and Kley [71] have rebuilt the Montsouris apparatus and compared its performance with the UV-photometer in current use, found the Montsouris technique highly accurate, results differing within 3 %.

### The Schönbein Method

Schönbein, the discoverer of ozone, invented one of the most widely used chemical methods. His method involves filter or blotting paper soaked in potassium iodide and starch solution exposed to air after having been dried for 12–24 h, well protected from sun and rain. These exposed papers, when moistened, change their colour to violet/blue. The amount of ozone present in air is evaluated from the colour of the strip comparing against a chromatic scale. This test involves the following reactions:

$$\begin{aligned} O_3 + 2\,I^- + 2\,H^+ &\rightarrow I_2 + O_2 + H_2O \\ I^- + I_2 &\rightarrow I_3^- \\ \hline \text{Net: } O_3 + 3I^- + 2H^+ &\rightarrow I_3^- + O_2 + H_2O \end{aligned}$$

In this reaction scheme, iodide is oxidised by ozone to the tri-iodide ion, which in the presence of starch forms a complex with the amylase helix. This complex has a strong absorption in the yellow region, and hence the Schönbein papers appear blue/violet. Anfossi et al. [72] evaluated their accuracy to be 33 %, which is equivalent to 2–3 ppb.

### The Ehmert Method

An accurate and sensitive method was initiated by Ehmert and Ehmert [73]. They used thiosulphate variant iodometry, where by adding sodium thiosulphate to the iodide solution, the oxidation was completed at pH = 5, using boric acid as buffer. The reaction sequence involved is given as:

$$\begin{aligned} O_3 + 2I^- + 2H^+ &\rightarrow O_2 + I_2 + H_2O \\ I_2 + 2\,S_2O_3^{--} &\rightarrow 2I^- + S_4O_6 \\ \hline \text{Net: } O_3 + 2H^+ + 2\,S_2O_3^{--} &\rightarrow O_2 + S_4O_6 + H_2O \end{aligned}$$

The liberated iodine oxidises the thiosulphate to tetrathionate, while titration is carried out using standard iodine solution. In certain ways there is similarity between this and the Montsouris method. In both the volatility of $I_2$ is overcome.

Chemical sensors have widely been used for ambient ozone measurements, at the ground, carried by aircraft and balloons.

## UV Absorption Techniques

### The Dobson Photoelectric Photometer

The Dobson spectrophotometer in current use is a specialised double beam monochromator (Fig. 3.12) and is used for determining total ozone by measuring the ratio of intensities of two selected wavelengths of solar UV. Its basic design is described by Dobson [74].

The Dobson instrument is used in three different modes, "direct sun" measurement, "zenith sky" measurement and "Umkehr mode". The four (rather five) wavelength pairs are (1) 305.5 and 325.4, (2) 308.8 and 329.1, (3) 311.45 and 332.4 (4) 317.6 and 339.8, all in nanometers (nm), designated, respectively as A, B, C, D (and also E: 332.4 and 453.6 nm) have been recommended for universal use by WMO. More often a combination of two wavelength pairs is preferred, the most widely used combination is that of pairs A and D.

The individual Dobson instruments are occasionally recalibrated by direct comparison at a common location with either the world primary standard (Dobson instrument No. 83, formerly the primary standard used as Dobson instrument No. 1, kept at Oxford) or with one of the secondary standards. This standard Dobson ozone spectrophotometer, which was the 83$^{rd}$ instrument manufactured of the Dobson type, was adopted in 1962 as the standard US instrument for the measurement of total ozone. In August 1977, Dobson No. 83 served as the reference spectrophotometer during an international intercomparison of regional secondary Dobson instruments held in Boulder, Colorado. In 1980 the instrument No. 83 was designated by WMO as the Primary Standard Dobson Ozone Spectrophotometer for the world.

The measurements with the Dobson spectrophotometer are based entirely upon the ability of molecular ozone to absorb UV radiation in the Huggins band, and have produced the only long-term record of total ozone in the atmosphere measured from ground-based stations.

### Filter Ozonometer

Since 1957, routine ground-based total column ozone measurements have been made at more than 40 stations in the former USSR using a filter ozonometer instrument designated as M-83 (not to be confused with the Dobson No. 83 discussed before). The filter ozonometer is based upon the same principle as the Dobson spectrophotometer in using different absorption of UV in the 300–350 nm Huggins band of ozone. The M-83 instrument, however, uses two broadband filters and measures the relative attenuation of the solar UV radiation

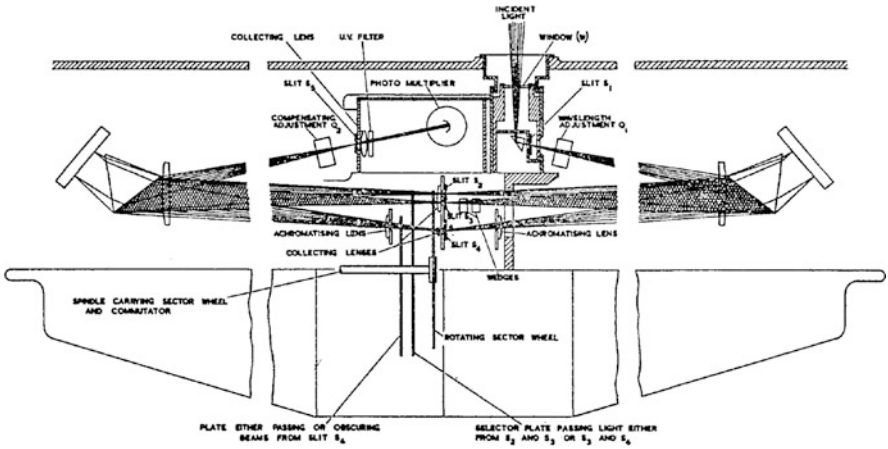


**Fig. 3.12** The basic design of the Dobson photoelectrical spectrophotometer (after Ref. [10] of Chap. 2)

either directly from the Sun or indirectly from the zenith sky [75]. Direct intercomparisons between M-83 and the Dobson spectrophotometers prior to 1971 [76] revealed that the M-83 recorded 6 % less ozone when the observations were restricted to $\mu > 1.5$, and 20–30 % more ozone when data were taken at $\mu > 2.0$. A strong dependency on turbidity was detected, with 9–14 % higher readings when the surface visibility was less than 5 km. The strong deviations for $\mu > 2.0$ made many of the high-latitude measurements in the former USSR very uncertain.

Improved filters were introduced into M-83 instruments starting 1972–1973 [77]. The new filters have maximum transmittance at 301 nm and 326 nm, and their band passes are less than those in the earlier version: 22 nm (291–312 nm) and 15 nm (319–334 nm). Comparison with NIMBUS-4 BUV satellite overpasses over M-83 stations in the USSR demonstrated a standard deviation of about 50 Dobson Unit (DU) before 1973 and 25 DU afterwards. The NIMBUS-4 overpasses of Dobson stations maintained a standard deviation of about 17 DU during the 1970–1977 lifetime of the satellite. A much newer and improved instrument designated as M-124 has been installed in many stations since 1986 (Gustin 80).

### Brewer Grating Spectrophotometer

An improved optical and electronic scheme for total ozone observation was proposed by Brewer [78]. The instrument has one diffraction grating (1,800 lines per mm) and five slits corresponding to five wavelengths in the 306–320 nm spectral band. The resolution is 0.6 nm as compared to 0.9–3.0 nm of the Dobson instrument. Combination of the data from all five wavelengths provides additional information about the total column content of $SO_2$, a potential interference for the Dobson instruments in $SO_2$ polluted air.

## Vertical Distribution of Ozone

### The Umkehr Method

During an expedition to Spitsbergen in 1929, F.W.P. Götz who operated a Dobson spectrophotometer, discovered, when measuring sky radiation from the zenith, that the intensity ratio of the used UV wavelength pair decreases with increasing solar zenith angle (decreasing solar elevation); a surprising reversal (German: Umkehr) of this decrease when the sun was close to the horizon. At very low solar elevations this ratio passed through a minimum and increased again with solar elevation decreasing further (during sunset). At low solar elevations during sunrise the situation is reversed. Götz concluded this effect resulting from the layered structure of the ozone distribution and that the "Umkehr" curves can be used for analytically deriving the vertical ozone profile. In collaboration with Meetham and Dobson he developed a method for solving the integrals involved in the estimation of the vertical ozone distribution [79]. Of course this method can be applied under suitable meteorological conditions only, as a large fraction of the sky needs to be cloudfree. As the evaluation of ozone profiles from Umkehr curves is a very elaborous method, only few profiles were derived during these early years. It was not before in the 1950s Dütsch and Mateer had developed a standardised routine method that the wealth of 20 years' Umkehr data achieved within the Dobson network could be exploited [80]. The Umkehr method is still in use providing vertical ozone profiles, along with total ozone values, at many stations of the global Dobson network. Although balloon-borne electrochemical sondes (bubblers) are flown at many stations (see next paragraph), the Umkehr measurements are superior, especially above 30 km altitude, because the bubbler solution usually evaporates at this height.

### Balloon Sondes

Two general types of ozonesonde are in use today, the Brewer-Mast bubbler [81] and the electrochemical concentration cell [82]. Both are based on the reaction of ozone with potassium iodide (KI). During the ascent, the ambient ozone/air mixture is pumped through the reaction cell (bubbler), and two electrodes with suitable voltage between them, provide the electrical signal to be transmitted to the ground station. Difficulties associated with these instruments are discussed by Logan [83], who also provides careful intercomparisons of different radiosonde sets and with satellite data. As the bubblers are electrochemical cells, difficulties mainly arise through chemical interference with other chemical substances in polluted air, especially $SO_2$. Logan's paper is an excellent review, on trends and relation to measurements carried out with other techniques, with satellite sensors, too.

### Ozone Measured from Satellite-Born Sensors

The advent of Earth's satellites created an enormous potential for remotely sounding the atmosphere on a global basis. Ozone was one of the first constituents to be investigated through satellites. Its strong and distinct spectral features in the UV, visible and IR regions of the spectrum, together with its abundance and distribution, make ozone a relatively easy species to detect and to carry out quantitative investigations. The advantage of regular global satellite monitoring is that it provides good information on spatial and temporal variations that allows us to address entirely new types of problems. The beginning of the long series of measurements of total ozone from space was made in April 1970, from the NIMBUS-4 satellite by the onboard BUV (Backscatter-Ultraviolet) spectrometer. The instrument was capable of daily measurements covering the entire sunlight portion of the globe, that means all but the Earth's surface area within the 24-h polar darkness. The BUV measurement was forerunner of SBUV (Solar Backscatter Ultraviolet), and due to a few of its inherent limitations the data from BUV were poorer and sparse compared to those from SBUV, the more advanced version. The BUV spectrometer, after working well for about 2 years, encountered problems resulting in fewer daily readings. With these drawbacks it operated until 1977. On 23 October 1978, with two instruments, TOMS (Total Ozone Mapping Spectrometer) and SBUV spectrometer on board, both capable of monitoring total ozone from the entire sunlit globe, the NIMBUS-7 satellite was launched. The SBUV instrument provided measurements of both, total ozone and its vertical profile up to about 50 km altitude, but only in the nadir mode (see Fig. 3.13). By sweeping through a series of slant angles, TOMS provided a much denser pattern of daily measurements of total ozone.

A detailed description of these satellite sensors is given in the WMO Report No. 18 [84]. The TOMS instruments on board of NIMBUS-7, Meteor-3 and Earth Probe (EP) operated, respectively, since October 1978 to May 1993, August 1991 to December 1994 and August 1996 onwards. NIMBUS-7 TOMS total ozone has an absolute error of 3 %, a random error of 2 % and the uncertainty in the drift for 14 years is 1.5 %, somewhat higher at high latitudes. For Meteor-3 TOMS the respective numbers are 3 %, 3 %, 1 % [27, 85].

The SBUV-2 instrument designated for flights on board of the NOAA series of satellites as part of its meteorological satellite program was first launched in December 1984. Its design was based on the NIMBUS-7 instrument, with a major difference that the onboard Hg-lamp on NIMBUS-7 used only for wavelength calibration was used in SBUV-2 for monitoring of the reflectivity of the diffuser plate, too. Other changes made were in the exploitation of the photomultiplier output and in the design of the grating drive. The SBUV instrument on board of NIMBUS-7 and SBUV-2 on board of NOAA-9, NOAA-11 and NOAA-14 covered, respectively, the periods November 1978-May1990 and January 1989-October 1994, and measured both total ozone and its vertical distribution. The data generated are based on measurements of the Earth's albedo at several wavelengths.

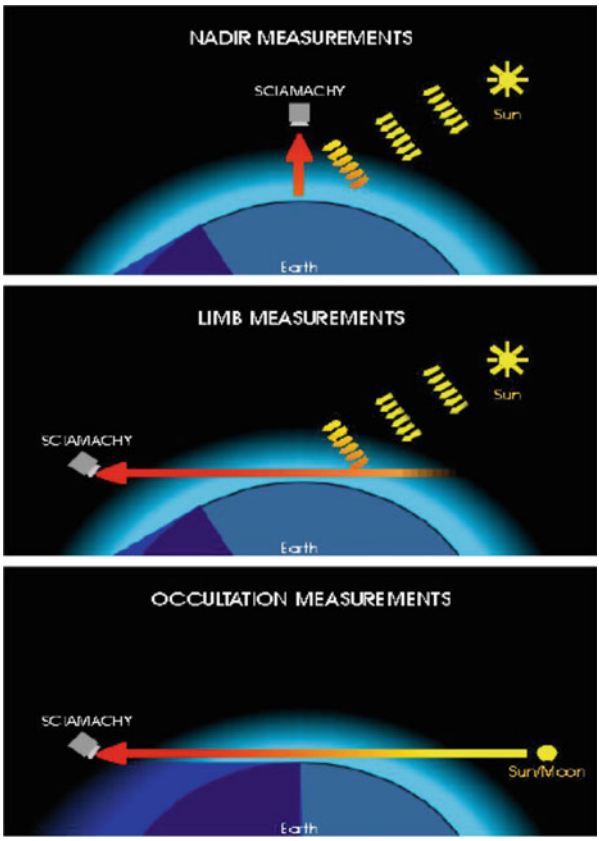


**Fig. 3.13** Configuration of modes used for satellite measurements of ozone and other atmospheric trace gases. *Upper figure*: Nadir mode, *middle figure*: limb measurements allowing profile measurements by using the radiation emitted by the different layers. *Lower mode*: occultation making use of the Sun at low elevation. Figure provided by IUP Breman: See http://www.iup.uni-bremen.de/sciamachy/instrument/modes/index.html

An inversion algorithm then produces ozone profile estimates with relatively poor vertical resolution, more or less similar to the Umkehr profile (about 5 km over 25–45 km). Errors and uncertainties are discussed in [27].

The Television Infrared and Observational Satellite (TIROS)-N Operational Vertical Sounder (TOVS) units on NOAA polar-orbiting satellites can provide estimates of stratospheric ozone. The 9.7 μm High Resolution Infrared Sounder (HIRS) ozone channel is well suited for measuring low-stratospheric ozone. But the measurements in the 9.7 μm channel are insensitive to middle stratospheric and tropospheric ozone changes. TOVS ozone retrievals are sometimes complicated by cloud effects, water vapour absorption and surface emissivity [27].

An excellent overview of satellite ozone measurements and trends is given by Rusch et al. [85, 86].

### Satellite Measurements of Tropospheric Ozone

The measurement of tropospheric ozone from space is not straightforward by using the satellite sensors discussed before. This is mainly due to the fact that the tropospheric ozone column is very small compared to the stratospheric and mesospheric column. When looking from space this is like trying to see a small item behind a mountain. Therefore several tricks have been applied to measure tropospheric ozone from space despite this difficulty.

Jiang and Yung [87] have derived concentrations of tropospheric ozone from TOMS data. They concentrated on tropical South America and use the TOMS signal from the high Andes as upper limit of the troposphere. Thereby they provide tropospheric data as differences of the total and the mountain data representing the high atmosphere only. Thus data and trends are published for the 1979–1992 period.

Another method successfully applied for deriving tropospheric ozone concentrations from TOMS data is the development of a modified residual method [88].

## References

1. Chapman S (1930) A theory of atmospheric ozone. Mem R Met Soc 3:103–125
2. Nicolet M (1974) An overview of aeronomic processes in the stratosphere and mesosphere. Can J Chem 52:1381–1396
3. Dütsch HU (1968) The photochemistry of stratospheric ozone. Q J R Meteorol Soc 94:483–497
4. Wulf OR, Deming LS (1937) The distribution of atmospheric ozone in equilibrium with solar radiation and the rate of maintenance of the distribution. Terr Magn Atmos Elect 42:195–202
5. Brewer AW (1949) Evidence for a world circulation provided by the measurements of helium and water vapour distribution in the stratosphere. Q J R Meteorol Soc 75:351–363
6. Brewer AW, Wilson AW (1968) The regions of formation of atmospheric ozone. Q J R Meteorol Soc 94:249–265
7. Dobson GMB (1956) Origin and distribution of poly-atomic molcules in the atmosphere. Proc Roy Soc London A236:187–193
8. Newell RE (1963) Transfer through the tropopause and within the stratosphere. Q J R Meteorol Soc 89:167–178
9. Fabian P, Libby WF (1974) The stratospheric residence time of odd nitrogen and the effect of the SST, studied in a two-dimensional model derived from high-altitude sampling of radioactive debris. US Department of Transportation, third conference on CIAP, pp 103–116
10. Garcia RR, Hartmann DL (1980) The role of planetary waves in the maintenance of the zonally averaged ozone distribution of the upper stratosphere. J Atmos Sci 37:2248–2264
11. Holton JR (1990) On the global exchange of mass between the stratosphere and troposphere. Mon Weather Rev 47:392–394
12. Holton JR, Hayes PS, McIntyre ME, Douglass AR, Rood RB, Pfister L (1995) Stratosphere-troposphere exchange. Rev Geophys 33:403–439
13. Loyola D, Coldewey RM, Dameris M, Garny H, Stenke A, Van Roozendael M, Lerot C, Balis D, Koukouli M (2009) Global long-term monitoring of the ozone layer – a prerequisite for predictions. Int J Remote Sens 30:4295–4318

14. Bates DR, Nicolet M (1950) The photochemistry of atmospheric water vapour. J Geophys Res 55:301–327
15. Hampson J (1964) Photochemical behaviour of the ozone layer. Can Am Res Develop Estab., Tech. Note 1627/64, Valcartier, QC, 280 p
16. Hesstvedt E (1968) On the effect of vertical eddy transport on atmospheric composition in the mesosphere and lower thermosphere. Geofis Publ 27(4):35–42
17. Crutzen PJ (1970) The influence of nitrogen oxides on the atmospheric ozone content. Q J R Meteorol Soc 96:320–325
18. Johnston HS (1971) Reduction of atmospheric ozone by nitrogen oxide catalysts from supersonic transport exhaust. Science 173:517–522
19. Bates DR, Hays PB (1967) Atmospheric nitric oxide. Planet Space Sci 15:643–676
20. Stolarski RS, Cicerone RJ (1974) Stratospheric chlorine: a possible sink for ozone. Can J Chem 52:1610–1615
21. Molina MJ, Rowland FS (1974) Stratospheric sink for chlorofluoromethanes: chlorine atom catalyzed destruction of ozone. Nature 249:810–814
22. Yung YL, Pinto JP, Watson RT, Sander SP (1980) Atmospheric bromine and ozone perturbations in the lower stratosphere. J Atmos Sci 37:339–353
23. Fabian P, Pyle JA, Wells RJ (1982) Diurnal variations of minor constituents in the stratosphere modeled as a function of latitude and season. J Geophys Res 87:4981–5000
24. Fabian P (1980) Der gegenwärtige Stand des Ozonproblems. Naturwissenschaften 67:109–120
25. Pitari G, Visconti G (1991) Sensitivity of stratospheric ozone to heterogeneous chemistry on sulfate aerosols. Geophys Res Lett 18:833
26. Hofmann DJ, Solomon S (1989) Ozone destruction through heterogeneous chemistry following the eruption of El Chichon. J Geophys Res 94:5029
27. World Meteorological Organization (WMO) (1999) Scientific Assessment of Ozone Depletion: 1998, Global Ozone Research and Monitoring Project, Report No. 44, Geneva
28. Tevini M (1992) Global change research- enhanced UV-B radiation: a risk for plant growth? Global Change Prisma 12, 4–6, Federal Ministry for Reseach and Technology. Bonn, Germany
29. Vogelmann A, Ackerman TP, Turco RP (1992) Enhancement of biologically effective ultraviolet radiation following volcanic eruptions. Nature 359:47–49
30. World Meteorological Organization (WMO) (2006) Global Ozone Research and Monitoring Project- Report Number 50: Scientific Assessment of Ozone Depletion. NOAA, NASA, UNEP, WMO, European Commission
31. Seckmeyer GA, Bais A, Bernhard G, Blumenthaler M, Booth CR, Disterhoft P, Eriksen P, McKenzie RI, Miyauchi M, Roy C (2001) Instruments to measure Solar Ultraviolet Irradiance, Part I: Spectral instruments, Global Atmospheric Watch, Report 125, 30pp. WMO Geneva, Switzerland
32. Kylling A, Webb AR, Bais AF, Blumthaler M, Schmitt R, Thiel S, Kazantzidis A, Kift R, Misslbeck M, Schallhart B, Schreder J, Topaloglou C, Kazadzis S, Rimmer J (2003) Actinic flux determination from measurements of irradiance. J Geophys Res 108(D16):4506. doi:10.1029/2002JD003236
33. Schallhart B, Huber M, Blumthaler M (2004) Semi-empirical method for the conversion of spectral UV global irradiance data into actinic flux. Atmos Environ 38(26):4341–4346
34. Krotkov NA, Herman JR, Fioletov V, Seftor C, Larko D, Vasilikov A, Labow G (2004) Boundary layer absorbing aerosol correction of an expanded UV irradiance database from satellite Total Ozone Mapping Spectrometer. Proc, Quadrnnial Ozone Symposium Kos, Greece
35. WMO (1997) Report of the WMO-WHO Meeting of Experts on Standardization of UV Indices and their Dissemination to the Public. Report 127, WMO/WHO, Les Diablerets, Switzerland

36. Levelt PF, Hilsenrath E, Leppelmeier GW, van der Oord GHJ, Bhartia PK, Tamminen J, de Haan JF, Veefkind JP (2006) Science objectives of the ozone monitoring instruments. IEEE Trans Geosci Remote Sens 44(5):1199–1208
37. Tanskanen A, Krotkov NA, Herman JR, Arola A (2006) Surface ultraviolet irradiance from OMI. IEEE Trans Geosci Remote Sens 44(5):1267–1271
38. Thorne RM (1980) The importance of energetic particle precipitation on the chemical composition of the middle atmosphere. Pure Appl Geophys 118:128–151
39. Crutzen PJ, Solomon S (1980) Response of mesospheric ozone to particle precipitation. Planet Space Sci 28:1147
40. Heath DF, Krueger AJ, Crutzen PJ (1977) Solar proton event and the atmospheric ozone layer. Science 197:886
41. Fabian P, Pyle JE, Wells RJ (1979) The August 1972 solar proton event and the atmospheric ozone layer. Nature 277:458–460
42. Reagan JB, Meyerott RE, Nighingale RW, Gunton RC, Johnson RG, Evans JE, Imhof WL, Heth DF, Krueger AJ (1981) Effects of the August 1972 solar particle event on stratospheric ozone. J Geophys Res 86:1473–1494
43. Jackman CH, Frederick JE, Stolarski RS (1989) Production of odd nitrogen in the stratosphere and mesosphere: an intercomparison of south strengths. J Geophys Res 85:7495–7505
44. Solomon S, Crutzen PJ (1981) Analysis of the August 1972 solar proton event including chlorine chemistry. J Geophys Res 86:1140–1146
45. McPeters RD, Jackman CH, Stassinoupoulos EG (1981) Observations of ozone depletion associated with solar proton events. J Geophys Res 86:12071–12081
46. Gaines EE, Chenette DL, Imhof WL, Jackman CH, Winningham JD (1995) Relative electron fluxes in My 1992 and their effect on the middle atmosphere. J Geophys Res 100:1027–1033
47. Jackman CH, Fleming EL, Vitt FM (2000) Influence of extremely large solar proton events in a changing atmosphere. J Geophys Res 105:11659–11670
48. Palmer AS, van Ommen TD, Curran MAJ, Morgan V (2001) Ice-core evidence for a small solar-source of atmospheric nitrate. Geophys Res Lett 28:1953–1956
49. Angell JK, Korshover J (1973) Quasi-binnal and longterm fluctuations in total ozone. Mon Weather Rev 101:426
50. Paetzold HK, Piscalar F, Zschörner H (1973) Secular variation of the stratospheric ozone layer over middle Europe the solar cycles from 1951 to 1972. Nature Phys Sci 140:106
51. Penner JE, Chang JE (1980) The relation between atmospheric trace species variabilities and solar UV variabilities. J Geophys Res 85:5523–5528
52. Keating GM (1979) Relation between monthly variations of global ozone and solar activity. Nature 274:873–874
53. Chandra S (1984) An assessment of possible ozone-solar cycle relationship inferred from NIMBUS 4 BUV data. J Geophys Res 89:1373–1379
54. Garcia RR, Solomon S, Roble RG, Rusch DW (1984) A numerical response of the middle atmosphere to the 11-year solar cycle. Planet Space Sci 32:411–423
55. Angell JK (1989) On the relation between atmospheric ozone and sunspot number. J Clim 2:1404–1416
56. McCormack JP, Hood LL (1996) Apparent solar cycle variation of upper stratospheric ozone and temperature: Latitude and seasonal dependences. J Geophys Res 101:20933–20944
57. Shindell D, Rind D, Balachandran N, Lean J, Lonergan P (1999) Solar cycle variability ozone, an climate. Science 284:35–308
58. Wuebbles DJ, Wei C-F, Patten KO (1998) Effects on stratospheric ozone and temperature during the Maunder Minimum. Geophys Res Lett 25:523–526
59. Whitten RC, Cuzzi J, Borucki WJ, Wolfe JH (1976) Effect of nearby supernova explosion on atmospheric ozone. Nature 263:398

60. Ruderman MA (1974) Possible consequences of nearby supernova explosions for atmospheric ozone and terrestrial life. Science 184:1079
61. Hunt GE (1978) Possible climatic and biological impact of nearby supernova. Nature 271:430
62. Reid GC, Isaksen ISA, Holzer TE, Crutzen PJ (1976) Influence of ancient solar proton events on the evolution of life. Nature 259:177
63. Thiemens MH, Savarino J, Farquhar J, Bao H (2001) Mss-independent isotopic compositions in terrestral and extraterrestrial solids and their aplications. Acc Chem Res 34(8):645–652
64. Thiemens MH, Heidenreich J III (1983) The mass independent fractionation of oxygen: a novel effect and the possible cosmochemical implications. Science 219:1073–1075
65. Mauersberger K (1981) Measurement of heavy ozone in the stratosphere. Geophys Res Lett 8:935
66. Krankowsky P, Lämmerzahl P, Mauersberger K (2000) Isotopic measurements of stratospheric ozone. Geophys Res Lett 27:2593
67. Mauersberger K, Lämmerzahl P, Krankowsky P (2001) Stratospheric ozone isotope enrichments-revisited. Geophys Res Lett 28:3155
68. Thiemens MH (2002) Mass-independent isotope effects and their use in understanding natural processes. Isr J Chem 42:43–54
69. Yung YL, DeMore WB, Pinto JP (1991) Isotopic exchange between carbon dioxide and ozone via O(1D) in the stratosphere. Geophys Res Lett 18:13–16
70. Fabian P, Rollenbeck R, Spichtinger N, Dominguez G, Brothers L, Thiemens MH (2009) Sahara dust, volcanoes, biomass burning: pathways of nutrients into Andean rainforests. Adv Geosci 22:85–94
71. Volz A, Kley D (1988) Evaluation of the Montsouris series of ozone measurements made in the nineteenth century. Nature 332:240–242
72. Anfossi D, Sandroni S, Viarengo S (1991) Tropospheric ozone in the nineteenth century: the Moncalieri series. J Geophys Res 96:17349–17532
73. Ehmert A, Ehmert H (1941) Über die chemische Bestimmung des Ozongehaltes der Luft, Forschung und Erfahrung Ber. RWD A 13, 1941, reprinted in Ber. Dt. Wetterdienstes US Zone 11, 67-71, Bad Kissingen, 1949
74. Dobson GMB (1931) A photoelectric spectrometer for measuring the amount of atmospheric ozone. Proc Phys Soc Lond 43:324–339
75. Gustin GP (1963) Universal Ozonometer. Proc Main Geophys Obs Leningrad 141:83–98
76. Bojkov RD (1969) Differences in Dobson spectrophotometer and filter ozonometer measurements of total ozone. J Appl Meteorol 8:362–368
77. Gustin GP, Sokolenko SA, Kovalyov VA (1985) Total ozone measuring instruments used at the USSR measuring network in atmospheric ozone. In: Zerefos CS, Ghazi A (eds) Proc Quadrennial Ozone Symposium Halkidiki/Greece, 1984. D.Reidel, NL, pp 543–546
78. Brewer AW (1973) A replacement of Dobson spectrophotometer. Pure Appl Geophys 106–108:919–927
79. Götz FWP, Meetham AR, Dobson GMB (1934) The vertical distribution of ozone in the atmosphere. Proc R Soc Lond A 145:416–446
80. Dütsch HU (1959) Vertical ozone distribution from Umkehr observations. Arch Met Geophys Bioclim A 11:240–251
81. Brewer AW, Milford JR (1960) The Oxford–Kew ozone sonde. Proc R Soc Lond A 256:470–495
82. Komhyr WD (1969) Electrochemical concentration cells for gas analysis. Ann Geophys 25:203–210
83. Logan JA (1994) Trends in the vertical distribution of ozone: an analysis of ozonesonde data. J Geophys Res 99:25553–25585
84. World Meteorological Organization (WMO) (1989) Global Ozone Research and Monitoring Project, Report Nr. 18, Geneva
85. McPeters RD, Hollandsworth SM, Flynn LE, Herman JR, Senor CJ (1996) Long-Term ozone trends derived from the 16 years combined NIMBUS-7/Meteor-3 TOMS version 7 record. Geophys Res Lett 23:3699–3702

86. Rusch DW, Clancy RT, Bhartia PK (1994) Comparison of satellite measurements of ozone and ozone trends. J Geophys Res 99:20501–20511
87. Jiang Y, Yung YL (1996) Concentrations of Tropospheric Ozone from 1979 to 1992 over Tropical Pacific South America from TOMS Data. Science 272:714–716
88. Hudson RD, Thompson AM (1998) Tropical tropospheric ozone from total ozone mapping spectrometer by a modified residual method. J Geophys Res 103:22129–22145

# Chapter 4
# Ozone in the Troposphere

## 4.1 The Natural Troposphere: Early Ozone Measurements

The troposphere is the lowest atmospheric layer whose upper boundary, the tropopause, extends from about 18 km altitude in the tropics to 8 km in the polar region. Thus, it comprises about 90 % of the total mass of the Earth's atmosphere. It contains the air we breathe and the water we drink. Biogenic source gases produced in soils and in the ocean are released into the troposphere, where they are carried along and mixed by winds and turbulences related to the weather systems. It is the troposphere, too, which we use as a waste dump for all kinds of waste gases of human civilisation, from industry, power plants, heating, transportation and other sources.

The natural atmosphere consists of nitrogen, oxygen and argon, whose fractions by volume are 78.09 %, 20.95 % and 0.93 %, respectively. The remaining 0.03 % are made up of traces of noble gases (neon, helium, krypton) and trace gases such as $CO_2$ (pre-industrial fraction by volume: 270 ppm = 0.027 %), $CH_4$, $H_2$, $N_2O$ and $CH_3Cl$ (in the order of their abundances). Different from these, atmospheric water vapour ($H_2O$) is not homogeneously distributed but highly variable in time and space. Depending on evaporation, transport and rainout processes, tropospheric $H_2O$ abundances can vary between almost zero and 4 %.

None of these constituents can be photolysed at tropospheric levels, since solar UV radiation of wavelengths shorter than 390 nm is completely absorbed by $O_2$ and $O_3$ in the middle atmosphere. Thus, photochemical ozone production in the troposphere, similar to that in the middle atmosphere, is very unlikely.

Nevertheless, ozone has been measured in the troposphere, long time before it became polluted. Its fraction by volume was small, between about 10 and 20 ppb, whereas today 50 to more than 100 ppb are common.

The early Montsouris series (1876–1910) using iodine catalysed oxidation of arsenite shows near surface ozone annual means varying between 5 and 15 ppt [1, 2]. A 26 years (1868–1893) data series of daily ozone readings performed at Moncalieri, northern Italy, using the Schönbein test paper, shows average monthly

P. Fabian and M. Dameris, *Ozone in the Atmosphere*,
DOI 10.1007/978-3-642-54099-8_4, © Springer-Verlag Berlin Heidelberg 2014

averages around 10 ppb [1]. Records of surface ozone data collected twice a day using Schönbein papers at Montevideo, Uruguay (1883–1885) and Cordoba, Argentina (1886–1892) showed average monthly ozone mixing ratios between about 8 and 15 ppb [2].

A review by Junge [3] shows that even during the 1950s, annual means of tropospheric ozone mixing ratios were still low in many parts of the world hardly exceeding 15–25 ppb. Several stations, however, showed episodically higher values, of up to 50 ppb. Similar findings are reported for Val Joyeux close to Paris and Dumont D'Urville (Terre Adélie, Antarctica) [4]. It appears that the 1950s mark a gradual transition to higher tropospheric ozone levels, at least for central Europe and North America. Warmbt [5] reports on data of the surface ozone network of the former German Democratic Republic, with monthly means ranging between about 10 and 30 ppb. In the early 1960s Hering and Borden [6] presented results obtained within the US Airforce ozone radiosonde network, with near surface mixing ratios ranging between 10 and 55 ppb, while those measured in remote Antarctica were still ranging between 10 and 30 ppb [7].

It is generally accepted that these low tropospheric ozone levels are due to dynamics by which stratospheric ozone is mixed to the troposphere. Stratospheric–tropospheric exchange was conceived in the early Brewer–Dobson scheme already (see Sect. 3.1.2), by which stratospheric ozone is transported on sloped surfaces, polewards and downwards, with downward transport through the lower stratosphere and transfer into the troposphere, where ozone is finally destroyed, mainly near the ground. Today stratospheric–tropospheric exchange is seen in the context of the general circulation, as will be outlined in the next chapter.

## 4.2 Stratospheric–Tropospheric Exchange

The troposphere is the lowest region of the atmosphere which is characterised by sharply decreasing temperatures with increasing altitude, at a rate of roughly 6 K $km^{-1}$ on average. Since the cloudless atmosphere is almost transparent to solar radiation, it is essentially heated from the surface, with dynamically induced vertical mixing shaping the vertical temperature structure. The tropopause may be viewed as a transition region in which temperatures reach a minimum, before they begin to rise in the next layer, the stratosphere. According to the World Meteorological Organization (WMO), the tropopause is defined as "the lowest level at which the temperature lapse rate decreases to 2 K $km^{-1}$ or less, and the lapse rate averaged between this level and any level within the next 2 km does not exceed 2 K $km^{-1}$".

The stratosphere extends from the tropopause to about 50 km, where heating by the absorption of solar UV radiation leads to increasing temperatures with increasing altitudes. It should be noted that, due to the decrease of air density with altitude, the temperature maximum at 50 km does not coincide with the maximum of ozone

partial pressure (see Fig. 2.5). Above this temperature maximum called stratopause, temperatures decrease with altitude in the mesosphere.

With respect to their chemical composition and static stability, the troposphere and stratosphere are fundamentally different, and thus air mass exchange between these two regions is of great interest. They are separated by the tropopause which in the tropics largely coincides with the 380 K potential temperature surface, at a height of 15–18 km. (The potential temperature is derived from the first law of thermodynamics as $\Theta = T(P_0/P)^{\kappa}$, with $T$, $P$ and $P_0$ denoting temperature, pressure and reference surface pressure, respectively, and $\kappa = R/mc_p$ with the universal gas constant $R$, and $m$ and $c_p$ denoting the molecular weight and specific heat at constant pressure of dry air, respectively.) It slopes downwards towards the poles where it may be as low as 6–8 km, at a potential temperature of 290–320 K [8].

In the atmosphere $\Theta$ generally increases with altitude, more so in the stratosphere. Thus, the static stability $(-\delta\Theta/\delta P)$, a measure of the resistance of air to vertical displacement, is much larger in the stratosphere than in the troposphere. Under adiabatic conditions (with no addition or subtraction of energy), air parcels conserve entropy and move along isentropes just undergoing expansion or compression. Moving air across isentropic surfaces requires energy that is constrained by the magnitude of net diabatic processes, ultimately of dynamical origin. In particular, long-term transport between troposphere and stratosphere is achieved by the interplay of waves and eddies and thus placed in the framework of the general circulation.

As Holton et al. [9] pointed out, the main drivers are waves and eddies in the extratropical stratosphere. There, wave-induced forces drive a kind of global-scale "fluid-dynamical suction pump", which withdraws air upward and poleward from the tropical lower stratosphere and pushes it poleward and downward into the extratropical troposphere. The resulting global-scale circulation drives the stratosphere away from equilibrium conditions. As the strongest wave-induced forces occur in the Northern Hemisphere winter season, the exchange rate is also a maximum during that season.

The extratropical "suction pump" which drives the large-scale ascent in the tropical stratosphere seems to influence upwelling of air in the tropical troposphere as well. Moist convection plays an important role, and few cumulonimbus clouds even penetrate the tropopause. On passing the cold tropical tropopause, the air is freeze-dried and retains the saturation water vapour mixing ratio corresponding to these low temperatures. The fact that the whole stratosphere (the extratropical one as well) is extremely dry testifies that most air enters the stratosphere via tropical upwelling [10, 11].

A further piece of evidence is that the signal of the water vapour mixing ratio at the tropopause level is maintained by the air parcel as it rises through the stratosphere for up to 18 months. That way, seasonal variations of the water vapour mixing ratios induced by seasonal variations of tropopause temperatures are recorded as a layering of water vapour mixing ratios (the "tape recorder mechanism"). The layered structures move upwards in the tropical stratosphere and are still observable at the 20 hPa level [12].

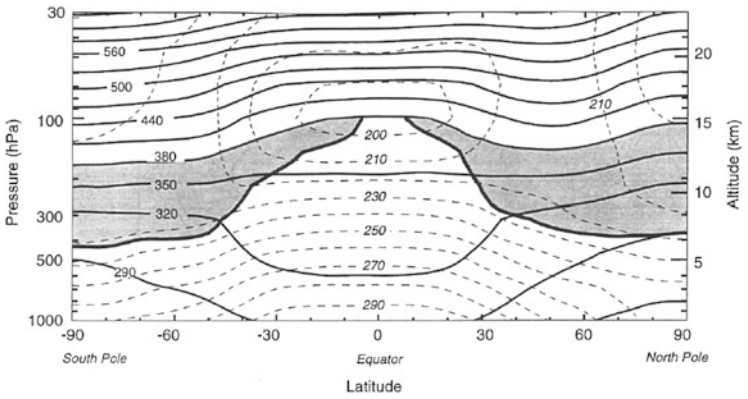


**Fig. 4.1** Dynamical aspects of stratosphere–troposphere exchange. The tropopause is shown by the *thick line*; *thin lines* are isentropic surfaces labelled in Kelvin (K). The *heavily shaded region* is the "lowermost stratosphere" where isentropic surfaces intersect the tropopause. The region above the 380 K surface is the "overworld", in which the isentropes lie entirely within the stratosphere [8, 9]

The dynamical aspects of stratospheric–tropospheric exchange as outlined by Holton et al. [8, 9] are illustrated in Fig. 4.1. The tropopause is shown by the thick line; isentropic surfaces shown by thin lines are labelled in Kelvins. The heavily shaded region is the "lowermost stratosphere" where isentropic surfaces intersect the tropopause. The region above the 380 K surface is called the "overworld" in which isentropes lie entirely within the stratosphere. The region of wave-induced forcing, the driver of the extratropical "pump", is marked by light shading. At midlatitudes, exchange through the tropopause marked by the wavy arrows can occur in both directions, induced by cut-off cyclones and tropopause folds. Here, however, tropospheric air can enter the lowermost stratosphere only, where backward transport to the troposphere may occur as well.

Efficient transport of tropospheric air to the stratospheric overworld is largely achieved by upwelling and large-scale ascent in the tropics. This is the way that natural source gases as well as manmade pollutants are carried to the stratosphere, as confirmed by various measurements. $CO_2$, for instance, is a natural gas whose atmospheric mixing ratio would be constant up to the mesopause if there would be no anthropogenic emissions leading to a tropospheric excess $CO_2$ growing by about 1.5 ppm/year. Stratospheric $CO_2$ measurements up to 35 km showed midlatitude $CO_2$ mixing ratios between 20 km and 35 km being constant with altitude, growing by 1.5 ppm/year, but about 7 ppm smaller than respective tropospheric values. This implies about 4–5 years for excess $CO_2$ to arrive in the midlatitude stratosphere via tropical upwelling and wave-induced stratospheric mixing [13].

Similar findings based on measurements of $CO_2$ and other long-lived trace gases, such as $SF_6$, HF, HCl and $CF_4$, are presented in a review article by Waugh and Hall [14], based on the concept of the "age of stratospheric air", the transit time since stratospheric air last made tropospheric contact [15]. Observational estimates of mean

ages in the 25–30 km range vary between 3.5 years and 6 years, for tropical to mid/high latitude measuring sites, respectively. It appears that the time for entering the tropical stratosphere is relatively short, not much more than 1 year (Ref. [16] of Chap. 3), and that meridional spreading to extratropical latitudes is inhibited by a barrier. By analysing $N_2O$ and $H_2O$ measurements taken from the Upper Atmosphere Research Satellite (UARS), Randel et al. confirm that indeed such a barrier exists [16].

While troposphere–stratosphere transport, which is largely achieved in the tropics, is most important for trace gases of tropospheric origin, the reverse stratosphere–troposphere transport affecting constituents which are produced in or introduced into the stratosphere, mainly occurs at middle and high latitudes, where large-scale subsidence and exchange from the lowermost stratosphere to the troposphere take place (see Fig. 4.1).

This process proceeds faster than the upward transport of tropospheric air to the overworld. From fallout data of bomb-produced Strontium 90, an overall stratospheric "residence time" of 1.6 years was derived [17] which is less than half the time constants shown for the reverse process. Stratospheric residence times as function of latitude and altitude computed by means of a model, whose transport parameters had been tuned with stratospheric 2D data of bomb-produced Zirconium 95, are shown in Fig. 4.2 [18].

This is associated with synoptic-scale processes such as those occurring at tropopause folds in the vicinity of the polar jetstream first studied by Danielsen [19]. Later work revealed that synoptic-scale processes at the subtropical jet, in mesoscale convective complexes and thunderstorms, and due to breaking gravity waves, contribute to the intrusion of stratospheric air into the troposphere as well (see the review by Stohl et al. [11] and the references given therein).

Typically, the intruding stratospheric air forms filamentary structures which have been observed as laminae of ozone profiles [20], as filamentary features on water vapour satellite images [21], and they are even evident by ozone lidar measurements demonstrating that they can subside deep into the troposphere [22].

Midlatitude transport of tropospheric air to the lowermost stratosphere has been observed as well. Stohl [23] emphasised the role of warm conveyor belts, airstreams ahead of cold fronts associated with extratropical cyclones, for rapid transfer of tropospheric air into the lower stratosphere. However, against the large-scale descent from the overworld and in view of the high stratospheric stability, this influx of tropospheric air does not reach the overworld (see [11] and the references given therein).

Intrusions of stratospheric air into the troposphere are rich in ozone [19] and, because of the long chemical life time of $O_3$ in the free troposphere, which is of the order of months [24], contribute to the tropospheric $O_3$ budget. The quantitative contribution has been a subject of debate for long, but it is evident that during pre-industrial times, when no tropospheric ozone sources existed, at least most of the ozone observed in the troposphere must have been intruded from the stratosphere. The transition from the pre-industrial pristine atmosphere to an atmosphere polluted by human activities has occurred gradually, with large regional differences. It is thus impossible to determine when the impact of pollution on the

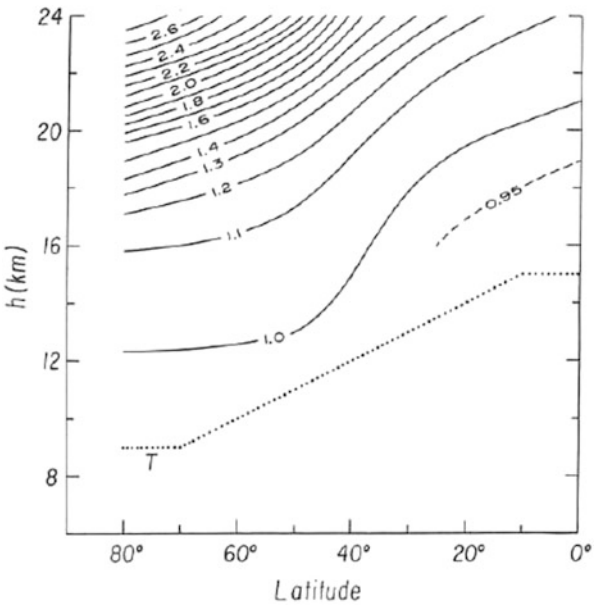


**Fig. 4.2** Stratospheric residence time (e-fold) as function of latitude and altitude. Units: years, T shows the tropopause [18]

tropospheric ozone budget began. It is very likely, though, that the early ozone measurements reported in the previous chapter mostly reflect pre-industrial conditions. This would imply that an average tropospheric ozone level of 10 to not more than 20 ppb is maintained by stratosphere–troposphere exchange. The photochemistry related to these pristine conditions is discussed in the following chapter.

## 4.3 Photochemistry in the Troposphere

### *4.3.1 Oxidation Capacity*

The shortwave solar radiation is entirely absorbed in the middle atmosphere by oxygen and ozone. Thus, the troposphere receives radiation of wavelengths $\lambda > 290$ nm only which cannot photolise the main constituents making up the unpolluted atmosphere. As these substances do not react with each other there would hardly be, without a suitable primer, tropospheric chemistry at all. Indeed, it is ozone which acts as such a primer.

Thus, ozone found in the unpolluted troposphere has its main origin in the stratosphere from where it is carried downward by synoptic-scale processes as discussed in the previous chapter. Like in the stratosphere, it is photolised throughout the wavelength range $\lambda < 1{,}200$ nm [Eq. (3.3), Sect. 3.1.1]. At wavelengths $\lambda < 310$ nm, however, this photolysis leads to the production of excited ($^1$D)-O

atoms [Eq. (3.10), Sect. 3.1.3]. These can react with $H_2O$ which is highly abundant in the troposphere forming hydroxyl radicals

$$H_2O + (^1D)\text{-}O \rightarrow 2OH \tag{3.10}$$

OH is the dominating oxidiser in the troposphere. It reacts with the natural source gases $CH_4$, $H_2$ and $CH_3Cl$ (see next chapter). It initiates the oxidation chains of pollutants such as $SO_2$ and $NO_2$ leading to $H_2SO_4$ and $HNO_3$, respectively, which are soluble in water and thus are washed out in rain and fog droplets. In the absence of OH, with dry deposition being the only removal process, pollutants would generally accumulate to higher levels. OH, due to its conversion of pollutants to water soluble species which are readily washed out (see Fig. 4.3), is therefore called "detergent" of the atmosphere.

OH determining the atmospheric "oxidation capacity" is a short-lived radical which exists under daylight conditions only. Its diurnal variation follows the solar elevation as shown in Fig. 3.2 for the stratosphere (see [25]). At ground level, maximum noon concentrations of OH vary between $9 \times 10^5$ $cm^{-3}$ and $12 \times 10^5$ $cm^{-3}$, the highest OH concentrations being observed in the humid tropics [26].

### 4.3.2 Methane Oxidation

One of the most important processes is the oxidation chain of $CH_4$ which is initiated by its reaction with OH

$$CH_4 + OH \rightarrow CH_3 + H_2O \tag{4.1}$$

followed by

$$CH_3 + O_2 + M \rightarrow CH_3O_2 + M \tag{4.2}$$

(with M being third body, see Sect. 3.1.1).

The following reaction chain (see [25]) eventually leads to the formation of formaldehyde HCHO, from which the formyl radical HCO is produced via

$$HCHO + OH \rightarrow HCO + H_2O$$

and

$$HCHO + h\nu \rightarrow HCO + H$$

which finally leads to the formation of the source gas CO.

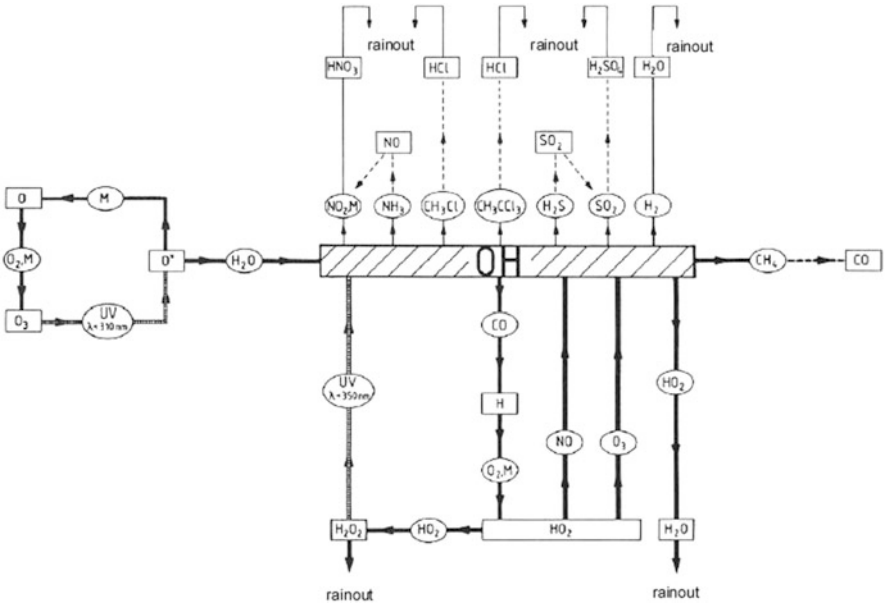


**Fig. 4.3** The photochemistry of the OH radical largely controls the tropospheric trace gas composition. OH formation (*left part*) from excited $^1$D-O atoms produced by ozone photolysis is the primer of subsequent chemical reactions. Reactions controlling the concentration of OH are shown in the *lower part*. The *upper part* shows oxidation reactions of OH with major source gases forming water soluble sink gases which are washed out with cloud and rain droplets

Another photolysis reaction of formaldehyde leads to the formation of the source gases $H_2$ and CO via

$$\mathrm{HCHO} + h\nu \rightarrow \mathrm{H_2} + \mathrm{CO}$$

About 95 % of HCHO (and consequently of $CH_4$) eventually end up as CO; only a smaller fraction produces $H_2$ [26].

As CO is oxidised to $CO_2$ by OH via

$$\mathrm{CO} + \mathrm{OH} \rightarrow \mathrm{CO_2} + \mathrm{H} \tag{4.3}$$

all carbon contained in $CH_4$ eventually ends up in $CO_2$.

H formed in (4.3) is converted to $HO_2$ via

$$\mathrm{H} + \mathrm{O_2} + \mathrm{M} \rightarrow \mathrm{HO_2} + \mathrm{M} \tag{4.4}$$

Loss reactions of the $HO_2$ radical include

$$HO_2 + OH \rightarrow H_2O + O_2$$

producing water and

$$HO_2 + HO_2 \rightarrow H_2O_2 + O_2$$

leading to the formation of hydrogen peroxide which, being soluble in water, acts as a strong oxidiser in cloud droplets.

The methane oxidation chain thus leads to the formation of the source gases CO, $H_2$ (see next chapter), $H_2O$ and $HO_x$ radicals which are highly important for photochemistry, both in the troposphere and stratosphere.

For the tropospheric ozone budget reactions (4.3) and (4.4) are of fundamental importance. Depending on the abundances of $NO_x$ and $O_3$, they either lead to a production or a destruction of ozone. In the unpolluted troposphere $NO_x$ levels are very low, and for NO mixing ratios below about 10 ppt ($10^{-12}$) the oxidation of CO to $CO_2$ is a loss reaction for ozone according to the left branch of

$$CO + OH \rightarrow CO_2 + H \tag{4.5}$$

$$H + O_2 + M \rightarrow HO_2 + M \tag{4.6}$$

$HO_2 + O_3 \rightarrow OH + 2\,O_2$

$HO_2 + NO \rightarrow OH + NO_2$

$NO_2 + h\nu \rightarrow NO + O$

$O + O_2 + M \rightarrow O_3 + M$

---

---

**Σ** $\mathbf{CO + O_3 \rightarrow CO_2 + O_2}$

**Σ** $\mathbf{CO + 2\,O_2 \rightarrow CO_2 + O_3}$

For low $NO_x$ each oxidation step of CO to $CO_2$ consumes one $O_3$ molecule (left branch), which might have reflected the conditions of the unpolluted atmosphere. For NO mixing ratios above that threshold, the right branch reactions dominate leading to the production of ozone. Herein $HO_2 + NO \rightarrow OH + NO_2$ is the key reaction which proceeds so fast that it dominates the loss reactions of $HO_2$ [27, 28]. The product $NO_2$ is a direct precursor of O and thus $O_3$, as it photolyses at wavelengths up to about 420 nm which are abundant throughout the entire daylight troposphere.

If we assume that the natural atmosphere was low in $NO_x$, generally below the threshold of 10 ppb, the methane oxidation chain would have been a major ozone sink, along with ozone decomposition at the surface.

In fact this has been a subject of debate: Before the methane oxidation had been identified as a mechanism for in-situ production of ozone in the troposphere [29, 30] it was generally accepted that the stratosphere is the only source , from where ozone is mixed to the troposphere and finally decomposed at the Earth's surface [31, 32]. It was assumed that the low ozone levels measured during these early years (see Sect. 4.1) reflected this concept, and indeed, the annual variations of tropospheric ozone generally showed a maximum during spring concurrent with stratosphere–troposphere exchange being strongest.

Natural $NO_x$ sources were identified in processes such as lightning, the oxidation of biogenic $NH_3$ by OH (see Fig. 4.3) and the direct outgassing of NO and $NO_2$ from soils and ocean surfaces. Some $NO_x$ from stratospheric $N_2O$ breakdown may be mixed to the troposphere. Altogether, these natural sources make up less than 30 % of all $NO_x$ produced in the present atmosphere, most of which by energy use and biomass burning [33]. As no $NO_x$ measurements are documented from the early years, when air pollution was negligible, the exact transition cannot be identified. Nevertheless, tropospheric ozone levels clearly began to rise, since the 1950s, at different rates in different parts of the world. This clearly reflects the growing influence of $NO_x$ and other pollutants from human activities shifting the effect of the methane oxidation chain to the right branch of ozone production.

Figure 4.4 shows an example of the present global ozone distribution in the troposphere, monthly mean fields of $O_3$ at 850 hPa (about 1 km altitude), for June 2003, from reanalysis of ground based and satellite data. Low ozone values between 20 and 40 ppb prevail in the Southern Hemisphere, while up to 80 ppb are documented for tropical and Northern midlatitudes. These high levels certainly reflect massive photochemical ozone production in the troposphere, but even the low ozone levels of the Southern Hemisphere are higher than those to be expected in a pristine troposphere. $NO_x$, CO and a variety of hydrocarbons are precursors leading to photochemical ozone production, as will be discussed in Sect 4.4.

## 4.4 Natural Source Gases

### *4.4.1 Biogenic Sources*

The large fraction of oxygen, almost 21 % of the air we breathe, has accumulated over more than two billion years as a result of photosynthesis of organisms living in the oceans and on land. Ozone formed from atmospheric oxygen thus is a product of biological activity, too.

Besides oxygen, the metabolism of organisms liberates huge amounts of other gaseous substances such as the source gases $CH_4$, $N_2O$ and $CH_3Cl$.

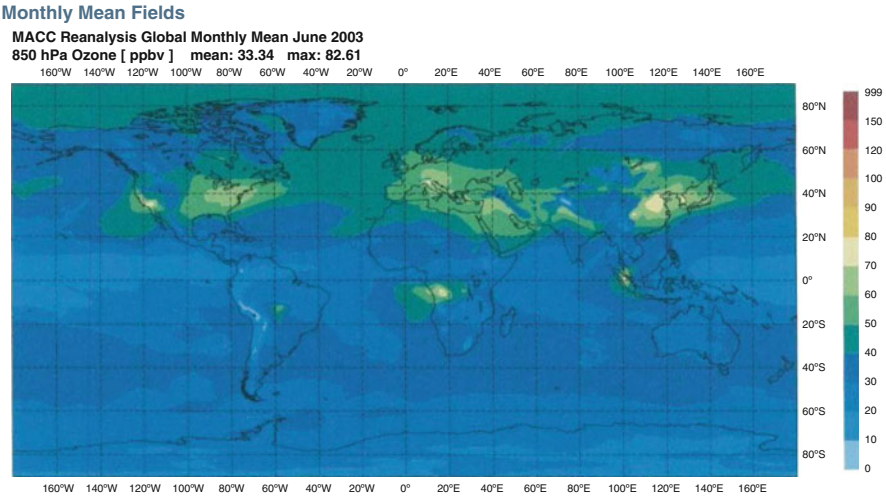


**Fig. 4.4** Global ozone distribution at 850 hPa in ppbv: monthly mean for June 2003 based on satellite data and reanalysis [34]

The six elements carbon (C), hydrogen (H), oxygen (O), nitrogen (N), phosphorus (P) and sulphur (S) are the main constituents of all living organisms making up about 95 % of the biosphere. Organic tissue largely consists of carbohydrates and water. N is contained in proteins, with a typical C/N ratio of about 50 for most organisms. P is needed for adenosine triphosphate (ATP) molecules regulating the energy transfer of photosynthesis, while S, along with the trace elements calcium (Ca), magnesium (Mg) and sodium (K), is an indispensible nutrient.

For the elements C and N the atmosphere is the main source, while P, Ca, Mg and K enter the soils by rock weathering. Water, precondition for all life, is provided by the global water cycle.

While organisms are growing they pick up nutrients and release waste products. After death, organisms decay releasing elements back to the environment. Thus, the biosphere closely interacts with the atmosphere, the ocean and the Earth's crust. The distribution of species in the system is regulated by fluxes between the subsystems determining the essential pathways in global biogeochemical cycles.

The most important of these biogeochemical cycles, the carbon cycle and the nitrogen cycle, are closely related to the emission of hydrocarbons and nitrogen compounds which play an important role in the photochemistry of ozone. They are thus briefly discussed here.

### 4.4.2 The Global Carbon Cycle

The Earth's atmosphere evolved, like the atmospheres of our neighbouring planets Mars and Venus, from outgassing of the liquid planet body. Like for volcanic exhalations observed today, water vapour, carbon dioxide and sulphur compounds have been the bulk substances in this process. Different from our neighbouring planets, however, Earth orbits the Sun just at the "right" distance, where the radiative equilibrium of solar energy gain and thermal energy loss yields surface temperatures for liquid water to exist. Thus, most of the outgassed water has accumulated in the oceans thus providing an ideal solvent for carbon dioxide, which, over geologic times, was chemically converted to calcium- and magnesium carbonate and deposited in the ocean floor sediments.

Venus orbits closer to the Sun and thus has experienced higher temperatures at which an ocean never could have formed. Thus, the bulk of the outgassed carbon dioxide makes up a 90 bar $CO_2$ atmosphere leading to a tremendous greenhouse effect and deadly 735 K surface temperatures. Mars, orbiting the Sun at a larger distance, has been colder from the beginning, and with about 220 K surface temperature is so cold that water is likely to be in the ice phase.

Life on Earth began to evolve in the oceans, with photosynthesis of blue-green algae as early as about four billion years ago. The early oxygen thereby produced was mostly bound up in the oxidation of iron and sulphur compounds dissolved in the oceans. Free oxygen could begin to escape to the atmosphere about two billion years ago, as documented by the ages of continental red sandstone formations (red beds). When atmospheric oxygen had accumulated to about 10 % of the present atmospheric level (0.1 PAL), with a corresponding ozone layer having formed shielding against the lethal UV radiation of the Sun, life is likely to have begun conquering the continents. The accumulation of oxygen and the evolution to higher forms of living organisms seem to be related. While the metabolism energy of primitive early organisms living under anaerobic conditions was provided by fermentation, oxygen breathing in an aerobic environment, about 14 times more efficient than fermentation, was the likely progress leading to the rapid evolution of higher forms of life, about 1.5–0.6 billion years ago. The present atmospheric level of about 21 % was probably reached during the carboniferous period, about 350 million years ago [35].

Dead organisms generally decompose, their constituents being recycled to the environment. Under aerobic conditions they are eventually oxidised with an equivalent amount of oxygen consumed. That way organic carbon is recycled back to the environment as $CO_2$. Under anaerobic conditions, fermentation may occur converting organic carbon to $CH_4$. Protected from oxygen, organic matter may accumulate and survive for long. That way huge amounts of organic carbon sediments were formed.

The sediments of the Earth's crust contain the enormous amount of $10^{22}$ g ($10 \times 10^6$ Gigatons, 1 Gt = $10^9$ t) organic carbon from dead organic substance. This is about 20,000 times more than the amount of carbon stored in all organisms

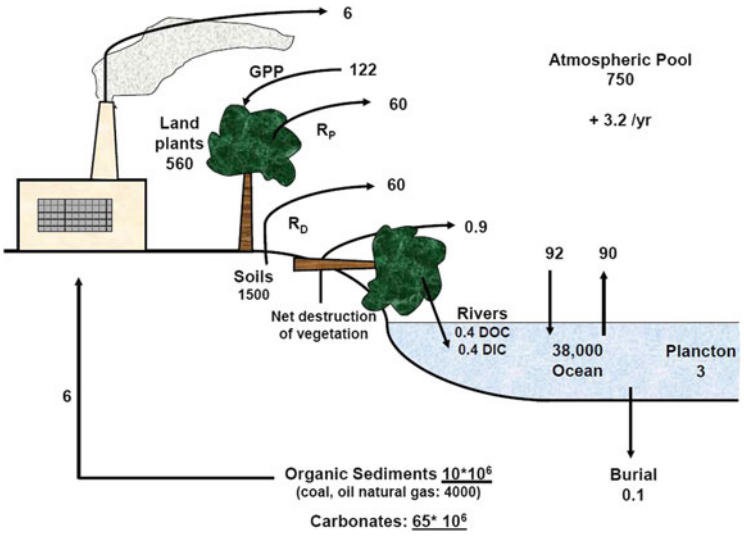


**Fig. 4.5** The present-day global carbon cycle. All pools are expressed in units of $10^{15}$ g C (Gigatons C), all annual fluxes in units $10^{15}$ g C/year, averaged over the 1980s, after [37]

living today. By far the largest amount of it is widely spread, just a small fraction of 1 % forms mineable coal, oil and gas deposits [36]. Would we attempt to burn all mineable coal, oil and gas within shortest time, the equivalent oxygen amount of $2.7 \times 10^{19}$ g would be used, just 2 % of all atmospheric oxygen. Thus, for the atmospheric oxygen budget the burning of fossil fuels has a negligible effect. $CO_2$, however, the product of this fossil fuel burning, causes the atmospheric greenhouse effect to rise, with severe consequences for climate on Earth.

Today, outgassing, for instance from volcanoes, still releases carbon dioxide and other compounds to the atmosphere. In the modern carbon cycle, however, where large short-term fluxes between the carbon pools and anthropogenic emissions dominate, it is generally disregarded (see Fig. 4.5).

The Earth contains about $10^{23}$ g ($100 \times 10^6$ Gt, 1 Gt $= 10^9$ t) carbon, most of which is buried in sedimentary rocks as carbonate ($65 \times 10^6$ Gt) and organic carbon ($10 \times 10^6$ Gt). The total active carbon pool near the Earth's surface, however, amounts to about 40,000 Gt only, most of which is dissolved in the oceans (dissolved inorganic carbon, DIC, see Fig. 4.5), with an enormous buffering capacity towards atmospheric $CO_2$ variations. The atmosphere contains 750 Gt C stored in $CO_2$. The living biomass on land, 90 % of which is made up by forests, contains 560 Gt, while 1,500 Gt of carbon are stored in soils.

The largest annual fluxes of C, about 90 and 120 Gt C/year, are exchanged between the atmosphere and ocean, and between the atmosphere and the terrestrial ecosystems, respectively. Plants annually take up about 120 Gt of carbon from the atmosphere for photosynthesis and release 60 Gt via respiration. With 60 Gt, from the decay or organic matter in the soil, being returned to the atmospheric carbon

pool, this cycle is closed. The net uptake of 60 Gt/year implies that, on average every 12.5 years, all $CO_2$ molecules contained in the atmosphere cycle through the biosphere.

The fact that plants take up additional 2 Gt/year for photosynthesis shows that this cycle is not balanced at present. As Fig. 4.5 demonstrates, about 7 Gt of carbon are released from anthropogenic sources, about 6 Gt by burning fossil fuel and 1 Gt from biomass burning. This anthropogenic C input is still rising and amounts to about 9 Gt C/year at present. It appears that present growth rates of forests are accelerated thus buffering 2 Gt of the anthropogenic carbon input [37–39].

Another 2 Gt of carbon are buffered by the ocean whose annual exchange with the atmospheric carbon pool amounts to about 90 Gt, about 1/3 by photosynthesis of plankton and 2/3 by inorganic solution of $CO_2$ in seawater [37]. Thus, on average every 8 years all atmospheric $CO_2$ cycles through the ocean. Nevertheless, despite this rapid exchange, the atmospheric life time of $CO_2$ is about 100 years. In fact, the rapid exchange involves surface water $CO_2$ only. The removal of a disturbance such as the anthropogenic input of $CO_2$ requires that excess carbon is carried to the deep ocean, for which a mixing time of the order of 350 years has to be considered. Thus, the $CO_2$ uptake capacity of the ocean critically depends on the mixing of the surface water with the deep ocean. A perfectly stirred ocean could accommodate about 6 Gt carbon per year and thus eliminate the anthropogenic input [40].

After all, of the 7 Gt annually added to the atmospheric carbon pool by human activities, 2 Gt are eliminated by the ocean. Another 2 Gt are buffered by the biosphere, mostly by accelerated growth of trees. Thus, the net increase of the atmospheric carbon pool just amounts to "mere" 3 Gt per year. Nevertheless, this atmospheric $CO_2$ increase causes a continuously growing greenhouse effect and severe climate changes on a global scale. Since the beginning of the industrialisation, the atmospheric carbon pool has increased from 590 Gt (285 ppm $CO_2$) to more than 800 Gt (390 ppm $CO_2$) at present. $CO_2$ is still rising: on 10 May 2013 the Mauna Loa record reached 400 ppm.

Carbon sedimentation is of the order of 0.2 Gt/year. If we assume that the slow carbon exchange with the Earth's crust is balanced, an equal carbon amount has to be returned to the atmosphere by sediment weathering and volcanism. In fact, volcanic emissions of 0.02–0.05 Gt carbon per year [37] make this flux plausible. This would imply that the turnover time of the sediments amounts to $75 \times 10^6/0.02$ years $= 375 \times 10^6$ years.

Compared to this slow geologic cycle, the anthropogenic burning of fossil fuels proceeds much too fast. Over the past $300 \times 10^6$ years, the burial of organic carbon occurred at an average rate of about 0.05 Gt carbon/year [41]. Thus, the burning of 6 Gt carbon /year by man proceeds 120 times faster than the rate at which the excess carbon can return to the sediments.

The exchange of $CO_2$ between the atmospheric pool and the biosphere can directly be seen in Fig. 4.6 showing the course of $CO_2$ mixing ratios measured in the free troposphere at Mauna Loa, Hawaii, from the fairly regular annual variation with a maximum in winter and a minimum in summer. In spring, with the beginning of the vegetation period, $CO_2$ from the atmosphere is taken up by plant

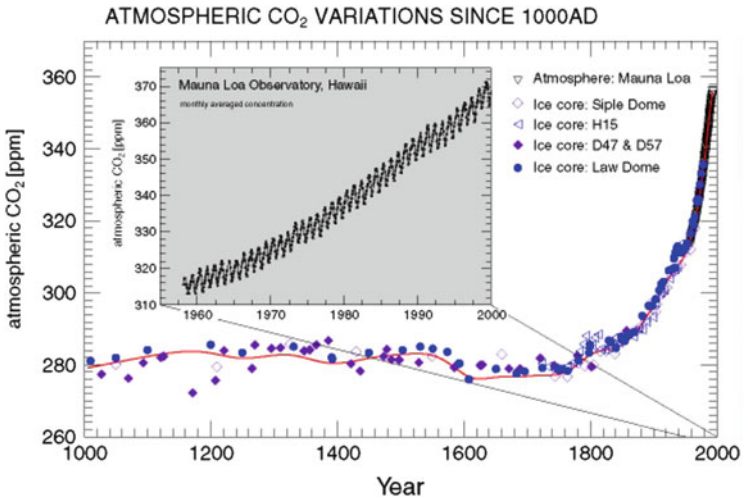


**Fig. 4.6** Atmospheric carbon dioxide at Mauna Loa Observatory (19°N) 1958–2010, after [41]

photosynthesis. During autumn and winter, when plant growth decreases and biomass decays, $CO_2$ is returned to the atmosphere. For Mauna Loa (19°N) the amplitude of this annual oscillation is about 6 ppm corresponding to 13 Gt carbon. This value differs from the global value of 60 Gt shown in Fig. 4.5, since photosynthesis and respiration do not proceed synchronously everywhere. A quantification requires the detailed modelling of the biosphere [42]. The overall increase of atmospheric $CO_2$ as a result of human activities can also be seen in Fig. 4.6.

The carbon cycle and $CO_2$ fluxes discussed so far have no obvious direct relation to atmospheric ozone (if we disregard the impact of global warming caused by the increase of $CO_2$ in the atmosphere, see Sect. 5.4). A small fraction of biospheric carbon, however, is released in the form of other carbon compounds, such as $CH_4$ and higher hydrocarbons, which are oxidised in the atmosphere and eventually end up as $CO_2$. Although the fluxes of these are about three orders of magnitude smaller than those of $CO_2$ as shown in Fig. 4.5, they play an important role in the photochemistry of ozone.

$CH_4$ is a major product of biomass fermentation under anaerobic conditions. It can directly be released or undergo anaerobic oxidation with $CO_2$ being returned to the atmosphere. Large amounts of $CH_4$ are oxidised to $CO_2$ by bacteria in marine sediments and thus are prevented from escaping to the environment [43]. A significant fraction of $CH_4$ produced over geologic times, in soils and waters, has not been released to the atmosphere at all. It is sequestered in crystallised water structures called methane hydrates that have formed in the ocean under specific temperature and pressure conditions, at depths below about 400–500 m. At several continental slopes, where high plankton productivity provided ample biomass, methane hydrate layers, up to 1,000 m in thickness, have formed over geologic times. Smaller amounts are found in Russian and Canadian permafrost soils as well.

Altogether, an estimated amount of 7,500–10,000 Gt C are stored as methane hydrates [44], about twice as much as in the fossil fuel carbon pool (Fig. 4.5).

Upon warming, at normal pressure, $CH_4$ is liberated. The curiosity of "burning ice" has been known for long: At room temperature, the escape rate of $CH_4$ from a chunk of methane hydrate is generally sufficient for maintaining a steady flame. Thus, the large methane hydrate deposits are not only a significant carbon pool but also a latent threat to the environment: Global warming is likely to liberate $CH_4$, a greenhouse gas 21 times more efficient than $CO_2$, from this carbon pool.

### *4.4.3 The Global Nitrogen Cycle*

Nitrogen ($N_2$) makes up about 78 % of the Earth's atmosphere. This atmospheric nitrogen pool of $4 \times 10^{21}$ g N ($4 \times 10^9$ Megatons N) is by far the largest nitrogen pool against which the other pools appear small: Nitrogen accumulated in living plants and dead biomass amounts to about $3.5 \times 10^{15}$ g N (3,500 Mt N) and $100 \times 10^{15}$ g N (100,000 Mt N), respectively. Thus, average C/N ratios of living and dead biomass amount to 160 and 15, respectively [37].

For all living organisms nitrogen is an indispensible element. However, it is not the inert $N_2$ from the huge atmospheric pool that plants can use for their metabolism. Nitrogen rather needs to be "fixed", i.e. converted into substances such as ammonium ($NH_4^+$) and nitrate ($NO_3^-$) plants can take up, along with other nutrient elements, with the soil water solution. Natural nitrogen fixation occurs through lightning in the atmosphere, by blue-green algae and bacteria in soils and waters, in particular in symbiosis with leguminous plants.

Lighting discharges produce $NO_x$ which is converted to $HNO_3$ by OH radicals (see Sect. 3.1.3). $HNO_3$ dissolved in rain and fog water droplets thus feeds nitrate to the biosphere. The total amount of nitrogen fixed by lightning each year is estimated to range between 5 and 20 Mt N. As Fig. 4.7 shows, this nitrogen fixation rate is much smaller than the rate of biological nitrogen fixation amounting to about 140 Mt N/year. Microorganisms thereby produce ammonium and nitrate in the soil which can be taken up by plant roots with the soil water solution. The global rate of 140 Mt N/year corresponds to an average nitrogen deposition of 10 kg N/year per hectare land surface.

The net primary production of the total land vegetation amounts to 60 Gt C/year (Fig. 4.5). Based on a C/N ratio of 50 this would require a nitrogen equivalent of 1,200 Mt N/year, about eight times more than available from natural nitrogen fixation. It is thus assumed that internal cycling between living and dead biomass provides most of the required nitrogen (Fig. 4.7). Thereby losses occur through denitrification (reduction of $NO_3^-$) and nitrification (oxidation of $NH_4^+$).

A fraction of ammonium and nitrate compounds solved in water, about 36 Mt N/year, are lost to rivers. Thus under conditions undisturbed by human activities, these losses are obviously compensated by natural fixation of atmospheric nitrogen.

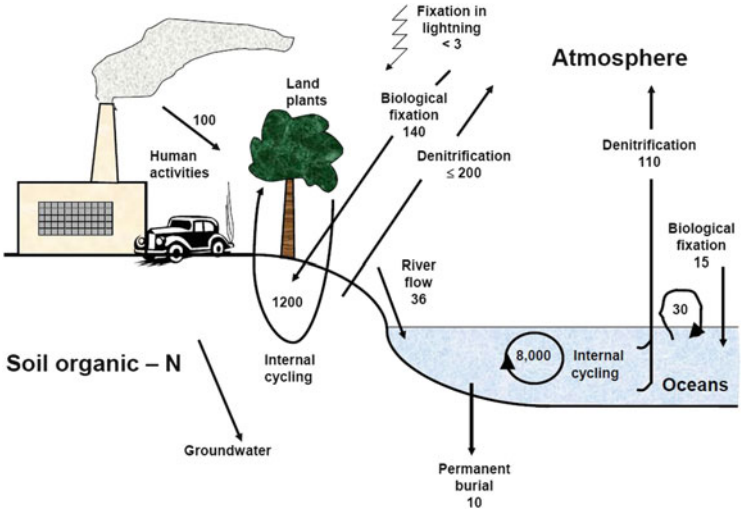


**Fig. 4.7** The global nitrogen cycle. Fluxes are shown in units of $10^{12}$ g N/year, from [37]

Human activities have a tremendous impact on the nitrogen cycle: About 80 Mt N/year nitrogen fertiliser are applied to arable soils, and 20 Mt N/year are emitted to the atmosphere as $NO_x$ by combustion, most of it from automobile exhaust, which ends up as nitrate in the soil as well [45]. Moreover, the cultivation of leguminous plants enhances the biological nitrogen fixation. Thus, more than 100 Mt N/year are added to the biosphere from anthropogenic sources, about 40 % of the total nitrogen input.

The atmospheric part of the cycle is closed by processes in which dead biomass is mineralised releasing nitrogen back to the atmosphere. Soil bacteria thereby produce $NH_4^+$ and $NO_3^-$ both of which can be taken up by living plants. Denitrifying bacteria finally reduce $NO_3^-$ to $N_2$ which thereby gets lost from the soil and returns to the atmosphere. That way up to 200 Mt N/year return to the atmospheric pool.

A by-product of bacterial nitrification is nitrogen monoxide (NO) which escapes as gas to the atmosphere. Between 1 and 3 % of the cycling nitrogen is thus released corresponding to a global NO source of 10 Mt N/year [46]. The NO emission of soils depends on soil temperature and humidity. It is particularly high when nitrification is stimulated by the application of ammonium fertiliser [47]. On the other hand, under high atmospheric NO concentrations, soils take up NO and thus act as NO sink. The compensation point, at which neither uptake nor release occurs, depends on several parameters. For clean air conditions, with NO levels below 10 ppb, far below the compensation point, most land ecosystems thus are likely to act as NO sources. NO is an important trace gas for ozone photochemistry (see Sect. 4.3).

A by-product of bacterial denitrification is, along with small amounts of NO, nitrous oxide ($N_2O$), known as laughing gas (Sect. 4.4.4). The ratio $N_2/N_2O$

depends on the pH value and the fractions of $NO_3^-$ and $O_2$ in the soil and thus varies in wide ranges. The presently accepted median value of 22 [37] would imply that almost 5 % of nitrogen recycled from the biosphere by denitrification, about 15 Mt N/year, is emitted to the atmosphere as $N_2O$. $N_2O$ is an efficient greenhouse gas. Being inert in the troposphere it gets mixed to the stratosphere, where it is a source of $NO_x$ radicals which catalytically destroy ozone (see Sect. 3.1.3).

For the oceanic part, internal cycling of nitrogen is even more pronounced than for terrestrial ecosystems (Fig. 4.7). The small input of 36 Mt N/year from the rivers is the main source, while biological fixation amounts to 15 Mt N/year only. On the other hand, the huge amount of 8,000 Mt N/year from dead organisms is recycled for uptake of living plankton. Most of the nitrogen input by rain (30 Mt N/year) is recycled as well over the ocean.

While photosynthesis and internal nitrogen fluxes are confined to the oceanic surface layer, the deep ocean forms a relatively large nitrogen pool of $570 \times 10^3$ Mt N fed by sunken remains of dead organisms and excrements. As only 10 Mt N/year are buried in the sediments, a large fraction of the nitrogen input to the ocean is returned to the atmosphere. About 110 Mt N/year from denitrification in the deep anaerobic ocean are thus recycled back to the atmospheric $N_2$ pool.

If we disregard the anthropogenic input, about 200 Mt N/year cycle through the global biosphere. Thus, the atmospheric nitrogen pool passes through the biosphere once every $20 \times 10^6$ years. The biosphere itself is a small nitrogen pool. Without denitrification, by which nitrogen is recycled to the atmosphere, a large amount of nitrogen would thus form nitrate which would be carried away by the rivers finally ending up in the ocean. Moreover, most atmospheric oxygen would be used up in this process. Thus, the complicated interplay of biological processes coupling the biogeochemical cycles is an essential condition for maintaining life conditions on our planet [35].

### *4.4.4 Nitrous Oxide ($N_2O$)*

Nitrous oxide is the major source of nitrogen oxides ($NO_x$) in the stratosphere, with the latter contributing significantly to ozone depletion. In addition, $N_2O$, which has an atmospheric life time of about 120 years, is an important greenhouse gas. Its global warming potential per molecule is 310 times that of $CO_2$. It is emitted at the Earth's surface by a large number of sources.

About $300 \times 10^6$ t N/year are released to the atmosphere by denitrification from soils and the oceans (Fig. 4.7). If we assume that almost 5 % of this nitrogen is emitted as $N_2O$, this global source of $N_2O$ would amount to about $15 \times 10^6$ t N/year.

As was shown in the previous chapter, the global nitrogen cycle and hence the $N_2O$ budget is not balanced, as additional $100 \times 10^6$ t N/year from anthropogenic sources are applied to the biosphere resulting in enhanced $N_2O$ liberation. Natural and anthropogenic sources of $N_2O$ are compiled in Table 4.1. With $8 \times 10^6$ t

**Table 4.1** Global budget of $N_2O$: natural and anthropogenic sources as well as photochemical decomposition in $10^6$ t N/year, after [46, 48–50] (for converting to $10^6$ t $N_2O$ multiply by 44/28 = 1.57)

| | Range | Global average |
|---|---|---|
| Emission from soils | | 6 |
| Emission from oceans | | 3 |
| **Total natural sources** | | **9** |
| Biomass burning | 0.2–3 | 1.6 |
| Nitrogen fertilisation | 0.4–3 | 1.0 |
| Sewage and manure | 0.3–3 | 1.5 |
| Irrigation, wet farming | 0.8–2 | 0.8 |
| Cattle and feed lots | 0.3–1 | 0.5 |
| Traffic | 0.1–2 | 0.8 |
| Nylon production | | 0.7 |
| Global warming | 0.1–1 | 0.3 |
| Land use changes | | 0.7 |
| **Total anthropogenic sources** | **5–10** | **8** |
| **Total all sources** | | **17** |
| **Photochemical loss in the stratosphere** | **9–16** | **12.5** |

N/year, anthropogenic sources are almost as high as the natural liberation of $N_2O$ from soils and the ocean together. Basically, more than 65 % of the anthropogenic $N_2O$ release can be considered "natural" as well, as it results from $NH_4^+$ and $NO_3^-$ input to the biosphere. Alone through agricultural practices, such as the application of nitrogen fertilisers, irrigation, cattle breeding and biomass burning, more than $5 \times 10^6$ t N/year are added to the biosphere. Global warming and land use changes are likely $N_2O$ sources as well, and even abiotic processes [51] might be relevant to the $N_2O$ budget.

In the troposphere, due to lacking decomposition processes, $N_2O$ behaves like a noble gas. In the stratosphere and mesosphere, its major photochemical sink reactions are

$$N_2O + \left(^1D\right)\text{-}O \rightarrow 2NO$$

(see Sect 3.1.3),

$$N_2O + \left(^1D\right)\text{-}O \rightarrow N_2 + O_2,$$

and

$$N_2O + h\nu(\lambda < 240\,\text{nm}) \rightarrow N_2 + O$$

by which about $12.5 \times 10^6$ t N/year are returned to the atmospheric N pool. The contribution of the first of these reactions, which is the major source of $NO_x$, is about 10 % to this photochemical sink.

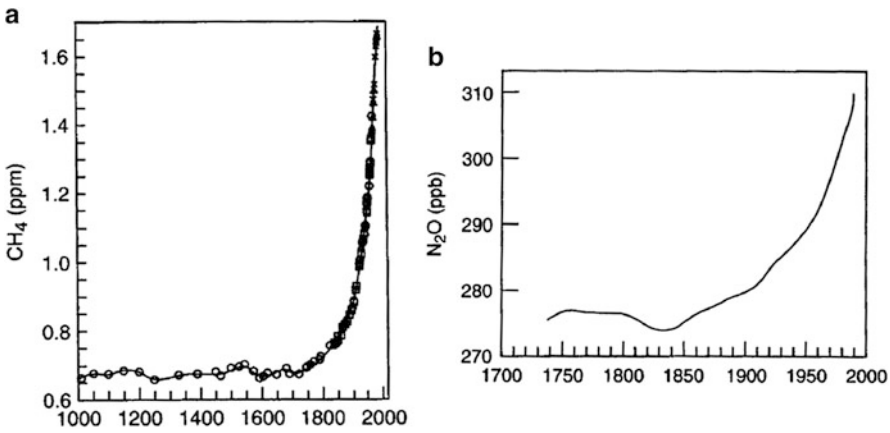


**Fig. 4.8** Atmospheric abundances of $CH_4$ (**a**) and $N_2O$ (**b**) over past centuries, after [54]

The vertical distribution of $N_2O$ as shown in Fig. 4.9 clearly illustrates that no significant destruction occurs in the troposphere, while above the tropopause photochemical decomposition causes mixing ratios to decrease with altitude. Due to the stability of the $N_2O$ molecule, its breakdown and thus the decrease with altitude are slow. Thus, a small fraction of $N_2O$ survives stratospheric decomposition: $N_2O$ analysed from a mesospheric air sample collected by a rocket-borne whole-air sampler showed a mixing ratio of 2.8 ppb at about 60 km altitude, about 1 % of the tropospheric $N_2O$ abundance [52].

The present atmospheric fraction of $N_2O$ is close to 320 ppb which corresponds to an atmospheric $N_2O$ pool of $1.5 \times 10^9$ t N, about $4 \times 10^{-7}$ of all atmospheric nitrogen. Dividing through the photochemical sink rate, we obtain an overall atmospheric life time of 120 years for $N_2O$.

Due to this long atmospheric life time and the lack of tropospheric sinks, the global distribution of $N_2O$ is found to be fairly homogeneous despite considerable inhomogeneities of the sources. From ice core gas analyses, preindustrial $N_2O$ levels were found to be about 265 ppb [53]. Due to human activities, $N_2O$ began to rise in the early nineteenth century (Fig. 4.8b). Over the last decade the increase was about 0.7 ppb/year. The present $N_2O$ mixing ratio (2006) is about 320 ppb, about 20 % higher than the preindustrial value.

### *4.4.5 Methane ($CH_4$)*

Methane is the longest lived and most abundant organic molecule in the atmosphere. It is photochemically important, both in the troposphere and stratosphere.

**Table 4.2** Global $CH_4$ budget: natural and anthropogenic sources as well as photochemical decomposition rates in $10^6$ t C/year, after [57, 58] (for conversion to $10^6$ t $CH_4$/year multiply by 16/12 = 1.33)

| | Range | Global average |
|---|---|---|
| Swamps, marshes | 75–150 | 85 |
| Lakes | 1–20 | 5 |
| Oceans | 5–15 | 10 |
| Termites, other natural sources | 10–75 | 30 |
| **Total natural sources** | **91–260** | **130** |
| Cattle farming | 50–75 | 60 |
| Rice fields | 45–130 | 80 |
| Biomass burning | 40–75 | 45 |
| Waste dumps | 25–50 | 30 |
| Coal mining | 20–35 | 25 |
| Natural gas | 20–40 | 35 |
| **Total anthropogenic sources** | **200–405** | **275** |
| **Total $CH_4$ sources** | **291–665** | **405** |
| **Photochemical loss by OH reactions** | **50–600** | **400** |

Moreover, because of its IR absorption properties, it is an efficient greenhouse gas with a global warming potential per molecule 21 times that of $CO_2$.

Fermentation of biomass under anaerobic conditions is the main source of methane. $CH_4$ has been found to be formed not only in swamps, marshes, tropical rainforests, tundra soils and the ocean but also in the digestive tract of ruminants. Termites contribute to the natural $CH_4$ sources as well [55]. Altogether, between 100 and 150 $\times$ $10^6$ t C/year are liberated to the atmosphere as $CH_4$ [56] .

In the overall global budget, the emission rates of $CH_4$ from anthropogenic sources even exceed those from natural ones. Wet farming, rice paddies, in particular, and cattle farming cause about 140 $\times$ $10^6$ t C/year to be released as $CH_4$ to the atmosphere (Table 4.2). Although these emissions are due to biological processes, they are caused by man and thus are to be regarded anthropogenic providing $CH_4$ fluxes about as large as those from all natural sources together. Another 45 $\times$ $10^6$ t C/year and 30 $\times$ $10^6$ t C/year are emitted from forest fires and waste dumps, respectively. Through mining and processing of coal, oil and natural gas, about 60 $\times$ $10^6$ t C/year are liberated. With a total of 275 $\times$ $10^6$ t C/year anthropogenic sources contribute about twice as much to the global methane budget compared to all natural sources.

The most important loss process of $CH_4$ is the reaction with OH in the troposphere (reaction (4.1) in Sect. 4.3.2) initiating a chain of further reactions which eventually lead to the formation of CO, $CO_2$ and $H_2$. The quantification of the annual $CH_4$ loss by this process requires knowledge of the global OH distribution. Regarding related uncertainties, the global tropospheric $CH_4$ sink is found to range between 150 and 600 $\times$ $10^6$ t C/year or 200–800 $\times$ $10^6$ t $CH_4$/year (Table 4.2).

About 10 % of the amount of $CH_4$ emitted at ground level escapes tropospheric degradation and is mixed to the stratosphere, where the following loss reactions occur:

$$CH_4 + OH \rightarrow CH_3 + H_2O \quad \text{(reaction (4.1))}$$

$$CH_4 + \left(^1D\right)\text{-}O \rightarrow CH_3 + OH$$

$$CH_4 + \left(^1D\right)\text{-}O \rightarrow H_2CO + H_2$$

The first of these initiates, like in the troposphere, the oxidation chain leading to the formation of CO, $CO_2$ and $H_2O$. For the dry stratosphere, whose water content is controlled by the low tropopause temperature; this in-situ production is an important source of $H_2O$.

In the second reaction $CH_3$ is produced as well, along with OH which plays an important role in catalytic ozone destruction cycles (see Sect. 3.1.3).

In the third reaction the source gas $H_2$ is formed, along with formaldehyde, an intermediate product in the methane oxidation chain (see Sect. 4.3.2), which eventually leads to the formation of CO, $CO_2$ and $H_2$. About 95 % of the $H_2CO$ (and consequently of the $CH_4$) end up as CO and $CO_2$; only a smaller fraction generates $H_2$, mainly through photolysis of $H_2CO$

$H_2CO + h\nu \rightarrow H_2 + CO$ ([26], see Sect. 4.3.2).

The present global average $CH_4$ mixing ratio at the surface is 1,777 ppb [53] corresponding to a total atmospheric methane load of about $4 \times 10^9$ t $CH_4$ or $3 \times 10^9$ t C.

If we take the average value of $400 \times 10^6$ t C/year for the photochemical sink (Table 4.2), a mean atmospheric life time of 7.5 years is obtained for the $CH_4$ molecule. This time is long compared to tropospheric mixing times, and hence $CH_4$ is relatively well mixed over the globe, although the sources, being largely concentrated on the continents, are extremely inhomogeneous. As Fig. 4.10 shows, however, areas of increased $CH_4$ emission over the continents can clearly be identified by $CH_4$ values up to 10 % above the global average.

The vertical $CH_4$ distribution shown in Fig. 4.9 is characterised by mixing ratios almost constant with altitude in the troposphere and gradually falling off above the tropopause. $CH_4$ can even reach the mesosphere where 56 ppb were measured at about 60 km altitude, more than 3 % of the surface mixing ratio [52].

From the preindustrial value of about 700 ppb (Fig. 4.8a), the abundance of methane has more than doubled, as a result of human activities, to 1,777 ppb today. The global growth rate has varied from 14 ppb/year in 1985 to near zero in 2000, but with significant interannual variability. Since 2000 no significant growth has been observed, but in view of the large uncertainties in the $CH_4$ budget the reasons for this levelling-off are unclear. Obviously, individual sources such as biomass

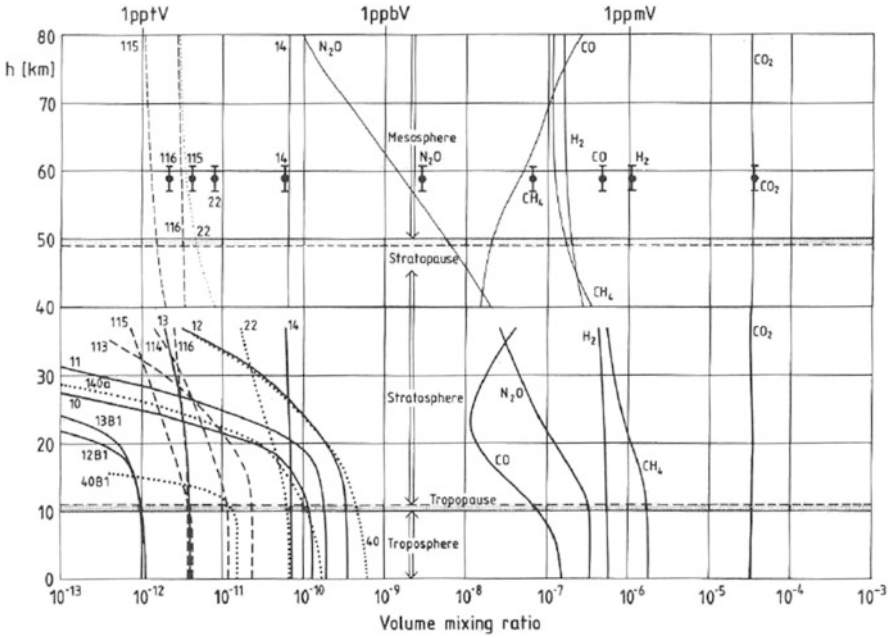


**Fig. 4.9** Vertical distribution of source gases as measured at Northern midlatitudes, from [52]

burning and emissions from the former Soviet Union have seen substantial changes during the past decades [53].

About 7,500–10,000 $\times$ $10^9$ t C are sequestered as $CH_4$ in gas hydrates on the seafloor and in permafrost soils. Global warming is likely to liberate $CH_4$ from these deposits thereby adding another source.

### *4.4.6 Carbon Monoxide (CO)*

Carbon monoxide is a reactive trace gas which plays an important role in photochemical ozone formation. Its main natural source is the oxidation of $CH_4$ and other hydrocarbons from biogenic sources, while direct emissions of CO seem to be insignificant.

The major anthropogenic sources are the incomplete combustion of fossil fuels and biomass burning providing an average global CO emission of 450 $\times$ $10^6$ t C/year, almost half the annual emission from all sources (Table 4.3).

Through reaction (4.1) (see Sect. 4.3.2)

$$CO + OH \rightarrow CO_2 + H$$

about 90–95 % of tropospheric CO are oxidised to $CO_2$ using up OH. $HO_2$ formed in the follow-up reaction (4.2)

**Table 4.3** Global budget of CO: natural and anthropogenic sources in $10^6$ t C/year, after [59] (for conversion of C to CO: multiply by 28/12 = 2.33)

| | $10^6$ t CO/year | $10^6$ t C/year |
|---|---|---|
| Methane oxidation | 760 | 325 |
| Oxidation of other hydrocarbons | 683 | 295 |
| **Total natural sources** | **1,443** | **620** |
| Burning fossil fuels | 300 | 130 |
| Biomass burning | 748 | 320 |
| **Total anthropogenic sources** | **1,048** | **450** |
| **Total CO sources** | **2,491** | **1,070** |

$$H + O_2 + M \rightarrow HO_2 + M$$

is important for tropospheric ozone formation.

Thus, CO has a significant influence on the OH distribution and hence the tropospheric oxidation potential, which decreases (increases) for rising (falling) CO levels [60]. The atmospheric residence time of CO is determined by reaction (4.1). It varies, according to the OH distribution, between a few weeks up to about 3 months.

Due to this short life time, the global CO distribution is highly variable. Except for the oxidation of methane, all other sources of CO are concentrated on the land surfaces. About 50 ppb CO are found over most of the Southern Hemisphere oceans, with higher values over Southern continents reflecting the emission from biomass burning (Fig. 4.10). On the Northern Hemisphere where anthropogenic burning of fossil fuels dominates, the oceanic CO mixing ratios are about twice those over the southern ocean, while in the industrialised regions of North America, Europe and Asia CO mixing ratios up to the ppm range are observed.

Long-term measurements, beginning in the 1970s, showed a slight increase of about 1 %/year levelling off during the end of the 1980s. Since then no significant CO trend is reported [54].

The short atmospheric life time of CO is reflected in the vertical distribution, too. Different from the longer-lived $CH_4$ and $N_2O$, CO mixing ratios fall off with height well below the tropopause already. Above a minimum at about 25 km altitude CO mixing ratios begin increasing with altitude. At about 60 km a CO mixing ratio of 425 ppb was measured [52], about four times the value typical for the surface level over the Northern Hemisphere ocean. The increase shown in Fig. 4.9 is a unique feature of CO. It is due to the production of CO by $CH_4$ oxidation and, especially at altitudes above 50 km, photolysis of $CO_2$ by shortwave UV radiation.

### *4.4.7 Hydrogen ($H_2$)*

Molecular hydrogen contributes, like methane and carbon monoxide, to the formation of $HO_x$ radicals. Its main natural sources are the $CH_4$ oxidation (see

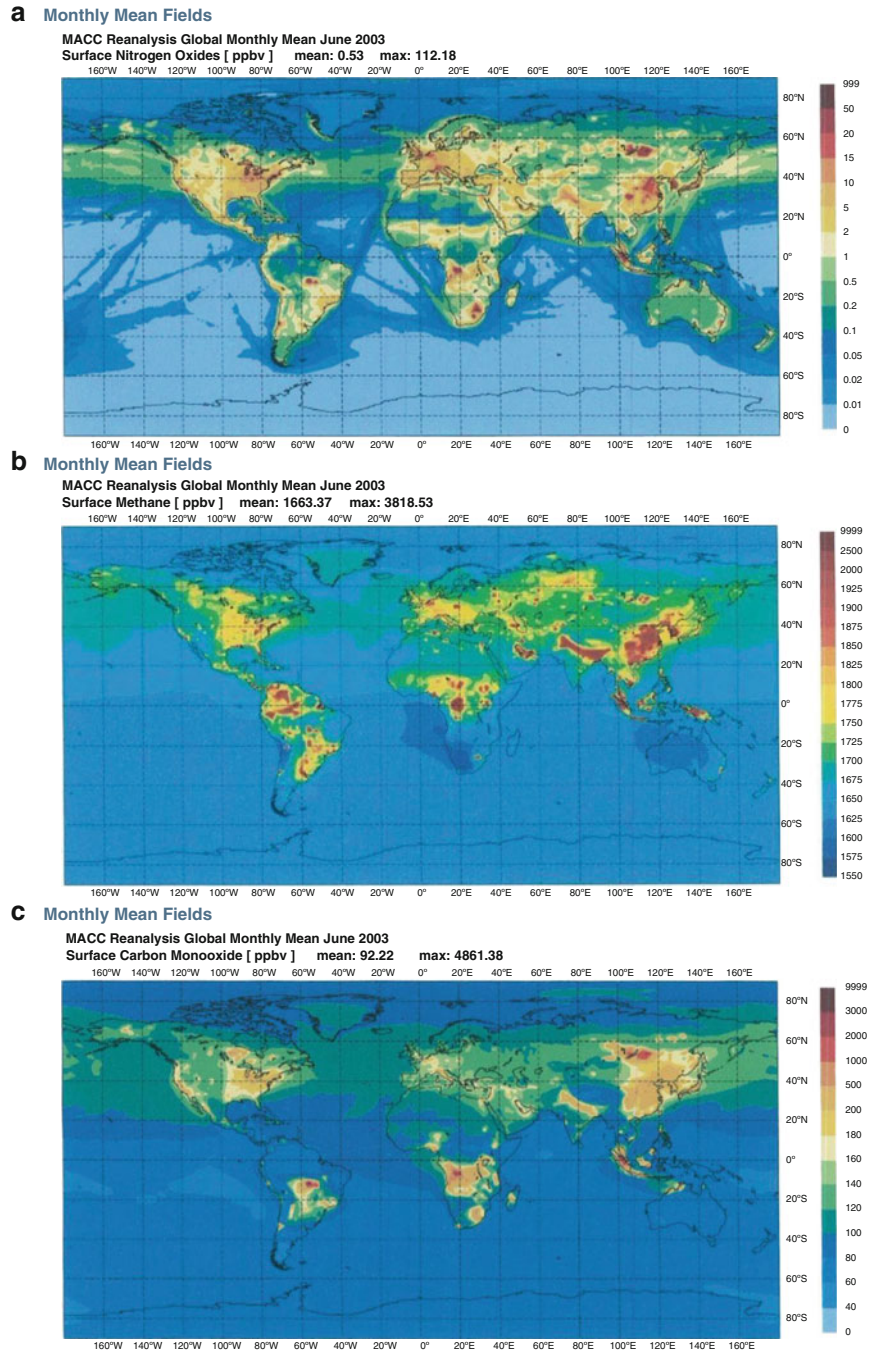


**Fig. 4.10** Global surface distributions of nitrogen oxides ($NO_x$) (**a**), methane ($CH_4$) (**b**) and carbon monoxide (CO) (**c**), monthly means for June 2003, same source as for Fig. 4.4 [34]

**Table 4.4** Global budget of $H_2$: natural and anthropogenic sources and sinks are given in $10^6$ t $H_2$/year, after [26]

| | Range | Global average |
|---|---|---|
| $N_2$ fixation ocean | 3–9 | 6 |
| $N_2$ fixation land | 1–5 | 3 |
| Photochemical production from | | |
| Methane | 15–31 | 23 |
| VOCs | 1–25 | 18 |
| **Total natural sources** | | **50** |
| Fossil fuel burning | 7–15 | 11 |
| Biomass burning | 9–21 | 15 |
| **Total anthropogenic sources** | | **26** |
| **Total $H_2$ sources** | | **76** |
| Oxidation by OH | 14–24 | 19 |
| Soil uptake | 40–90 | 60 |
| **Total sinks** | | **79** |

Sect. 4.3.2) and the oxidation of higher hydrocarbons, such as terpenes and isoprene emitted by certain vegetation species (see Sect. 4.4.10). This photochemical source contributes about 50 % to the total $H_2$ production (Table 4.4). The direct natural emission of $H_2$ plays a minor role, with nitrogen fixation under anaerobic conditions, both on land and in the oceans, contributing about 12 % to the overall budget only.

Anthropogenic sources, such as the incomplete combustion of fossil fuels and biomass burning, contribute about 15 % and 20 %, respectively, to the $H_2$ budget, about half the contribution of the natural sources. It should be noted, however, that the anthropogenic share of the $H_2$ sources is by far larger given the fact that 60 % of the sources of $CH_4$ (from which $H_2$ is formed) are anthropogenic. Thus, at present about 50 % of the total tropospheric $H_2$ production can be considered anthropogenic [26].

The $H_2$ sources are balanced by two sinks: The first one is the photochemical reaction with OH in the troposphere

$$H_2 + OH \rightarrow H_2O + H$$

whose contribution to the total loss of about 25 % is determined fairly accurately. The second and by far dominating one is the $H_2$ uptake by soils. Current estimates place it at about 75 % of the total loss. There are, however, large uncertainties involved because of the large variety of soils and biomass that have to be considered (see review by Ehhalt and Rohrer [26] and references given therein).

Different from the sources, with about 50 % of $H_2$ being emitted at the Earth's surface and the other 50 % being formed photochemically in the atmosphere, about 75 % of the loss of $H_2$ takes place at the surface, while photochemical loss in the troposphere contributes 25 % only.

The present tropospheric abundance of $H_2$ is 531 ppb, which corresponds to a total mass of $155 \times 10^6$ t $H_2$. There is no evidence for a trend in tropospheric $H_2$ [26]. Based on the sources and sinks given in Table 4.4, the atmospheric life time of

$H_2$ is about 2 years. Thus, $H_2$ is well mixed throughout the global troposphere, with small latitudinal variations. The annually averaged mixing ratios are highest at the equator, about 545 ppb, and decrease towards the poles.

As the anthropogenic sources are dominating on the Northern Hemisphere, mainly owing to the burning of fossil and bio-fuel, there is some debate about hemispheric asymmetries. With 64 % the excess of the Northern Hemisphere sources is not as large as about 70 % for the total losses. This results in a net deficit of the $H_2$ balance of the Northern Hemisphere maintaining the present interhemispheric gradient in the $H_2$ mixing ratio of about 3 % [26].

Due to the fact that about 50 % of $H_2$ is not emitted at the surface but rather is produced photochemically in the atmosphere, vertical profiles of the tropospheric $H_2$ mixing ratio generally show a slight increase with height [26]. This implies that there is almost no export of $H_2$ from the troposphere to the stratosphere. Stratospheric $H_2$ originates to a large extent from in situ methane oxidation (see vertical profiles shown in Fig. 4.9).

### *4.4.8 Methyl Chloride ($CH_3Cl$)*

Methyl chloride, the most abundant halocarbon in the atmosphere, is derived largely from natural sources (other halocarbons, most of which are from anthropogenic sources, are discussed in Sect. 5.1). Until the 1990s, most of the input to the atmosphere was considered to originate from oceanic sources. Recent investigations, however, indicated that terrestrial sources, in particular tropical and subtropical forests, dominate the global budget of $CH_3Cl$, while oceanic sources are much less important than hitherto appreciated.

From high concentrations of $CH_3Cl$ measured in and above tropical forests, a global source strength of (820–8,200) $\times$ $10^6$ t $CH_3Cl$/year was derived [53], the largest term among all sources compiled in Table 4.5. Significant amounts of $CH_3Cl$ are emitted from senescent or dead leaves and biomass, too. The oceanic source of (380–500) $\times$ $10^6$ t $CH_3Cl$/year is small compared to the terrestrial sources and much smaller than assumed 20 years ago. All sources, however, remain uncertain within large ranges.

By far the largest sink of $CH_3Cl$ from the atmosphere is the reaction with the OH radical $CH_3Cl + OH \rightarrow$ products, which amounts to (3,800–4,100) $\times$ $10^6$ t $CH_3Cl$/year. All other sinks listed in Table 4.5 appear to be less important, although large uncertainty ranges, in particular those related to decomposition by soils, might still bear surprises.

Observations from various networks suggest an average global abundance of (0.55 $\pm$ 0.03) ppb or (550 $\pm$ 30) ppt, with slightly higher values at low latitudes. Small interannual variations are reported, but there is no trend of $CH_3Cl$. From the sinks given in Table 4.5 an overall atmospheric life time of 1.3 years is estimated [53]. This allows a fraction of $CH_3Cl$ to be exported to the stratosphere.

A midlatitude vertical profile of $CH_3Cl$ (marked 40) is shown in Fig. 4.9.

**Table 4.5** Global sources and sinks of atmospheric $CH_3Cl$ from observations and model studies, in $10^6$ t $CH_3Cl$/year, after [53] (for conversion to $10^6$ t Cl/year multiply by 35/50 = 0.7)

| | Range | Average from 3D models |
|---|---|---|
| Tropical and subtropical plants | 820–8,200 | 2,640 |
| Senescent or dead leaves | 30–2,500 | |
| Oceans | 380–500 | 493 |
| Salt marshes | 95–440 | 170 |
| Fungi | 43–470 | 128 |
| Wetlands | 48 | 48 |
| **Total natural sources** | **1,416–12,158** | **3,479** |
| Biomass burning | 325–1,125 | 672 |
| Rice paddies | 2.4–4.9 | |
| Fossil fuel burning | | 5–205 |
| Waste incineration | 15–75 | 162 |
| Industrial processes | | 10 |
| **Total anthropogenic sources** | **357–1,420** | **834** |
| **Total $CH_3Cl$ sources** | **1,773–13,578** | **4,313** |
| Loss by reactions with OH | 3,800–4,100 | 3,922 |
| Loss to stratosphere | 100–300 | |
| Cl reaction | 180–550 | |
| Loss to soils | 100–1,600 | 256 |
| Loss to polar waters | 93–145 | 149 |
| **Total $CH_3Cl$ sinks** | **4,273–6,695** | **4,327** |

### *4.4.9 Methyl Bromide ($CH_3Br$)*

Methyl bromide is the only natural source gas which significantly contributes to the atmospheric bromine budget. (The role of other bromine compounds from anthropogenic sources will be discussed in Sect. 5.1). Its present average tropospheric mixing ratio of about 8 ppt (2005) corresponds to a total load of $0.13 \times 10^6$ t $CH_3Br$.

Bromine released in the stratosphere is about 50 times more efficient in catalytically destroying ozone than chlorine. Thus, even the low abundance of $CH_3Br$ makes it an important ozone depleter and, in view of its anthropogenic sources, a target of emission controls set by the Montreal Protocol (see Chap. 6).

The oceans are the major natural reservoirs of bromine and thus have generally been regarded as the principle natural sources of $CH_3Br$. The oceans, however, have been identified to act as efficient sinks for $CH_3Br$ as well. Other natural sources include the emission from soils and the fraction of biomass burning from natural fires. As recent reviews show [53] a quantification of the natural sources appears to be impossible as yet.

$CH_3Br$ is removed from the atmosphere by reactions with OH radicals. This sink is quantified fairly well (see [61, 62]). It appears that the oceans provide additional sinks of the same order of magnitude, within large uncertainty ranges, however. $CH_3Br$, being a polar molecule and strong methylating agent, is subject to

significant dry deposition, too. Thus, as many field experiments have shown, soils are efficient sinks for $CH_3Br$. Respective sink strengths published so far vary within large ranges [53, 61, 62].

Despite these severe uncertainties related to sources and sinks, the preindustrial abundance of $CH_3Br$ has been determined fairly well, from air trapped in ice and firn, to range between 5 and 6 ppt [53].

During the 1900s, $CH_3Br$ levels have been increasing as a result of anthropogenic emissions. The largest sources have been from agricultural and allied usage, with $CH_3Br$ being used as a fumigant controlling a wide spectrum of pests, including pathogens, insects, rodents and nematodes. Exact figures on production and sales of $CH_3Br$ showing a steady increase until 1998 are documented, although the fraction eventually released to the atmosphere is less well known. Another important anthropogenic source of $CH_3Br$ is biomass burning. A minor source has been from gasoline additives during the years when leaded gasoline was used [61, 62].

$CH_3Br$ has been increasing until about 1998, the year of highest abundances in both hemispheres, of about 11 ppt and 8 ppt, at 82°N and 90°S, respectively [53]. The hemispheric difference is mostly due to the fact that most of the anthropogenic sources have been concentrated on the Northern Hemisphere. In view of the large uncertainties related to the natural sources and sinks, it cannot be argued to what extent these contribute to the hemispheric asymmetry as well.

Since 1998, $CH_3Br$ tropospheric abundances have been observed to decrease on a global scale as a result of regulations under the Montreal Protocol.

The overall atmospheric life time of $CH_3Br$ has been estimated to be about 1 year. Given the large uncertainties it may range between 0.7 and 1.3 years, long enough to enable $CH_3Br$ to be mixed to the stratosphere where it acts as source for $BrO_x$ radicals. A vertical profile of $CH_3Br$ is shown in Fig. 4.9 (marked 40B1).

### *4.4.10 Biogenic Hydrocarbons*

Volatile organic compounds (VOCs) are essential constituents of living organisms and thus part of the biosphere. They are released through leafs and needles, and their global emission amounts to several hundred $10^6$ t C/year, more than released from anthropogenic sources.

The spectrum of biogenic VOCs identified so far is huge and comprises more that 40,000 compounds, whose occurrence and distribution varies among hundred thousands of plant species. Forests making up about 90 % of all living biomass thus constitute by far the most important sources of VOCs, and the scent of “healthy forest air” is indeed due to such compounds.

Despite the huge variety of substances, most investigations have been concentrating on few groups of species, such as isoprene ($C_5$), monoterpenes ($C_{10}$), several alkanes, alkenes, alcohols and their reaction products (see [63–67]). According to a

recent review [26], the following global emission rates have been evaluated for these three groups of substances:

Isoprene: $500 \pm 250$, Monoterpenes: $140 \pm 20$, sum of other VOCs: $250 \pm 150$, all in $10^6$ t C/year.

Quantitatively, isoprene (2-methyl-1,3-butadiene, $C_3H_5$) is the most important VOC. With about $500 \times 10^6$ t C/year its worldwide emission is of the same order of magnitude as the $CH_4$ budget. Typical isoprene emitters are deciduous trees, several shrubs, ferns and a variety of plants and trees in tropical forests.

Monoterpenes are $C_{10}H_{16}$ compounds whose C atoms are arranged in ring and chain combinations. Their most important representatives are α- and β- pinene, camphene, limonene and carene. Monoterpenes are preferentially emitted not only by coniferous trees, but also from oaks, fruit trees and several bushes and trees in tropical forests [66, 68–70].

The emission of VOCs is largely controlled by environmental conditions such as temperature and light. Increasing temperatures generally lead to higher emission rates of isoprene and monoterpenes, while light seems to influence monoterpene more than isoprene emission rates. Thus, VOC concentrations, typically in the range up to a few ppb, show a pronounced diurnal variation, with highest values around noon [67, 71].

Besides isoprene and monoterpenes, alkanes, alkenes and alcohols are emitted [72, 73]. Most VOCs are unsaturated hydrocarbons with one or several double bonds. Being thus highly reactive they are rapidly oxidised by OH radicals. Typical atmospheric life times of VOCs range between minutes to hours [74]. The oxidation by OH yields CO whose global sources are fed by about 30 % from this process (see Sect. 4.4.6). In addition, a variety of secondary products is formed, such as aldehydes, carbonyles, ketones, furanes and acids.

Common species are methyl vinyl ketone (MVK), methacrolein (MACR) and 3-methyl-furane, which are secondary products of isoprene oxidation [71]. It is often difficult to assign measured VOCs to emitted or secondary substance groups, as several reaction paths are not fully understood as yet (see [26] and references therein).

The photooxidation of VOCs leading to particle formation is another important aspect. It is known for long that over extended forest areas, such as those of the Great Smoky Mountains National Park in the US state North Carolina, aerosols are formed during sunny days leading to remarkable turbidity of the otherwise clean air [74]. The aerosol forming potential of monoterpenes is fairly well known, and in smog chamber experiments it could be shown that from isoprene and β-pinene particles are formed photochemically [75]. Many processes are not fully understood, however.

Because of their short atmospheric life time, VOCs are of local to regional influence only. Through CO, the product of their oxidation by OH, however, they have global relevance. Another important aspect is the anthropogenic emission of $NO_x$ species which have caused enhanced photochemical ozone formation in many regions worldwide.

## References


1. Anfossi D, Sandroni S, Viarengo S (1991) Tropospheric ozone in the nineteenth century:The Moncalieri series.J. Geophys Res 96(D9):17349–17352
2. Sandroni S, Anfossi D, Viareng S (1992) Surface ozone levels at the end of the nineteenth century in South America. J Geophys Res 97(D2):2535–2539
3. Junge CE (1962) Global ozone budget and exchange between stratosphere and troposphere. Tellus XIV:363–377
4. Vassy A (1961) Données concernant les mesures d'ozone. Année Géophsique Internationale, Sér. II Fasc.3 Meteorologie et ozone. CNRS, Paris
5. Warmbt W (1966) Neuere Meßergebnisse des bodennahen Ozons. In: Meteorologie, Ergebnisse der Konferenz in Liblice 1964, Academia-Verlag, Prague, pp 51–62
6. Hering WS, Borden TR (1965) Mean distributions of ozone density over North America, 1963–1964. AFCRL-65-913, Environmental Research Papers No.162, US Air Force
7. Oltmans SJ, Komhyr WD (1976) Surface ozone in Antarctica. J Geophys Res 81:5359–5364
8. Holton JR (1990) On the global exchange of MAS between the stratosphere and the troposphere. Mon Weather Rev 47:392–394
9. Holton JR, Hayes PS, McIntyre PS, Douglass AR, Rood RB, Pfister L (1995) Stratosphere–troposphere exchange. Rev Geophys 33:403–439
10. Mahlman JD (1997) Dynamics of transport processes in the upper troposphere. Science 276:1079–1083
11. Stohl A, Bonasoni P, Cristofanelli P, Collins W, Feichter J, Frank A, Forster C, Gerasopoulos E, Gäggeler H, James P, Kentarchos T, Kromp-Kolb H, Krüger B, Land C, Meloen J, Papayannis A, Priller A, Seibert P, Sprenger M, Roelofs GJ, Scheel HE, Schnabel C, Siegmund P, Tobler L, Trickl T, Wernli H, Wirth V, Zanis P, Zerefos C (2003) Stratosphere-troposphere exchange: a review, and what we have learned from STACCATO. J Geophys Res 108(D12):27. doi:10.1029/2002JD002490
12. Mote PW et al (1996) An atmospheric tape recorder: the imprint of tropical tropopause temperatures on stratospheric waer vapour. J Geophys Res 101:3989–4006
13. Bischof W, Borchers R, Fabian P, Krüger BC (1985) Increased concentration and vertical distribution of carbon dioxide in the stratosphere. Nature 316:708–710
14. Waugh DW, Hall TM (2002) Age of stratospheric air: theory, observations, and models. Rev Geophys 40:4. doi:10.1029/2000RG000101
15. Boering KA et al (1996) Stratospheric transport rates and mean age distribution derived from observations of atmospheric CO2 and N2O. Science 274:1340–1343
16. Randel WJ, Gille JC, Roche AE, Kumer JB, Mergenthaler JL, Waters JW, Fishbein EF, Lahoz WA (1993) Stratospheric transport from the tropics to middle latitudes by planetary-wave mixing. Nature 365:533–535
17. Fabian P, Libby WF, Palmer CE (1968) Stratospheric residence time and interhemispheric mixing of Strontium 90 from fallout in rain. J Geophys Res 73:3611–3616
18. Fabian P (1974) The effect of the SST on the stratospheric distribution of odd nitrogen. Pure Appl Geophys 112:901–912
19. Danielsen EF (1968) Stratospheric-tropospheric exchange based on radioactivity, ozone and potential vorticity. J Atmos Sci 25:502–518
20. Dobson GMB (1973) The laminated structure of the ozone in the atmosphere. QJR Met Soc 99:599–607
21. Appenzeller C (1992) Davies HC (1992) Structure of stratospheric intrusions into the troposphere. Nature 358:50–572
22. Stohl A, Trickl T (2001) A textbook example of long-range transport: simltaneous observation of ozone maxima of stratospheric and North American origin in the free troposphere over Europe. J Geophys Res 104:30445–30462
23. Stohl A (2001) A 1-year Lagrangian "climatology" of airstreams in the northern hemisphere troposphere and lowermost stratosphere. J Geophys Res 106:7263–7279

24. Liu SC et al (1987) Ozone production in the rural troposphere and the implications for regional and global ozone distributions. J Geophys Res 92:4191–4207
25. Logan JA, Prather MJ, Wofsy SC, McElroy MB (1981) Tropospheric ozone: a global perspective. J Geophys Res 86:7210–7254
26. Ehhalt DH, Rohrer F (2009) The tropospheric cycle of H2: a critical review. Tellus 61B:500–535
27. Crutzen PJ (2000) Developments in tropospheric chemistry. In: Zerefos CS, Iaksen ISA, Ziomas I (eds) Chemistry and radiation changes in the ozone layer, NATO science series 8. Kluwer, Dordrecht, pp 1–12. ISBN 0-7923-6513-5 HB
28. Fishman J, Crutzen PJ (1978) The origin of ozone in the troposphere. Nature 274:855–858
29. Chameides W, Walker JCG (1973) A photochemical theory of tropospheric ozone. J Geophys Res 78:8751–8760
30. Crutzen PJ (1974) Photochemical reactions initiated by and influencing ozone in the unpolluted troposphere. Tellus 26:47–57
31. Danielson E, Mohnen V (1977) Project Duststorm: ozone transport, in situ measurements and meteorological analysis of tropopause folding. J Geophys Res 82:5867–5877
32. Fabian P, Pruchniewicz PG (1977) Meridional distribution of ozone in the troposphere and its seasonal variations. J Geophys Res 82:2063–2073
33. WMO Global Ozone Research and Monitoring Project-Report No.44: Scientific Assessment of Ozone Depletion 1998.ISBN:92-807-1722-7.Geneva 1999
34. Monitoring atmospheric composition and climate (MACC) 2010. http://www.gms-atmosphere.eu/d/services/ga/reanalysis/macc/macc_monthly_fields
35. Junge CE (1981) Die Entwicklung der Erdatmosphäre. Die Naturwissenschaften 68:236–244
36. Schidlowski M (1982) Content and isotopic composition of reduced carbon in sediments. In: Holland HD, Schidlowski M (eds) Mineral deposits and the evolution of the biosphere. Springer, Berlin, pp 103–122
37. Schlesinger WH (1997) Biogeochemistry, an analysis of global change, 2nd edn. Academic, San Diego, CA
38. Keeling CD, Chin JFS, Whorf TP (1996) Increased activity of northern vegetation inferred from atmospheric CO2 measurements. Nature 382:146–149
39. Myneni RB, Keeling CD, Tucker CJ, Asrar G, Nemani RR (1997) Increased plant growth in the northern high latitudes from 1981 to 1991. Nature 386:698–702
40. Keeling CD (1983) The global carbon cycle: what we know and could know from atmospheric, biospheric and oceanic observations. CONF 820970, Washington, DC, pp 3–62
41. Olson JS, Garrels RM, Berner RA, Armentano TV, Deyer MI, Yaalon DH (1985) The natural carbon cycle. In: Trabalka JR (ed) Atmospheric carbo dioxide and the global carbon cycle. US Department of Energy, Washington, DC, pp 175–213
42. Heimann M, Esser G, Haxeltine A, Kaduk J, Kicklighter DW, Knorr W, Kohlmaier GH, McGuire AD, Melillo J, Moore B, Otto RD, Prentice IC, Sauf W, Schloss A, Sitch S, Wittenberg U, Wurth G (1998) Evaluation of terrestrial carbon cycle models through simulations of the seasonal cycle of atmospheric CO2: first results of a model intercomparison study. Global Biogeochem Cy 12:1–24
43. Scheller S, Goenrich M, Boecher R, Thauer RK, Jaun B (2010) The key nickel enzyme of methanogenesis catalyses the anaerobic oxidation of methane. Nature 465:606–608
44. Kvensvolden KA (1993) Gas hydrates-geological perspective and global change. Rev Geophys 31:173–187
45. Müller J-F (1992) Geographic distribution and seasonal variation of surface emissions and deposition velocities of atmospheric trace gases. J Geophys Res 97:3787–3804
46. Potter CS, Matson PA, Vitonsek PM, Davidson EA (1996) Process modelling of controls on nitrogen trace gas emissions from soils worldwide. J Geophys Res 101:1361–1377
47. Skiba U, Smith KA, Fowler D (1993) Nitrification and denitrification as sources of nitric oxide and nitrous oxide in a sandy loam soil. Soil Biol Biochem 25:1527–1536

48. Khalil MAK, Rasmussen RA (1992) The global sources of nitrous oxide. J Geophys Res 97:14651–14660
49. Machida T, Nakazawa T, Fujii Y, Aoki S, Watanabe O (1995) Increase in the atmospheric nitrous oxide concentration during the last 250 years. Geophys Res Lett 22:2921–2924
50. Kroeze C, Mosier A, Bouwman L (1999) Closing the global N2O budget: a retrospective analysis 1500-1994. Global Biogeochem Cy 13:1–8
51. Samarkin V, Madigan MT, Bowles W, Casciotti KL, Priscu JC, McKay CP, Joye SB (2010) Abiotic nitrous oxide emission from the hypersaline Don Juan Pond in Antarctica. Nat Geosci 3:341–344. doi:10.1038/ngeo847
52. Duscha H, Borchers R, Fabian P, Bischof W (1990) First results of RASMUS: source gases in the mesosphere. Adv Space Sci 10(6):77–81
53. WMO (2007) World Meteorological Organization, Scientific assessment of ozone depletion: 2006. Global ozone research and monitoring project, Report No. 50, Geneva, Switzerland
54. Khalil MAK, Rasmussen RA (1995) The changing composition of the earth's atmosphere. In: Singh HB (ed) Composition, chemistry and climate of the atmosphere. Van Nostrand Reinhold, New York, pp 50–87
55. Zimmerman PR, Greenberg JP, Wandiga SO, Crutzen PJ (1982) Termites-A potentially large source of atmospheric methane, carbon dioxide and molecular hydrogen. Science 218:563–565
56. Houweling S, Dentener F, Lelieveld J (2000) Simulaion of preindustrial atmospheric methane to constrain the global source strength of natural wetlands. J Geophys Res 105:17243–17255
57. Cicerone RJ, Oremland RS (1988) Biogeochemical aspects of atmospheric methane. Global Biogeochem Cy 2:299–327
58. Khalil MAK, Rasmussen RA (1990) Constraints on the global sources of methane and an analysis of recent budgets. Tellus 42B:229–236
59. Holloway T, Levy H, Kasibhatla P (2000) Global distribution of carbon monoxide. J Geophys Res 105:12123–12147
60. Novelli PC, Masarie KA, Lang PM (1998) Distributions and recent changes of carbon monoxide in the lower troposphere. J Geophys Res 103:19015–19033
61. Singh ON, Fabian P (1999) Reactive bromine compounds. In: Fabian P, Singh ON (eds) Reactive halogen compounds in the atmosphere, The handbook of environmental chemistry, vol 4E. Springer, Berlin, pp 1–43
62. WMO (2003) Scientific assessment of ozone depletion: 2002, Global ozone research and monitoring project, Report No. 47. World Meteorological Organization, Geneva, Switzerland
63. Guenther A, Zimmerman P, Wildermuth M (1994) Natural volatile organic-compound emission rate estimates for United States woodland landscapes. Atmos Environ 28:1197–1210
64. Simpson D, Guenher A, Hewitt CN, Steinbrecher R (1995) Biogenic emissions in Europe I: estimates and uncertainties. J Geophys Res 100:22875–22890
65. Arey J, Atkinson R, Aschmann SM (1990) Product study of the gas phase reactions of monoterpenes with the OH radical in the presence of NOx. J Geophys Res 95:18539–18546
66. Geron C, Harley P, Guenther A (2001) Isoprene emission capacity for US tree species. Atmos Environ 35:3341–3352
67. Kesselmeier J, Staudt M (1999) Biogenic volatile organic compounds (VOC): an overview on emission, physiology and ecology. J Atmos Chem 33:23–88
68. Roberts JM, Fehsenfeld FC, Albritton DL, Sievers RE (1983) Measurement of monoterpene hydrocarbons at Niwot Ridge, Colorado. J Geophys Res 88:10667–10678
69. Juuti S, Arey J, Atkinson R (1990) Monoterpene emission rate measurements from a monterey pine. J Geophys Res 95:7515–7519
70. Kesselmeier J, Kuhn U, Wolf A, Andreae MO, Ciccioli P, Brancaleoni E, Frattoni M, Guenther A, Geenberg J, Vasconcellos PD, de Oliva T, Tavares T, Artaxo P (2000) Atmopheric volatile organic compounds (VOC) at a remote tropical forest site in central Amazonia. Atmos Environ 34:4063–4072

71. Finlayson-Pitts B, Pitts JN Jr (2000) Chemistry of the upper and lower atmosphere. Academic, San Diego, CA
72. McDonald RC, Fall R (1993) Detection of substantial emissions of methanol from plants in the atmosphere. Atmos Environ 27A:1709–1713
73. Goldan PD, Kuster WC, Fehsenfeld FC, Montzka SA (1993) The observation of a C5 alcohol emission in a North American pine forest. Geophys Res Lett 20:1039–1042
74. Went FW (1960) Blue hazes in the atmosphere. Nature 187:641–643
75. Pandis SN, Paulson SE, Seinfeld JH, Flagan RC (1991) Aerosol formation in the photo-oxidation of isoprene and beta-pinene. Atmos Environ A 25:997–1008

# Chapter 5
# Human Impact

## 5.1 Stratospheric Ozone Depletion

Martin Dameris

### *5.1.1 Ozone-Depleting Substances*

**Longer-Lived Source Gases** Stratospheric ozone depletion over the past three decades has resulted substantially from anthropogenic trace gas emissions and accumulation of these gases in the atmosphere. This was mostly caused by industrial and to a much less extent to agricultural activities. Consequently concentrations of chlorine, bromine, nitrogen, and hydrogen radicals have significantly increased in the stratosphere. These radicals are produced from longer-lived source gases (e.g. chlorofluorocarbons, CFCs; methane, $CH_4$; nitrous oxide, $N_2O$) which are transported into the stratosphere, because their atmospheric lifetimes are long compared with the transport time into the stratosphere. To protect the ozone layer, the international community of states has signed the Montreal Protocol in 1987 (and amendments thereafter) to ban the most important chlorine- and bromine-containing source gases. Due to the success of these agreements, emissions of these substances have been significantly reduced since the late 1980s. Hence, the global mean surface mixing ratios of the most abundant chlorine- and bromine-containing source gases are declining clearly since the middle 1990s, except CFC-12, which is going down significantly since 2005. Recent measurements show that global mean surface mixing ratios of the three most abundant HCFCs (i.e. HCFC-22, -142b, and -141b) are still continuing to increase (see Chap. 1 in [1]). The 2007 adjustments to the Montreal Protocol are expected to have an obvious impact on HCFC emissions in the coming years (Fig. 5.1).

P. Fabian and M. Dameris, *Ozone in the Atmosphere*,
DOI 10.1007/978-3-642-54099-8_5, © Springer-Verlag Berlin Heidelberg 2014

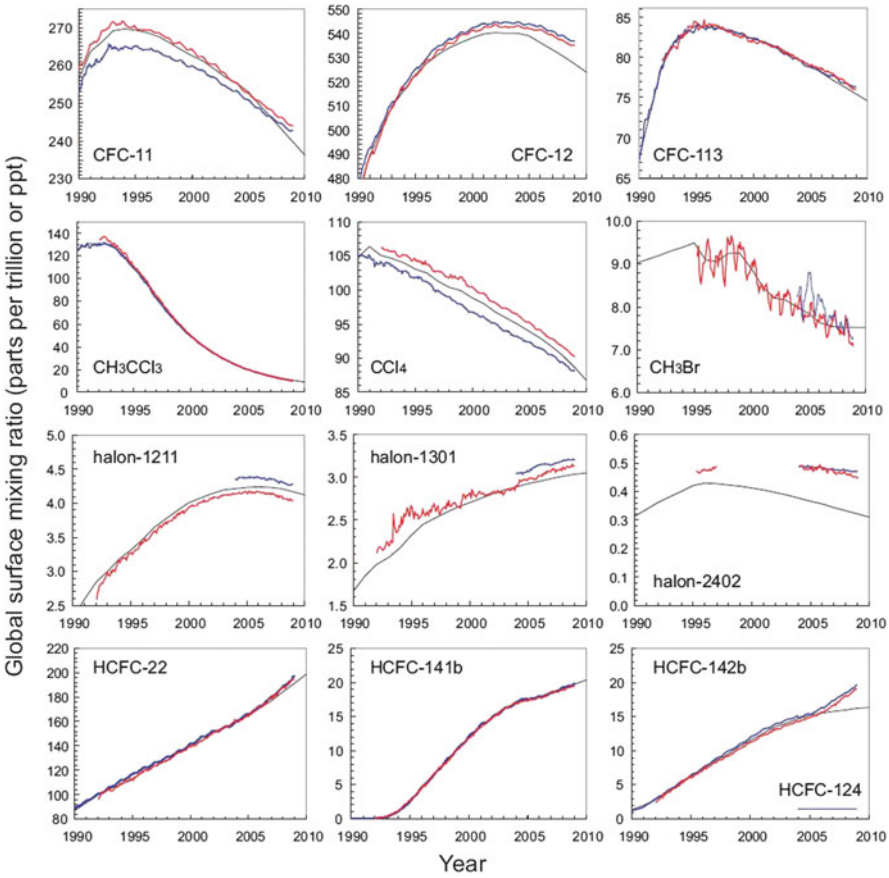


**Fig. 5.1** Mean global surface mixing ratios (expressed as dry air mole fractions in parts per trillion or ppt) of ozone-depleting substances from independent sampling networks and from scenario A1 of the Ozone Assessment (Chap. 1 in [1]) over the past 18 years. Measured global surface monthly means are shown as *red lines* (NOAA data) and *blue lines* (AGAGE data). Mixing ratios from scenario A1 from the previous Assessment (*black lines*) were derived to match observations in years before 2005 as they existed in 2005 [1]. The scenario A1 results shown in years after 2004 are projections made in 2005. Fig. 1.1 in [1]

***BOX*: Halogenated longer-lived source gases**

*Examples of important halogenated longer-lived source gases with relevance for the ozone layer (see Chap. 1 in* [2]):

- *Chlorofluorocarbons (CFCs): $CCl_2F_2$ (CFC-12, lifetime 100 years), $CCl_3F$ (CFC-11, 45 years), $CCl_2FCClF_2$ (CFC-113, 85 years), $CClF_2CClF_2$ (CFC-114, 300 years), $CClF_2CF_3$ (CFC-115, 1,700 years);*

(continued)

- *Hydrochlorofluorocarbons (HCFCs): $CHClF_2$ (HCFC-22, 12 years), $CH_3CCl_2F$ (HCFC-141b, 9.3 years), $CH_3CClF_2$ (HCFC-142b, 17.9 years), $CHClFCF_3$ (HCFC-124, 5.8 years);*
- *Halons: $CBr_2F_2$ (halon-1202, 2.9 years), $CBrClF_2$ (halon-1211, 16 years), $CBrF_3$ (halon-1301, 65 years), $CBrF_2CBrF_2$ (halon-2402, 20 years);*
- *Chlorocarbons: $CH_3Cl$ (methyl chloride, 1 year), $CCl_4$ (carbon tetrachloride, 26 years), $CH_3CCl_3$ (methyl chloroform, 5 years);*
- *Bromocarbons: $CH_3Br$ (methyl bromide, 0.7 years).*

**Halogenated Very Short-Lived Substances** Besides the longer-lived halogenated source gases, in particular short-lived halogenated substances also have to be considered with respect to depletion of the stratospheric ozone layer. So-called very short-lived substances (VSLS) are defined as trace gases whose local lifetimes in the troposphere are comparable to, or shorter than, tropospheric transport timescales. They are considered to be those compounds having atmospheric lifetimes of less than 6 months. Consequently their tropospheric distributions are non-uniform (see Chap. 1 in [1]). The efficiency of VSLS transport into the stratosphere results from the competition between fast vertical transport and chemical destruction or removal via washout of the source gases. That is why the amount of halogen from a VSLS that reaches the stratosphere depends on the location of the VSLS emissions. Conversion of the source gases to other gases, so-called product gases, reduces the efficiency of halogen transport to the stratosphere, for instance, if the product gas is taken up by aerosols and becomes washed out before reaching the stratosphere. So far substantial uncertainties remain in quantifying the full impact of chlorine- and bromine-containing VSLS on stratospheric ozone. Current results suggest that brominated VSLS contribute to stratospheric ozone depletion, particularly under enhanced aerosol loading. Future climate changes may influence the contribution of VSLS to halogen loading of the stratosphere and its influence on stratospheric ozone. Environmental changes in the future could affect both anthropogenic and natural VSLS contributions to stratospheric halogens.

***BOX: Halogenated very short-lived source gases***

*Prominent examples of VSLS affecting ozone chemistry are (see Chap. 1 in* [2]):

- *Chlorocarbons: $CH_2Cl_2$ (local lifetime: 140 days), $CHCl_3$ (150 days);*
- *Bromocarbons: $CH_2Br_2$ (120 days), $CH_2BrCl$ (150 days);*
- *Iodocarbons: $CH_3I$ (7 days), $CF_3I$ (4 days).*

### 5.1.2 Global Ozone Loss

Owing to the effect of catalytic reaction cycles of chlorine and nitrogen, global stratospheric ozone depletion outside the polar regions should be most obvious in the middle and upper stratosphere [3, 4]. Different measurements around the world have confirmed this expectation and with it the causes for the global depletion of the stratospheric ozone layer. For example, in middle latitudes stratospheric ozone content decreased between 35 and 45 km altitude from 1979 to 1995 by about 15 % (Fig. 5.2; [5]). Further analysis has confirmed that the middle and upper stratospheric ozone decline apparent from 1979 until the mid-1990s has stopped and ozone has stabilised since about 1995, depending on the latitude [1].

Representation of recent ozone changes in state-of-the-art chemistry-climate models (grey underlay in Fig. 5.2) is in good agreement with observations, indicating that the atmospheric model systems are considering the most relevant processes determining the evolution of stratospheric ozone content outside the polar regions. This emphasises that our overall knowledge and understanding of processes determining the temporal evolution of global stratospheric ozone are robust.

Taking a closer look at the global ozone loss, it shows obvious regional differences. Since most ozone is produced in the tropics, the global distribution on the one hand depends strongly on the intensity and temporal variability of stratospheric circulation (i.e. transport of ozone); on the other hand, it is determined as well through the spatially variable effect of (temperature dependent) ozone destroying chemical gas-phase reactions. A quasi-global (60°S–60°N) record of total ozone is shown in Fig. 5.3. The annual variation and the 11-year periodical component caused by the solar-activity cycle (i.e. relative ozone maxima detected around 1980, 1991, and 2002; minima around 1985 and 1995) are evident [1, 6]. The annual mean total ozone deviations for 25°S–25°N, 35°N–60°N, and 35°S–60°S latitude bands are presented in Fig. 5.4 for five independent data sets. In middle latitudes of both hemispheres, ozone values in the last few years stabilised at about 3.5 % for the Northern Hemisphere and 6 % for the Southern Hemisphere lower than the 1964–1980 average, with little sign of increase in recent years. In the tropical region a significant long-term reduction of the ozone amount is not detected.

The dominant reason of global ozone depletion is the influence of anthropogenic generated halogen compounds [1, 7]. In addition to chemically induced ozone destroying processes, the recent trend in middle latitudes is affected also by natural events, like large eruptions of volcanoes injecting significant amounts of sulphur into the stratosphere. For example, when the volcano Pinatubo erupted in the Philippines in June 1991, almost 20 million tons of sulphur dioxide ($SO_2$) were transported into the stratosphere. The $SO_2$ was oxidised in the stratosphere, and sulphuric acid droplets formed. In the atmosphere, these droplets have a very similar effect to that of Polar Stratospheric Clouds (PSCs), but with the difference

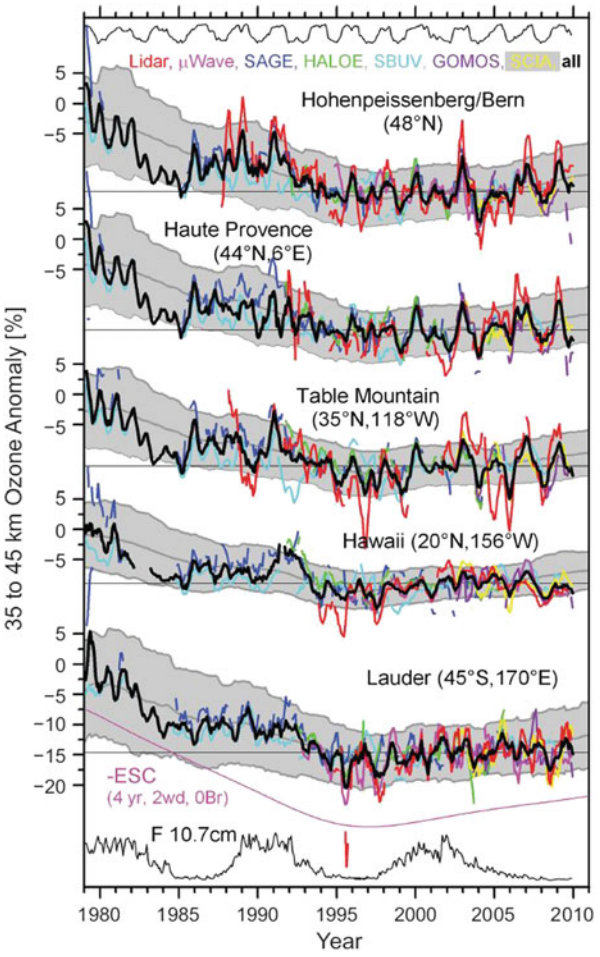


**Fig. 5.2** Ozone anomalies over the 1979 to early 2010 period from different data sets at five NDACC stations. Anomalies are averaged over the 35–45 km range. For details, see Fig. 2.5 in [1]

that the heterogeneous chemical reactions already start at higher temperatures (see Sect. 5.1.3).

In middle latitudes, the negative ozone trend in the 1980s and 1990s was most pronounced in the upper part of the stratosphere (see above). The stratosphere between 20 and 25 km over middle latitudes is another region where a statistically significant decline of about 7–8 % occurred between 1979 and the mid-1990s, followed by stabilisation or a slight (2–3 %) ozone increase thereafter [1]. In the Northern Hemisphere altitude range of about 20 km a distinctive seasonal variation was found, with stronger trends in winter and spring month [8]. They are related to transport of ozone-depleted air masses from the Arctic region (see Sect. 5.1.3) to middle latitudes.

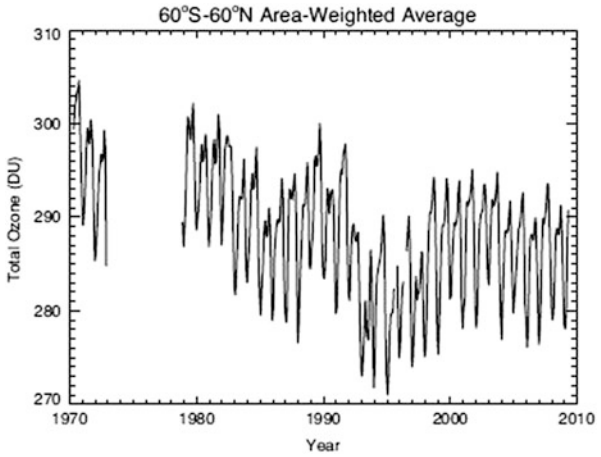


**Fig. 5.3** Quasi-global (60°N–60°S) average of total ozone distribution (Dobson Units, DU) for the period 1970–2009 from the BUV/TOMS/SBUV(/2) merged ozone data set. Figure 2.1 in [1]

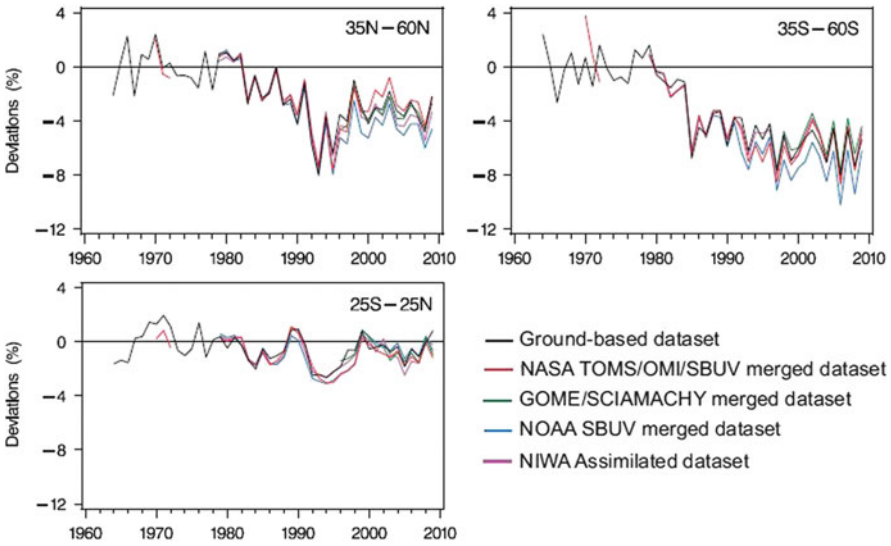


**Fig. 5.4** Annual mean area-weighted total ozone deviations from the 1964–1980 means for the latitude bands 25°S–25°N, 35°N–60°N, and 35°S–60°S, estimated from different global data sets: ground-based (*black*), NASA TOMS/OMI/SBUV(/2) merged satellite data set (*red*), National Institute of Water and Atmospheric Research (NIWA) assimilated data set (*magenta*), NOAA SBUV(/2) (*blue*), and GOME/SCIAMACHY merged total ozone data (*green*). Each data set was deseasonalised with respect to the period 1979–1987. The average of the monthly mean anomalies for 1964–1980 estimated from ground-based data was then subtracted from each anomaly time series. Deviations are expressed as percentages of the ground-based time average for the period 1964–1980. Parts of Fig. 2.2 in [1]

### 5.1.3 Polar Ozone Loss

**Polar Ozone Chemistry and Dynamics** Just like at lower and middle latitudes, ozone can also be depleted via $HO_x$-, $NO_x$-, $ClO_x$-, and $BrO_x$-catalysed cycles in the polar stratosphere. Here it is mainly chemical reactions on the surface of stratospheric ice particles, so-called heterogeneous reactions that are responsible for activating chlorine (or bromine) and then driving it to deplete ozone. This process starts during winter [9, 10]: in the cold lower polar stratosphere, Polar Stratospheric Clouds (PSCs) form during polar night. At typical lower stratosphere conditions with water vapour mixing ratios of about 4.5 mmol/mol and nitric acid mixing ratios of about 10 nmol/mol, PSCs are formed at temperatures below about 195 K (= −78 °C). Nitric acid trihydrate (= NAT; $HNO_3 \cdot 3H_2O$) crystals arise. Under these standard conditions in the lower stratosphere, NAT has an equilibrium temperature that is approximately 7 K higher than that of ice; ice is developing at temperatures below about 188 K (= −85 °C).

The lower stratosphere over the South Pole cools significantly more in winter (June–August) than the north polar stratosphere (December–February). Generally, the polar stratosphere during winter is dominated by a strong west wind vortex, the polar night jet [11]. Owing to different sea-land distribution in the Northern and Southern Hemisphere these wind vortices develop differently into the two hemispheres. Large-scale waves with several hundred kilometres wavelength (planetary waves) are generated in the troposphere, for example, during the overflow of air masses over mountain ridges. These waves propagate upward into the stratosphere and affect the dynamics there including the strength of the polar wind jets. The polar vortex in the Southern Hemisphere is less disturbed; therefore, the mean zonal stratospheric wind speed is stronger than in the Northern Hemisphere. In the Southern Hemisphere this leads to a stronger isolation of stratospheric polar air masses in winter and a more pronounced cooling of the polar stratosphere during polar night. Therefore, the climatological mean of polar winter temperatures of the lower Arctic stratosphere is about 10 K higher than that of the lower Antarctic stratosphere. Whereas the Antarctic stratosphere reaches temperatures below PSC-forming temperatures for several weeks every year, there is a definite year-to-year variability observed in the north polar stratosphere: relatively warm winters (e.g. 2010, 2012; see below) during which hardly any PSCs develop are observed and very cold winters, with conditions similar to that of Antarctica (e.g. 1997, 2011). This means that expansive PSC fields develop in the Antarctic stratosphere every year, but are seldom seen over the Arctic. PSC particles allow heterogeneous reactions to take place on their surfaces, which enables halogen compounds to be released from reservoir compounds (hydrogen chloride, HCl; chlorine nitrate, $ClONO_2$) and then be converted to a chemically more active form. Most important heterogeneous reactions are as follows:

$$\mathrm{ClONO_2(g) + HCl(s) \rightarrow HNO_3(s) + Cl_2(g)}$$
$$\mathrm{ClONO_2(g) + H_2O(s) \rightarrow HNO_3(s) + HOCl(g)}$$
$$\mathrm{HOCl(g) + HCl(s) \rightarrow Cl_2(g) + H_2O(s)}$$
$$\mathrm{N_2O_5(g) + H_2O(s) \rightarrow 2HNO_3(s)}$$
$$\mathrm{N_2O_5(g) + HCl(s) \rightarrow ClNO_2(g) + HNO_3(s)}$$

(herein the notation g: gaseous, s: solid)

After the polar night, when the sun returns in the polar spring, active molecules, such as $Cl_2$ or HOCl, are further converted into reactive Cl and ClO, and ozone depletion begins via the catalytic cycle. However, because of their size and weight, PSC particles (containing $HNO_3$) can sediment out and thus transport nitrogen compounds in the stratosphere to lower layers ('denitrification'). In the following, this reduces the chance of the destructive chlorine compounds being deactivated again shortly after the PSC particles melt. At certain altitudes, both the release and photolysis of gaseous $HNO_3$ and the formation of new $NO_2$ are decreased, which contributes to the deactivation of chlorine monoxide radicals by recombination (mostly via the reaction $ClO + NO_2 + M \rightarrow ClONO_2 + M$; there M is another molecule). The $NO_x$ cycle thus loses importance and the $ClO_x$ cycle accelerates owing to the released chlorine. In the lower polar stratosphere, the efficiency of the $ClO_x$ cycle increases, which is mainly due to the low number of oxygen atoms present under twilight conditions. The cycle does not run via the reaction $ClO + O \rightarrow Cl + O_2$, but rather via the formation of ClOOCl:

$$\mathrm{ClO + ClO + M \rightarrow ClOOCl + M}$$
$$\mathrm{ClOOCl + } h\nu \rightarrow \mathrm{Cl + ClOO}$$
$$\mathrm{ClOO + M \rightarrow Cl + O_2 + M}$$

The ClO dimer (ClOOCl) is photolysed slightly even when the sun is low and it releases Cl atoms, which deplete ozone [12]. As a result, the photolysis of ClO dimers plays a key ozone-depletion role in polar regions.

**The Antarctic Ozone Hole** Unusual low total ozone column values in the polar Southern Hemisphere have been firstly detected by Shigeru Chubachi, who measured low ozone over the Japanese Antarctic station Syowa in October 1982 (see Sect. 7.1). He reported about it at the Quadrennial Ozone Symposium at Halkidiki, Greece, in September 1984. The phenomenon of the Antarctic ozone hole was described in a scientific article first by Farman et al. [13] who analysed respective satellite data; this discovery has prompted considerable effort to develop the scientific basis necessary to understand the cause and effect chain and to model and predict polar ozone loss [10].

A decrease in the total amount of ozone of up to 70 % is seen during the Antarctic spring months of September and October (Fig. 5.5). Particularly in the lower stratosphere, ozone is almost completely depleted during this season. An

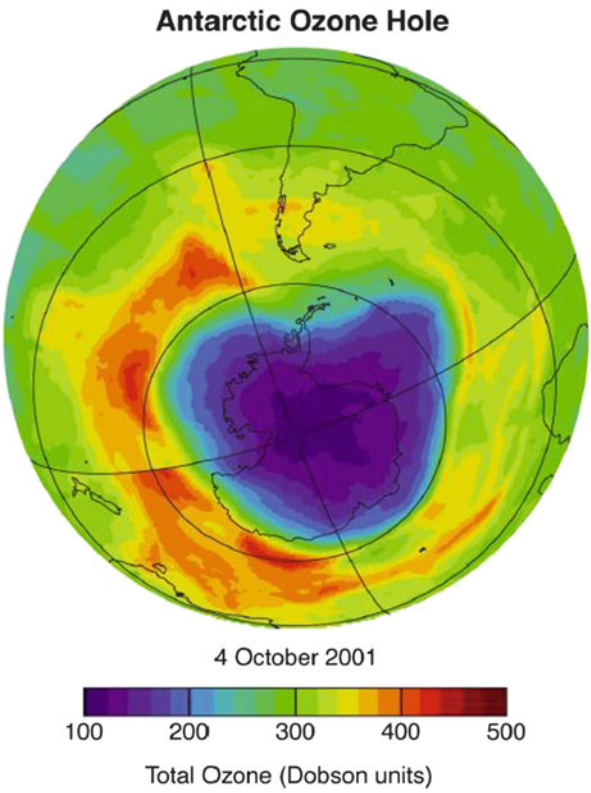


**Fig. 5.5** The ozone hole of the Southern Hemisphere on 4 October 2001

ozone hole is said to exist when the total ozone column sinks to values of less than 220 Dobson Units (DU), which is about 30 % under the norm. Dobson Units are column densities—a measure of the total amount of ozone in a column over a specific place. At standard pressure and temperature (i.e. 1,000 hPa, 0 °C), a 0.01-mm thick ozone layer corresponds to 1 DU. A 300-DU thick ozone layer at the Earth's surface would thus correspond to a pure ozone column of 3 mm.

The Antarctic ozone hole appears each spring since the beginning of 1980s. The seasonal evolution of Antarctic total ozone over the last decades has been mainly controlled by variations in stratospheric temperature and dynamical processes. The continued occurrence of an Antarctic ozone hole is expected because stratospheric chlorine and bromine have increased in recent decades and declined only moderately over the last decade. Relatively shortly after the discovery of the ozone hole, the extreme thinning of the ozone layer in the south polar stratosphere was explained as a combination of special meteorological conditions and changed chemical composition, based on industrially manufactured CFCs and halons (see above). In the years that followed, it became clear that the ozone layer was not just getting thinner over Antarctica, but over many other regions, too, although to a lesser extent (see above).

The springtime averages of total ozone poleward of 63° latitude in the Antarctic region are shown in the lower part of Fig. 5.6 (update of Fig. 2.8 from [1]; see [14]). As noted in the previous paragraph, the stratospheric chlorine burden reached its peak in the late 1990s and has since begun to decrease. During the period of increasing chlorine concentrations, the springtime polar ozone values decreased not only in the Antarctic stratosphere but also in the Arctic stratosphere (see next paragraph). Consistently low values in springtime ozone have been observed since the beginning of 1980s particularly in the Southern Hemisphere (Fig. 5.6 lower part). Inter-annual variability in polar stratospheric ozone abundance and chemistry is driven by variability in temperature and transport due to year-to-year differences in dynamics, which is much less pronounced in the Antarctic stratosphere.

Nevertheless, such dynamic events can be found also in the south polar region, affecting ozone depletion in a significant manner (Fig. 5.7). For example, a particular dynamical situation, the first major sudden stratospheric warming, was detected in the Southern Hemisphere in September 2002, splitting the polar vortex and the ozone hole, which led to remarkable high ozone levels, higher than in previous and in the following years. This major warming was astonishing because it was previously thought they only happened in the Northern Hemisphere, where the tropospheric forced planetary wave activity is much stronger (see above). This unprecedented event induced a clear reduction of the ozone hole area to less than 5 million $km^2$ as compared with more than 25 million $km^2$ in other years.

**Arctic Ozone Depletion** The Arctic polar ozone loss is much more variable (upper part of Fig. 5.6), depending not just on the stratospheric chlorine level but also on whether or not the winter is cold enough and of sufficient length for chlorine-catalysed ozone loss to occur. Because chlorofluorocarbons are long-lived, atmospheric chlorine loading is declining slowly. Obviously ozone depletion in the northern polar stratosphere is not as strong as in the southern polar stratosphere and the trend towards lower ozone amount is much less visible in the 1980s and 1990s. The inter-annual variability is high which can be explained by the variability of stratospheric dynamics (see above). Nevertheless, most clearly seen in years like 1997 and 2011, the dynamic situation of the Arctic stratosphere can be very similar to the Antarctic, i.e. showing a well-pronounced and undisturbed polar vortex in winter with temperatures low enough to form PSCs in large extent. On the other hand, in years like 1998, 1999, and 2010 when stratospheric temperatures are enhanced due to disturbed stratospheric dynamic conditions, total ozone values are much higher (Fig. 5.8).

The largest chemical ozone loss so far observed in the Arctic occurred in spring 2011. The degree of chemical loss was similar to that in early Antarctic ozone holes. This, together with anomalously low dynamical supply of ozone to high latitudes, led to a reduction in total ozone similar to that in Antarctic ozone holes. Column ozone remained higher than in Antarctic ozone holes, however, because of the generally thicker ozone layer in the Arctic compared to the Antarctic. Also, the depleted area was smaller than in Antarctic ozone holes. The exceptional ozone loss in the Arctic spring 2011 arose from particular meteorological conditions:

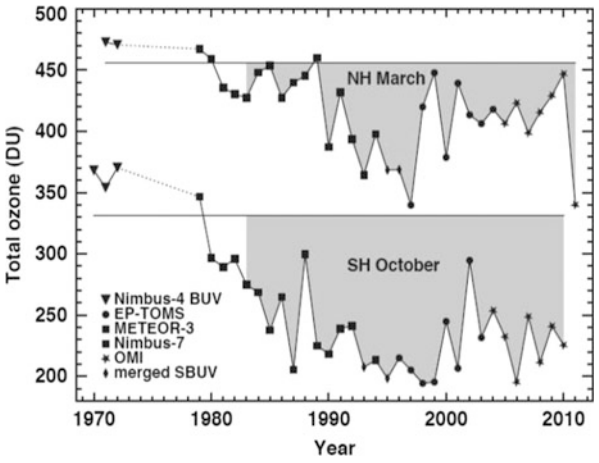


**Fig. 5.6** Total ozone average (Dobson Units) of 63°–90° latitude in March (Northern Hemisphere (NH)) and October (Southern Hemisphere (SH)). *Symbols* indicate the satellite data that have been used in different years. The *horizontal grey lines* represent the average total ozone for the years prior to 1983 in March for the NH and in October in the SH. Update of Fig. 2.8 in [1] which is originally based on Newman et al. [14]

persistent low temperatures and a prolonged and strong polar vortex. These circumstances resulted in a large degree of chemical loss that is well reproduced by state-of-the-art chemical transport model calculations, demonstrating that the respective chemical processes are sufficiently understood.

### *5.1.4 Future Evolution of Stratospheric Ozone*

As a result of the Montreal Protocol and its amendments, tropospheric CFC content has declined since the mid-1990s. Consequently, a slight decrease in stratospheric chlorine concentrations has also been detected for some years now. However, due to the long lifetimes of CFCs in the atmosphere, it will take until the middle of this century for the stratosphere's chlorine content to return to natural background conditions. Therefore, the ozone layer's thickness should build up again in the following decades; the ozone hole over Antarctica should close up with time. However, the speed at which the ozone layer will rebuild in future also depends on a range of other factors. Due to further increasing greenhouse gas concentrations, global atmospheric temperatures are expected to change over the coming decades: the troposphere will continue to warm up (the 'greenhouse effect'; [16]); the stratosphere will cool down further due to radiation effects (see Chap. 4 in [1]).

Owing to climate change, it is highly unlikely that the ozone layer will return to exactly the state it was before the time of increased concentrations of ozone-depleting substances. Exact predictions of the extent of the expected trends are difficult to make, since future emissions of greenhouse gases are uncertain. Furthermore, it must also be taken into account that, due to the expected back-formation of the ozone layer, heating of the stratosphere due to absorption of solar UV radiation by ozone will increase again, to some extent counteracting the intensified cooling due to rising greenhouse gas concentrations. However, as the

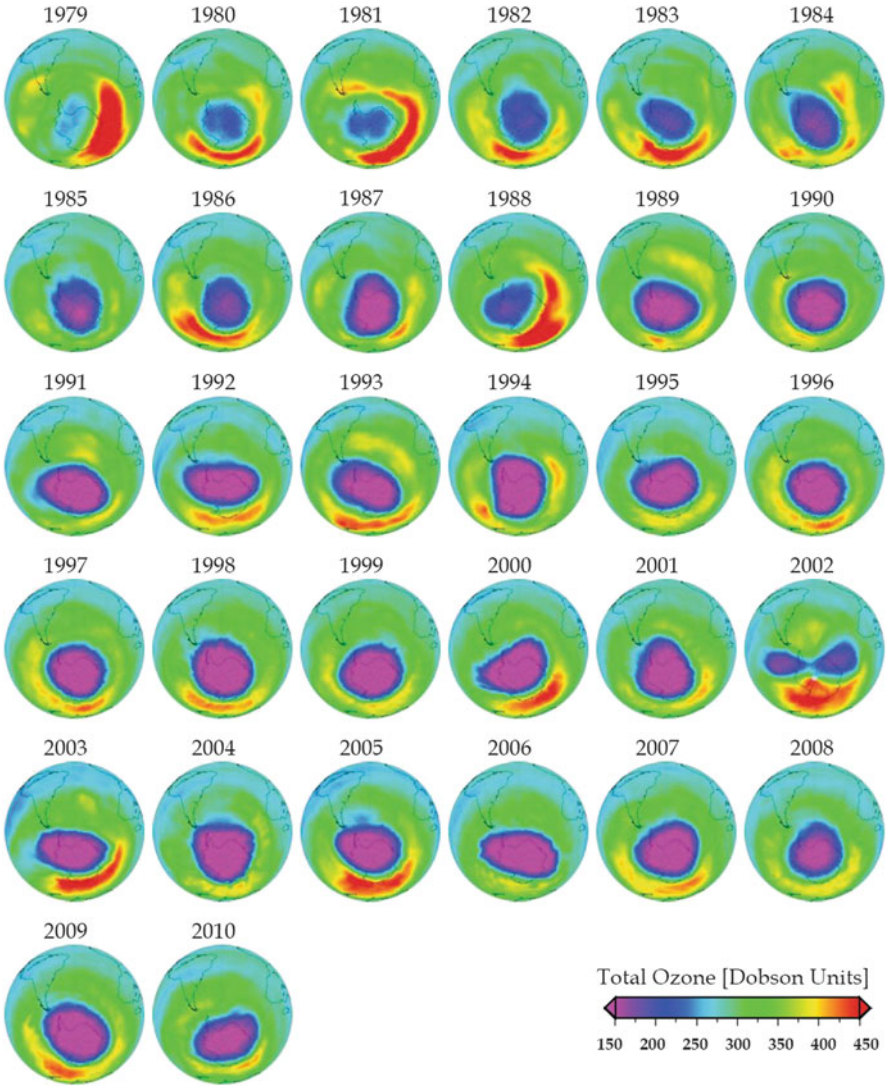


**Fig. 5.7** Evolution of the ozone hole over the Antarctic in early October [15]

ozone concentration depends largely on the background temperature, there will be some feedback. Since climate change also involves a change in stratospheric dynamics, 'dynamic' heating of the stratosphere can also occur, depending on the time of year and place, leading to local heating, rather than cooling. It is obvious that estimates of the future evolution of the stratospheric ozone layer are not trivial and bring uncertainties with them.

Due to these interactions, a further cooling of the stratosphere could, for instance, delay the recovery of polar ozone (because it would increase the

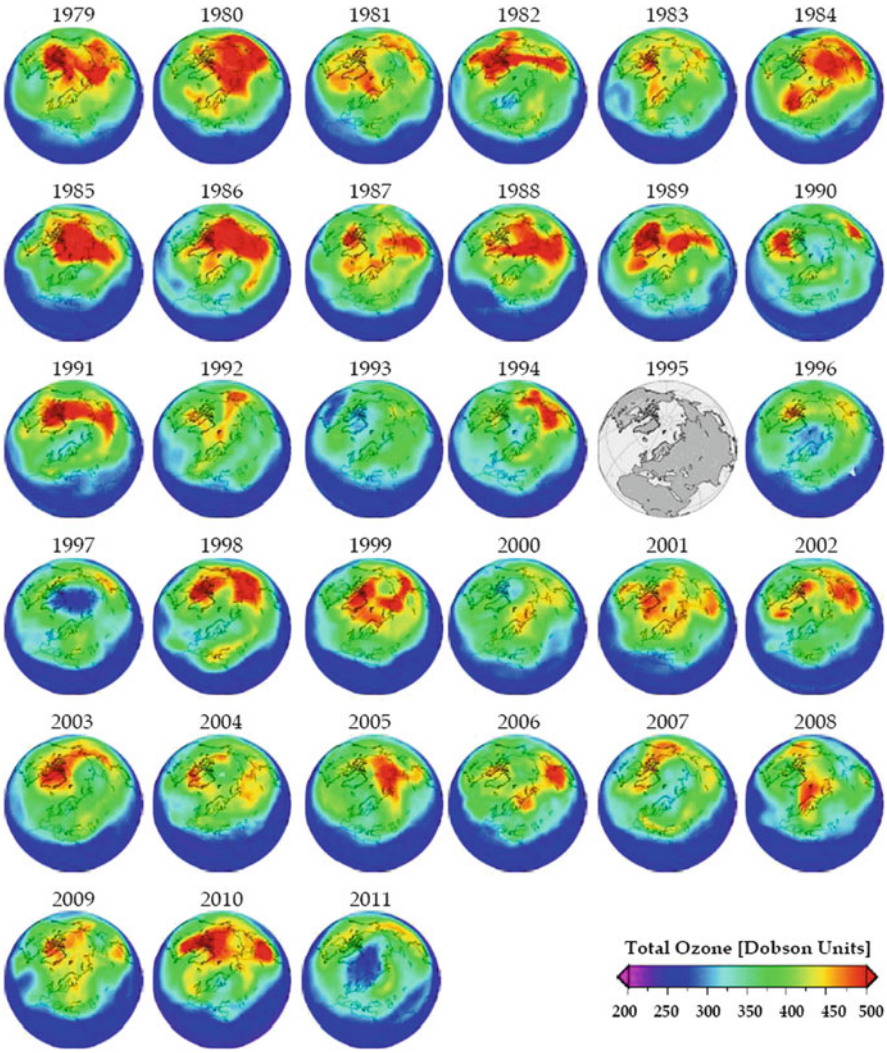


**Fig. 5.8** Evolution of the total ozone column over the Arctic in late March [15]

probability of PSC formation), while the ozone layer could rebuild faster in other areas of the stratosphere (e.g. in the upper stratosphere, where a cooling would slow down ozone destroying chemical reactions).

Changes in climate and the ozone layer can be estimated by means of climate models and Chemistry-Climate Models (CCMs). For example, CCMs consistently show that the ozone layer will build up again in the next decades [17]. Global annually averaged total column ozone is projected to return to 1980 levels before the middle of the century and earlier than when stratospheric halogen loading returns to 1980 levels (see Chap. 3 in [1]). As expected, a continued stratospheric

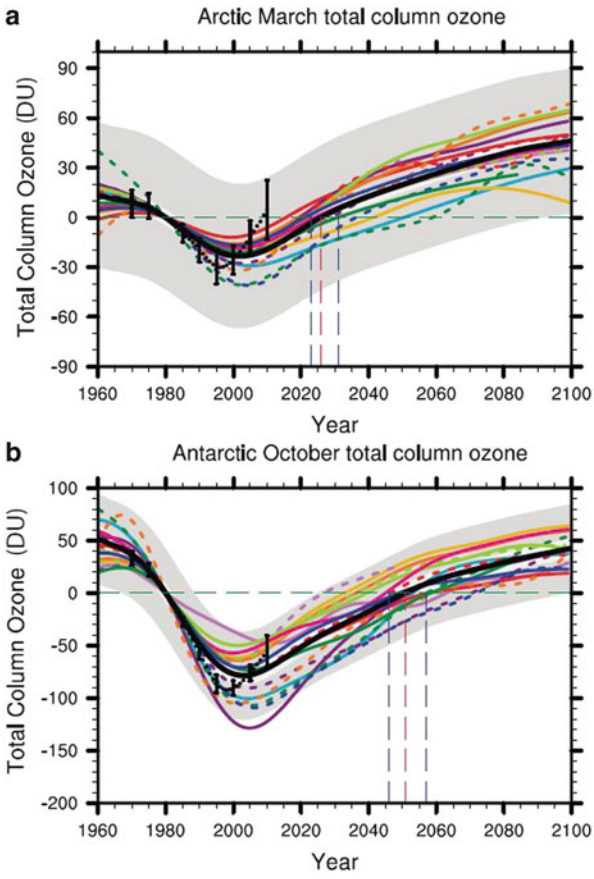


**Fig. 5.9** 1980 baseline-adjusted multi-model trend estimates of annually averaged total column ozone (in DU) for (**a**) the Arctic (60°N–90°N) in March and (**b**) the Antarctic (60°S–90°S) in October (see Chap. 3 in [1])

cooling will result in faster rebuilding of ozone in the middle and upper stratosphere. In the lower polar stratosphere, the re-creation of the ozone layer will slow down during spring, particularly in the Antarctic stratosphere (Fig. 5.9).

Due to climate change, it seems possible that the thickness of the ozone layer could exceed that of earlier years from then on. The results of the CCM simulations are consistent in this conclusion.

Prognostic studies regarding the future evolution of the ozone layer contain a number of uncertainties. Some of them arise from the numerical models themselves. Others result from insufficient knowledge about the future evolution of stratospheric constituents, like the chemically active greenhouse gas water vapour ($H_2O$) and nitrous oxide ($N_2O$).

For example, it is expected that tropospheric $H_2O$ concentrations will increase with rising tropospheric temperatures. This could enhance the amount of $H_2O$ being transported into the lower tropical stratosphere. Stratospheric $H_2O$ concentrations would also increase with rising methane ($CH_4$) concentrations (due to the oxidation of $CH_4$). Higher stratospheric $H_2O$ concentrations could increase the amount of

hydroxides ($HO_x$) in the stratosphere, which, in turn, would affect ozone depletion. Moreover, more $H_2O$ in the polar stratosphere would enhance the PSC-forming potential. Since $H_2O$ is also a key greenhouse gas, changes in its stratospheric concentration would influence the radiation balance of the stratosphere.

A further rise in atmospheric $N_2O$ concentrations (e.g. due to the production and use of artificial fertiliser) would increase the amount of nitrogen oxides ($NO_x$), decreasing the ozone content of the middle and upper stratosphere [18].

### *5.1.5 Impact of Aviation*

Aviation alters the composition of the atmosphere globally and could thus drive changes in climate and chemical composition, particularly the amount of ozone.

Emissions of $NO_x$ by aviation result in the formation of tropospheric ozone via atmospheric chemistry, a climate warming gas. Furthermore, aircraft $NO_x$ emissions result in the destruction of ambient methane ($CH_4$), also via atmospheric chemistry, which is accompanied by a loss of tropospheric ozone [19]. For instance, simulations with a coupled Chemistry-Climate Model (CCM) indicated that the 1990 aircraft $NO_x$ emissions contributed substantially to the Northern Hemisphere $NO_x$ (30–40 %) and ozone (3–4 %) tropospheric burdens [20, 21]. Ozone production rates are enhanced by air traffic $NO_x$ emissions in the mid- and upper troposphere, whereas ozone loss rates are increased in the lower troposphere. Sensitivity studies showed that feedback processes between chemical species and dynamics are not altered significantly by air traffic.

$NO_x$ emissions from current subsonic aviation do not appear to contribute towards ozone depletion in the stratosphere [20, 22].

In terms of a possible future supersonic aviation fleet flying in the stratosphere, the effects of emissions of $NO_x$ have been investigated for a considerable period of time. $NO_x$ emission of high flying supersonic aircraft results in destruction or increase of stratospheric ozone via atmospheric chemistry, depending critically upon the altitude of the emission: the 'crossover' point between ozone formation and destruction occurs at the height of approximately 16 km; above about 20 km, atmospheric models always predict ozone destruction [22].

## 5.2 Tropospheric Ozone Increases

Peter Fabian

### 5.2.1 Photochemical Smog

The term smog was coined at the end of the nineteenth century to classify the yellowish mixture of soot containing exhaust (smoke) and fog which took pains with the population of London at that time. This kind of air pollution also called London pea-soup was caused by the intensive emission of sulphur dioxide ($SO_2$) and soot from burning coal rich in sulphur. While the soot particles increased the tendency for fog formation which is high in that region, especially during winter months, $SO_2$ was dissolved in the fog droplets. Thereby, sulphurous acid ($H_2SO_3$) was formed which, within a chain of reactions, ends up as sulphuric acid ($H_2SO_4$). Through legislative actions the burning of sulphur containing coal has been banned in London and elsewhere, and thus the London type or winter smog is a phenomenon of the past, at least in this part of the world. Today, it is largely observed in China, where coal still is the major energy source.

Today the term smog is generally used for a photochemical phenomenon which, contrary to the London winter smog, is driven by solar radiation and thus is mostly confined to summer conditions. This photochemical or summer smog occurs when mixtures of oxides of nitrogen ($NO_x$), carbon monoxide (CO), and/or hydrocarbons (VOCs) are exposed to intense solar radiation. Thereby oxidising substances are formed, in particular ozone. The precursor substances from which photochemical smog is formed originate almost exclusively from burning processes. In urban and densely populated areas, automobile exhaust, domestic burning, and industry are the main sources, while in more remote regions agriculture and biomass burning often provide precursors for photosmog.

The end product of burning carbon containing fuel is carbon dioxide ($CO_2$), but, depending on the reaction conditions, a variety of unburnt hydrocarbons and carbon monoxide are released. The higher the reaction temperature, the more complete is the combustion and the more oxides of nitrogen ($NO_x$) are emitted, provided that oxygen is not limited.

The ozone formation in photosmog conditions is initiated by the photolysis reaction of $NO_2$

$$NO_2 + \text{light}(\lambda < 420\,\text{nm}) \rightarrow NO + O,$$

whereby atomic oxygen is released which, like in the stratosphere, reacts with $O_2$ forming $O_3$:

$$O + O_2 + M \rightarrow O_3 + M,$$

with M being a third-body collision partner.

Since the products of these reactions, NO and $O_3$, react rapidly with each other according to the ‘titration reaction’:

$$NO + O_3 \rightarrow NO_2 + O_2,$$

whereby ozone is removed again. Thus the abundance of $NO_x$ alone leads to low ozone levels only given by the equilibrium:

$$[O_3] = j[NO_2]/k[NO],$$

wherein $j$ and $k$ denote the rates of the photolysis of $NO_2$ and the titration reaction, respectively. As the anthropogenic emission of $NO_x$ generally occurs as NO, the titration reaction tends to lower existing ozone levels.

By CO and/or volatile hydrocarbons (VOCs), however, which generally are present in the mixture of precursor substances as well, the ozone equilibrium is shifted to higher levels, because their oxidation by OH leads to the formation of peroxides that bypass the titration reactions, i.e. convert NO to $NO_2$ without consuming $O_3$:

$$CO + OH \rightarrow H + CO_2$$
$$H + O_2 + M \rightarrow HO_2 + M$$
$$HO_2 + NO \rightarrow NO_2 + OH$$

and

$$RH + OH \rightarrow R + H_2O$$
$$R + O_2 + M \rightarrow RO_2 + M$$
$$RO_2 + NO \rightarrow NO_2 + RO$$

(herein the notation of VOCs by their group R is used. For instance in the notation of ethane ($C_2H_6$) as RH the group R is $C_2H_5$).

Thus the oxidation of CO to $CO_2$ initiates a cycle in which not only NO is converted to $NO_2$, but also $HO_2$ to OH. Likewise the oxidation of RH to $H_2O$ leads to a cycle in which, besides the conversion of NO to $NO_2$, peroxy radicals $RO_2$ are converted to aldehydes RO. The interplay of these cycles is schematically shown in Fig. 5.10. Thereby the decisive process is the photolysis of $NO_2$ providing O for the production of $O_3$, while CO and/or RH are the 'fuel' for the buildup of higher ozone concentrations.

Besides ozone, other substances are built up in photochemical smog episodes. From peroxy radicals aldehydes are formed whose organic groups are reduced by 1 compared to the group of the respective VOCs. Thus from $CH_4$ formaldehyde ($CH_2O$), from $C_2H_6$ acetaldehyde ($CH_3CHO$) is formed, etc. Aldehydes are relatively instable compounds readily reacting with radicals such as OH. The three-step decay reaction of acetaldehyde with OH and reaction with $NO_2$ lead to the formation of peroxy acetyl nitrate ($CH_3COO_2NO_2$). Peroxy acetyl nitrate is the most important representative of the peroxy acyl nitrates known as PANs. PAN

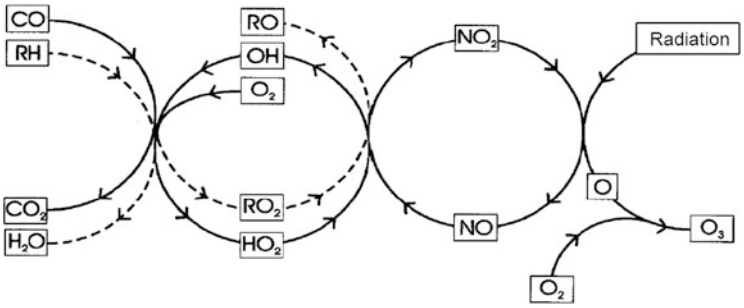


**Fig. 5.10** Schematics of the photochemical smog cycles. The photolysis of $NO_2$ providing atomic oxygen for the ozone formation (*right*) is decisive. Significant ozone levels, however, can only be built up when CO and/or hydrocarbons (RH) are present as well, which, being oxidised by OH to $HO_2$ and $RO_2$, respectively, serve as 'fuel' for photosmog

compounds are among the most instable and reactive substances that occur in photochemical smog.

Almost all VOCs contribute to photochemical smog formation, alkanes, alkenes, olefins, alcohols, and aromatics. Within every group the ozone formation potential increases with increasing reactivity towards OH, thus with increasing order. But also hydrocarbons from biogenic sources such as isoprene and several terpenes can contribute to photochemical smog [23, 24]. That way trees, whose natural VOC emission under clean air conditions leads to $O_3$ reduction, become $O_3$ producers when $NO_x$ levels are increased [25].

Many of the radicals formed in photosmog are attached on aerosol surfaces causing aerosol particles to grow. Furthermore, from the gas phase, new particles can be formed. Thus, besides elevated ozone and PAN concentrations, turbidity and reduced visibility are typical features observed during photochemical smog episodes. As an example, the brownish cloud of particles formed over the city of Los Angeles during a summer smog episode is shown in Fig. 5.11.

Typical diurnal variations of precursors, NO, $NO_2$, and CO, photochemical products, $O_3$ and PAN, and the global radiation observed during a photosmog episode in Athens are displayed in Fig. 5.12. The morning rush hour is characterised by the high CO and NO peaks. $NO_2$ increases with delay, $O_3$ for the titration of NO is mixed down from higher levels, and no $O_3$ is measurable at ground level. With sunrise (radiation curve) ozone and PAN begin to rise, while NO is converted to $NO_2$. Maximum values of $O_3$ and PAN occur around noon. In the afternoon, ozone production decreases with decreasing radiation, and ozone destroying processes progress. The cooling after sunset blocks the mixing with higher layers, and the remaining $O_3$ is destroyed during the night. During darkness, $HNO_3$ and $HNO_2$ are formed from $NO_2$ and VOCs (not shown here), which at sunrise are the first photochemical source of OH through which the diurnal cycle is driven again.

With respect to the precursor concentrations the photochemical ozone formation is a highly non-linear process, which predominantly depends on the VOC/$NO_x$ ratio. Urban regions and other areas of high traffic are usually characterised by $NO_x$

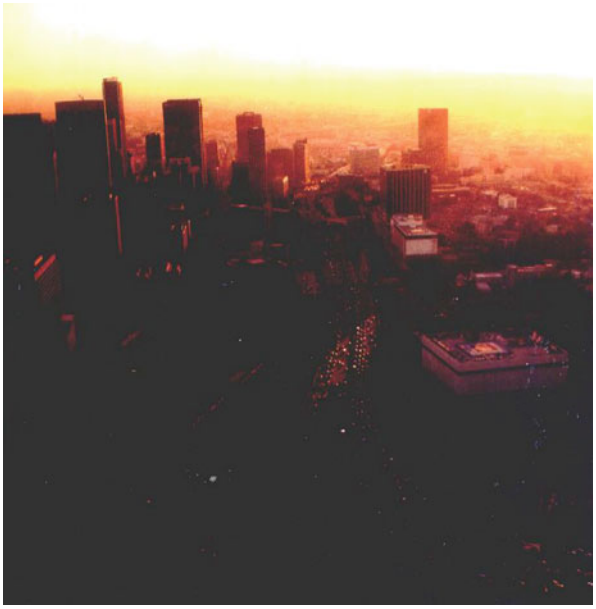

**Fig. 5.11** Photochemical smog over Los Angeles

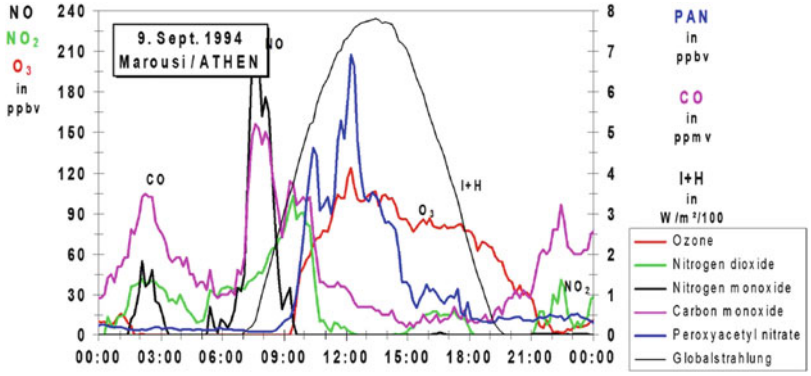


**Fig. 5.12** Typical diurnal variations of global radiation (I + H), precursors NO, $NO_2$, and CO, and the photosmog products $O_3$ and PAN in city air (Athens), after P. Suppan unpublished data

surplus, whereby the ozone production is largely controlled by the VOC emission. In these areas $NO_x$ increases tend to reduce ozone, while $NO_x$ decrease increases the ozone level. This is because $NO_x$ is largely emitted as NO which, by the titration reaction, is converted to $NO_2$ by using up ozone. The $NO_2$ thereby formed is 'potential ozone', which via the slower cycles shown in Fig. 5.10 is converted to ozone downwind at the transition from the VOC-limited to the $NO_x$-limited region. Depending on wind velocities and the distribution of the anthropogenic sources this

happens somewhere between 30 and 100 km downwind. Generally the $NO_x$ emissions of an urban source determine how much ozone is formed in the wake. While through titration every NO molecule can destroy not more than one ozone molecule, four ozone molecules per $NO_x$ molecule are formed downwind [26]. On the other hand, the VOC emissions in the urban centre determine how many ozone molecules are initially formed there. Especially in these VOC-limited regions biogenic VOC emissions from trees can be surprisingly efficient. Studies from Los Angeles [26] and Atlanta [23] show that biogenic emissions are responsible for about 30 % of the photochemical ozone level there.

### *5.2.2 Photosmog in Megacities*

Photochemical smog was first observed during the 1950s in the Los Angeles metropolitan area. A high density of automobile traffic, suitable meteorological conditions, and intense radiation made this area prone to extreme photosmog formation, long before photochemical ozone production was observed elsewhere in the world, and the term 'Los Angeles smog' became a synonym of photochemical smog.

The Los Angeles basin, exposed to the inflow of cool air from the Pacific Ocean in the west, is surrounded by a half cycle of mountains. The cool air causes the warm city air to rise, whereby an efficient inversion forms on most days of the year. This inversion cutting off the exchange with the higher atmosphere acts, in connection with the mountain barrier, like a cover on top of a reaction vessel, in which pollutants can accumulate over long periods and undergo photochemical reaction cycles driven by the intense solar radiation [27].

During the 1960s and 1970s, before significant emission regulations existed, the air quality in most parts of the Los Angeles area was quite bad, especially during the summer months. Ozone mixing ratios of up to 500 ppb were common, and aldehydes often exceeded these levels. A typical diurnal variation of photosmog components observed during these years is displayed in Fig. 5.13: During the morning rush hours NO increases to about 150 ppb. Although intense traffic continues, NO decreases due to its reaction with $HO_2$ forming $NO_2$. Around 8.00 a.m. the maximum $NO_2$ level is reached. At that time solar radiation is intense already, so that $NO_2$ photolysis leading to O and $O_3$ formation dominates the $NO_2$ production from NO. After 8.00 a.m. $NO_2$ decreases although traffic emissions continue until the end of the morning rush (around 9.00 a.m., maximum of the hydrocarbon level). Ozone is built up to a broad maximum which is reached in the early afternoon hours (after [29]).

Figure 5.14 shows a map of the Los Angeles metropolitan area with air monitoring stations and isolines of the number of days of 1980, when 1-h ozone averages exceeded the old California state standard of 100 ppb [30].

The new standard of 90 ppb for 1-h exposure was introduced 2010. With 175 the highest number of days and thus the highest ozone levels are documented in the area

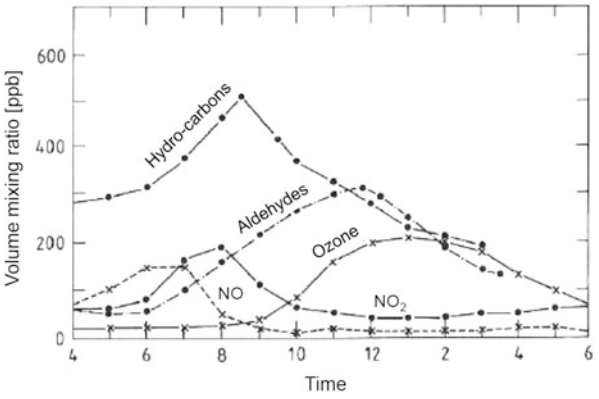


**Fig. 5.13** Typical diurnal variation of photosmog constituents observed in Los Angeles before the introduction of strict emission regulations (after [28])

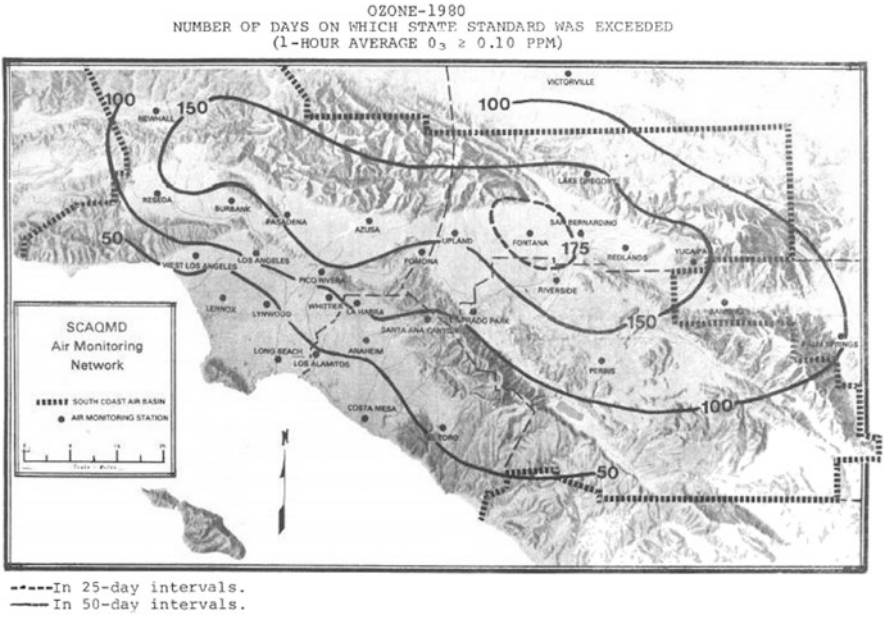


**Fig. 5.14** Los Angeles metropolitan area with air monitoring stations 1980. Isolines of the number of days on which the old state standard of 100 ppb 1-h average was exceeded [28]

of Fontana, about 50–60 km downwind of the area of the highest emissions, an axis reaching from Burbank over downtown Los Angeles further South-Eastwards towards Anaheim, which clearly shows the aforementioned effect of the NO titration reaction. Even in the area of Palm Springs, a desert oasis with little traffic

more than 100 km towards the East, ozone levels of more than 100 ppb were observed on 100 days of 1980.

Since efficient emission regulations were introduced in the 1980s, the air quality in the Los Angeles area has improved significantly. While maximum ozone levels in 1980 still were around 400 ppb, today about 170 ppb are not exceeded any more [31]. This still is a high burden but nevertheless a great achievement given the fact that the number of vehicles operating in this area has increased during this time to more than eight Million. It is fair to state that without the introduction of the three-way catalyst systems which reduce $NO_x$, CO, and hydrocarbons in the exhaust by about 90 %, many parts of the Los Angeles basin would not be habitable any more.

Photosmog and related higher ozone levels turned out to be common in many other metropolitan areas. Ozone levels of more than 100 ppb have been reported from London [32], Paris [33], Munich [34], Athens [30], Santiago de Chile [29], Mexico City [35], and Taipei [36], just to mention a few well-documented mega-cities. Due to the titration reaction, the highest ozone levels are generally not observed in the centres of these cities but rather 30–100 km downwind. There, due to $NO_x$ limitation, ozone is stable and not decomposed during the night, and thus the ozone burden in these 'clean air regions' downwind of the cities is much larger than in the centres where precursor emissions are highest. This is very well documented for the city plumes of New York City [37], Athens [30], and Santiago de Chile [29].

A land-sea circulation system prevailing in the Athens area during many days of the year carries the city plume inland towards popular residential areas in the North during daytime. Compared to the city centre, these are exposed to more than twice the ozone levels [30].

A similar situation is reported from Santiago de Chile where, due an efficient mountain-plain circulation, the city plume is carried towards the popular Las Condes residential areas in the Northeast during daytime, where ozone levels are highest accordingly [29].

Thus, ozone not destroyed in the city plumes is relatively stable, with lifetimes from days to weeks. This 'net ozone' escaping the pollution centres adds to the free tropospheric ozone level, an example of which is shown in Fig. 4.4. Here the main pollution centres are discernable, but they all contribute to the ozone level elevated almost everywhere on the Northern Hemisphere.

### *5.2.3 Biomass Burning*

Forest fires have been common as long as there are forests on Earth. They were caused by lightning and served, by mineralization of the biomass, to restore the respective ecosystem from time to time. Today, forest fires occasionally are ignited by lightning, too, but the vast majority of such fires are caused by man: by negligence in throwing away cigarette stubs and, in most cases, with the intention to remove the forest and use the ground for other purposes.

More than 80 % of the presently destroyed biomass is lost in the tropics; the main causes of this forest clearing by fire are the need for agriculture and pasture land and for building roads and settlements. Forest fires also occur outside the tropics, and the burning of straw and other remains of agricultural produce contributes to global biomass burning as well. Almost everywhere in the World the forested areas have been shrinking as a result of human activities. Between 1850 and 1980 the global forest area decreased from 59 to 50 million $km^2$, and since then about 200,000 $km^2$/year have been destroyed, mostly in the tropics [38].

By far the dominant product of biomass burning is $CO_2$ which thereby re-enters the atmospheric pool, an estimated amount of 3.7 Billion tons of $CO_2$ every year, equivalent to about 1 Billion t C/year. The global carbon cycle which has to cope with 6 Billion t C/year from the burning of fossil fuels thus is disturbed by a total of 7 Billion t C/year (see Sect. 4.4.2).

Besides $CO_2$, a vast variety of other substances originate, such as CO, $H_2$, $N_2O$, NO, $CH_3Cl$, COS, and HCN, as well as aerosol particles, mostly organic carbon particles and soot [39].

Furthermore, oxides of nitrogen are produced, like in any other open combustion process, in the heat of the fire. Thus biomass burning has a fourfold environmental impact:

1. It is a source of atmospheric trace gases and thus influences the biogeochemical C-, N-, and S-cycles as well as the budgets of several halogens (see Sect. 4.4).
2. Some of the emitted gases are greenhouse gases and thus have an impact on the climate system.
3. The pyrogenic aerosols enhance the albedo and thus induce a regional cooling.
4. Some of the emitted gases are precursors for photochemical ozone production.

Depending on the burning material and the burning conditions the composition of the products in the plume varies considerably. Table 5.1 illustrates that open flames with almost complete combustion lead to relatively low emission fractions of CO, VOCs, and particles, whereas smouldering fires reduce the $CO_2$ fraction and emit more CO, VOCs, and particles. Thus a global quantification is difficult and can only be a general guideline. Based on measurements carried out in Brazil, the total amount of VOCs and CO produced by biomass burning was estimated to 60 Million t C/year and 800 Million t C/year, respectively [39]. These are significant contributions to the global budget of these substances (see Sect. 4.4).

Several field campaigns have been carried out to investigate the effects of extended forest fires. Measurements during the SAFARI 92 campaign in South Africa [41] for instance showed that the array of VOCs comprises a variety of alkanes and alkenes, oxygenated and unsaturated compounds such as aldehydes, organic acids, and alcohols. Another substance typical for biomass burning is hydrogen cyanide (HCN). The simultaneous emission of $NO_x$, with $NO_x$/CO ratios varying between 0.02 and 0.10, makes the plume a highly reactive mixture of precursors for the formation of ozone and other photosmog products. Photochemically produced ozone in the plume of tropical vegetation fires in central South America, investigated by aircraft measurements, is documented in great detail

**Table 5.1** Emission factors of biomass burning for different conditions in gC/kg. NMHC is the sum of all VOCs except $CH_4$, from [40]

| Material | $CO_2$ | CO | NMHC | $CH_4$ | Particles | C-particles total | Soot |
|---|---|---|---|---|---|---|---|
| Pasture grass | 927 | 56 | 6 | 3.1 | 16 | 11.5 | 1.3 |
| Steppe | 928 | 57 | 7 | 3.7 | 9.6 | 6.6 | 1.0 |
| Forest (flames) | 913 | 60 | 7 | 7.9 | 16 | 10.2 | 1.1 |
| Forest (smouldering) | 831 | 120 | 17 | 125 | 26.6 | 19.4 | 1.5 |

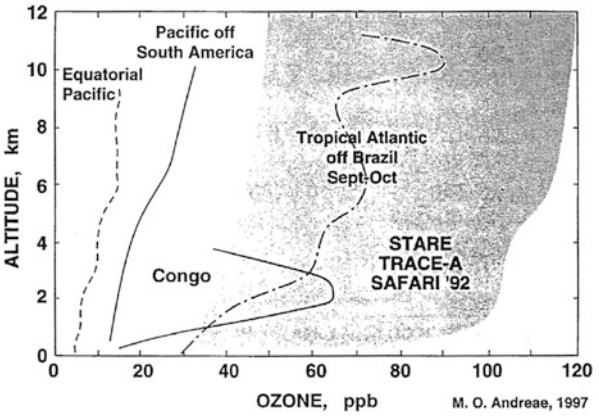


**Fig. 5.15** Enhanced ozone over wide areas of the tropics resulting from biomass burning [43]

[42]. The photochemical ozone production was shown to have occurred over the entire Cerrado region in central Brazil (Fig. 5.15).

The ozone plume resulting from biomass burning in tropical South America has even been shown to reach far out to the eastern Pacific Ocean [44]. Likewise, photochemically produced ozone from large-scale vegetation fires in southern Africa [41] has been shown to reach out to the adjacent southern Atlantic Ocean [45, 46]. Thus the impact of intensive biomass burning affects large regions.

Forest fires are an important source for halogen compounds, too. Among the emitted methyl halides, $CH_3Cl$, $CH_3Br$, and $CH_3I$, $CH_3Cl$ generally dominate, and $CH_3Cl/CO$ ratios of $(86...520) \times 10^{-6}$ have been documented for bush and forest fires in California [47]. Globally, about $640 \times 10^3$ t Cl/year are estimated to be emitted as $CH_3Cl$. Thus biomass burning constitutes an important source of methyl chloride (see Sect. 4.4). Besides, smaller amounts of dichloro methane ($CH_2Cl_2$) and chloroform ($CHCl_3$) are emitted [48].

Furthermore, forest fires emit $N_2O$, another important greenhouse gas. Lab experiments show that for well-inflamed fuels about 0.7 % of the nitrogen contained in the biomass is oxidised to $N_2O$ [49], from which a global source of $2.7 \times 10^5$ tN/year can be estimated, about 2 % of all global sources. From direct measurements close to forest fires in Canada biomass burning was found to even contribute up to 7 % to the global $N_2O$ sources [50].

The tropics are the zone of lowest ozone layer thickness and highest solar elevation and thus highest solar UV-B radiation fluxes worldwide. As the warm

tropical troposphere contains more water vapour than found anywhere else on the globe, the production of OH radicals and thus the oxidation capacity are highest (see Sect. 4.3.1). Therefore, the mixture of substances in the plume of tropical fires meets ideal conditions for the formation of ozone and other photosmog products. During rainy periods, when forest fires are more or less absent, tropospheric ozone levels vary around 10–20 ppb at most. With the onset of fires in the dry season ozone levels rise significantly, and 100 ppb and more have been measured in central Africa as well as Brazil [51, 52]. These ozone plumes can reach up to 5 km altitude and hundreds of km horizontally. Likewise, CO abundances which during the rainy season generally are below 100 ppb rise, with the onset of the fires, up to 700 ppb. Model calculations show that about 25 % of all ozone contained in the planetary boundary layer over Africa originates from biomass burning. A large fraction of it is carried by winds to other regions. Globally, biomass burning has been estimated to contribute about 9 % to all ozone found in the troposphere [53].

Extremely intensive forest fires were observed during the 1997/1998 El Nino event, the strongest reported ever. In Indonesia alone, about 100,000 $km^2$ dense forest were ablaze, and dense smoke plumes with low visibility dominated the entire region between Indonesia and North Australia for months. During September and October of 1997, extreme loads of airborne particles, up to 4,000 $\mu g/m^2$, were measured in several cities of that region [54]. Extreme CO fractions in the ppm range and high $NO_x$ served as precursors for effective photosmog formation. Interestingly, ozone levels were found to be quite low close to the dense clouds, hardly exceeding 20 ppb. Obviously, attenuation of solar radiation by the clouds prevented photochemistry. Likewise, ozone may have been destroyed on the surface of the aerosol particles, especially soot. Enhanced ozone levels of 80 ppb and more were found in regions of less cloud density [55]. After all, the photochemical ozone production was so effective that between August and November 1997 data of the satellite-borne TOMS instrument persistently showed total ozone enhancements of up to 30 DU that were interpreted as tropospheric ozone increases. Given the fact that the undisturbed tropospheric ozone column in that region amounts to about 20 DU, this disturbance favoured by the intense El Nino caused a doubling of tropospheric ozone for several months [56, 57].

### *5.2.4 Global Impact: Present Tropospheric Ozone Distribution*

The impact of the Indonesian fires could be followed by satellite instruments all the way to India. TOMS data clearly showed how the layers rich in ozone, gradually decoupling from the smoke layers below, were carried by the tropical easterlies well over the Indian subcontinent [57]. Spectroscopic measurements carried out on top of Mauna Loa/Hawaii showed, between September and November of 1997, significant spikes of CO, $C_2H_6$, as well as HCN, a typical substance originating in

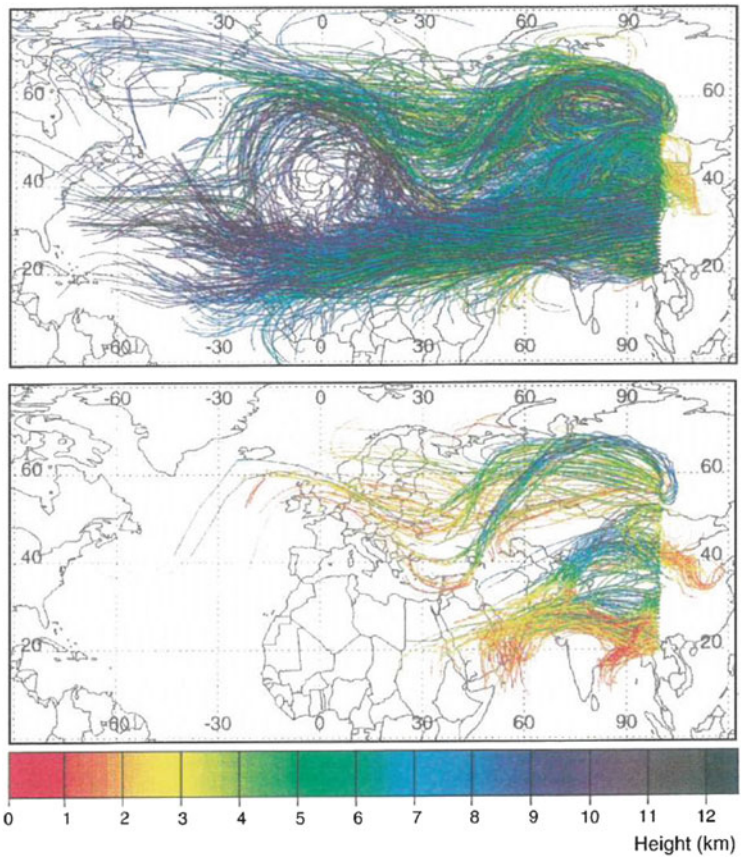


**Fig. 5.16** Back trajectories for 5 days, computed for a fictive 'wall' at 100° East, for March 1997. The trajectories in the *upper panel* start at altitudes above 2.5 km and those displayed in the *lower panel* below 2.5 km. The *colour scale* at the *bottom* shows the heights passed by the air parcels before reaching the 'wall'. After [60]

biomass burning. By means of trajectory analyses these spikes could be proven to originate from the forest fires in Indonesia [58].

Another interesting example is the tropical mountain forest on the eastern slopes of the Andes. This ecosystem was found to depend almost exclusively on nutrients carried in by long-range transport: products of biomass burning in Brazil, ocean spray, and even Sahara dust [59].

Thus the dispersion of photosmog products and other pollutants really has global dimensions. Especially in the tropics this is favoured by high reaching convection carrying, within shortest time, pollutants to higher layers where strong winds provide rapid horizontal transport. That way, photosmog pollutants, whose concentrations would otherwise rapidly decrease in the planetary boundary layer, by photochemical reactions and/or deposition, can be carried over intercontinental distances (Fig. 5.16).

In extratropical regions this long-range transport of pollutants can happen as well. Jet streams acting like conveyor belts provide effective horizontal transport over long distances (the term 'conveyor belt' is already well established in the respective literature). It could be shown for instance that forest fires in Eastern Siberia have an impact on CO and $O_3$ in near-surface air in Japan [61]. Such processes can be quantified by means of trajectory models: From an imaginary 'wall' formed by many 'particles' one reconstructs, using measured wind fields, back trajectories of these particles for the days before reaching the wall. From the resulting 'spaghetti plot' the origin and the transport of the single particles until reaching the wall can be investigated. Figure 5.16 shows an example: The wall extends at 100° Eastern latitude, from Bangkok to Siberia. A detailed analysis shows that during January and February about 30–40 % of the air arriving at 100° East originates from Europe and thus carries pollutants from there to the Far East [60].

Likewise, significant increases of CO, $NO_2$, $O_3$, and PAN measured during March/April of 1998 at the west coast of the USA could be attributed to polluted air from China and Japan [63]. Products of forest fires in Canada have been identified in Europe [64], and the plume from forest fires in Russia even could be followed all around the globe [65].

Thus air pollution is a global problem whose impact at a certain location is determined, besides local sources, by the background resulting from a multitude of sources elsewhere. On the Northern Hemisphere, pollution sources are so intense and densely spaced that there are virtually no clean air conditions anymore.

On the Southern Hemisphere, pollution mainly resulting from few megacities is largely dispersed over the oceans. Measurements carried out at Aspendale, Australia, at about 38°S, show an increase from about 20 ppb to 35 ppb, between 1964 and 1970, which mostly reflects the local pollution of the Melbourne metropolitan area [66]. On the global scale, the impact of biomass burning seems to be more important, and the extended plumes resulting from forest fires in South America and South Africa are a significant manifestation of photosmog substances and particles seen on many satellite images. This is nicely illustrated by the global distribution of tropospheric ozone shown in Fig. 4.4: While on the Northern Hemisphere ozone levels are elevated almost everywhere, most of the Southern Hemisphere shows ozone varying between 10 and 30 ppb. Except for a few spots in Africa and South America showing the effect of biomass burning, conditions close to undisturbed prevail. As the vast ocean areas and Antarctica are almost free from pollution sources there are still large regions on the Southern Hemisphere which can be characterised by clean air conditions.

The transition towards elevated ozone levels of the Northern troposphere occurred with the economic rise after World War II. Continuous measurements of near-surface ozone at various stations in East Germany show increases, from 15 to 20 ppb during the 1950s, to 25 to 30 ppb during the 1980s [67]. The long series of surface ozone measurements at Arosa/Switzerland showed an increase even by a factor of 2.2 over the same time span [68]. The analysis of regular radiosonde data from Hohenpeissenberg/Germany and Arosa showed that this trend continued and,

moreover, that part of it is due to intercontinental influx of polluted air from North America [69]. In central Europe this trend, about 0.4 ppb/year during the 1970s and 1980s, levelled off during the 1990s. Since then tropospheric ozone levels have remained high [70].

Ground level ozone trends over North America were mostly positive from the 1950s onwards. They levelled off by about 1980. Since then most regions in the USA experienced almost constant $O_3$ concentrations, and in the largest metropolitan areas, New York City, Los Angeles, and Chicago, even decreasing trends were observed [71]. This is most likely due to the effect of emission regulations. Over the time period 1980–1995 anthropogenic VOC emissions decreased by 12 %, while $NO_x$ emissions remained constant. The observed $O_3$ trends are consistent with the view that summertime $O_3$ production over the USA is $NO_x$ limited except in the main metropolitan areas where it is partly VOC limited. Decreasing ozone levels after 1980 were reported from Canadian ozone stations as well [72].

At several west coast stations, however, increasing background ozone levels were observed, even after 1980, by about 30 % between 1984 and 2002 [73]. These were interpreted to be due to changes in emissions of $O_3$ precursors from Asia. One can speculate to what extent growing energy use in developing countries is going to alter the emission patterns of $O_3$ precursors and thus the tropospheric ozone distribution. It is clear that air pollution is not restricted by national boundaries and that global cooperation is required to address environmental problems in the future.

### *5.2.5 Impact on Vegetation, Humans, and Materials*

The ozone molecule is instable and easily decays, thereby liberating an aggressive oxygen atom. Thus ozone is an effective oxidiser. It kills germs, and thus ozone generators providing high (toxic) ozone output are applied for various disinfection purposes. Ozone can attack all kinds of surfaces. A drastic example is the effect of rubber cracking observed in the Los Angeles basin during the 1950s and 1960s, the peak years of photosmog there, when ozone levels were so high that the lifetime of car tyres was generally less than 2 years; independent of the driven mileage rubber cracking by ozone caused tyres to fall apart within this time. It is interesting to note that during these years ozone monitoring instruments were ‘calibrated’ by exposing fresh rubber samples under a microscope in ambient air and measuring the time until the first crack was observed.

Plants take up ozone through their stomata, with ozone mostly decaying outside the plasma membrane. Thereby reactive oxygen radicals are formed which can attack sensible lipids and proteins of the membrane. Short-term exposure to very high ozone levels, of 1,000 ppb and more, leads to the destruction of the cell membrane and the inner cell compartment, and chloroses, necroses, and the loss of leaves and needles can be observed. Such high ozone concentrations, however, do not occur in the near-surface environment. Even from the Los Angeles

metropolitan area, where the highest ozone levels ever have been observed, such acute ozone effects have not been reported.

From the San Bernadino Mountains, downwind of the Los Angeles basin, long-term (chronic) effects of the heavy load of photooxidants are manifested in the annual growth rings of 30 years old Pinus ponderosa trees: Compared to those of the 30 years period 1910–1940, when air pollution was low, annual growth rings of the heavily polluted period 1941–1971 were about 2 mm narrower. This reduced growth, clearly an effect of ozone and other photooxidants, was observed on trees appearing healthy as well as those clearly showing the chronic stress [74].

But even moderate ozone levels, up to about 150 ppb, can lead to chronic effects on plants, such as reduced growth, and yield reduction of crops and thus losses in agricultural production. Phytotoxic effects on plant metabolism, ozone-induced genes, enzymes, and stress metabolites have been observed in herbaceous plants and forest trees. The quantification is difficult: numerous experiments have been performed using exposition chambers with regulated climate conditions. However, the translation of findings observed in chambers, under artificial conditions, to the free environment, has been an issue of heated debate.

The discussion of the impact of ozone on forest trees culminated during the 1970s and 1980s, when forests in Europe, North America, and Japan suffered from leaf and needle losses. Many trees even died under the impact of air pollutants and the related acidification of the soil, and the term 'Waldsterben' (forest decline) made headlines. It is far outside the scope of this book to cite the numerous experiments carried out to elucidate the impact of the different stress factors: pollutants (including ozone), soil acidification, and climate conditions. We just confine ourselves on the effects of ozone described in the review of Sandermann [75], the book of Lefohn [76], and the articles cited therein.

Since experiments carried out in exposition chambers are restricted to small plants, results obtained for tree species have been criticised: Effects found in small seedlings must not necessarily hold for mature trees as well. Open-top chambers allowed investigations at larger species, up to about 10 m height. But still there were wall effects, and grown-up trees clearly exceed the dimensions of open-top chambers.

Thus free-air exposure systems are required to scale up ozone research to mature trees. Two types of such systems have been used so far. The first one applies a ring tube with defined openings, through which ozone/air mixtures are continuously blown out. The ring diameter is about 30 m allowing fumigation of groups of trees inside the ring, up to about 15 m height. The ozone/air mixture is regulated such that the trees inside the ring are exposed to the intended ozone level. The ozone distribution, however, is far from being homogeneous: Close to the ring tube ozone concentrations are often so high that visible leaf damage occurs, while, depending on wind direction and velocity, ozone levels decrease towards the inner parts of the ring.

The second type leads the ozone/air mixture through a system of teflon tubes with defined openings directly inside the canopies. By means of a tube system hanging down from a scaffolding, with about 50 cm horizontal spacing, the ozone

field inside the fumigated area is quite homogeneous, and there is no restriction with respect to height and width [77].

The Kranzberg Ozone Fumigation Experiment (KROFEX) shown in Fig. 5.17 is of the second type. It was designed to double ambient ozone concentrations, and it has continuously been operating in a mixed group of mature beech and spruce trees for six complete vegetation periods [62]. KROFEX was operated within an interdisciplinary consortium for investigating the effects of controlled free-air fumigation with ozone. All effects studied in the fumigated area were compared to those in reference trees exposed to ambient ozone. Fumigation was limited to maximum levels of 150 ppb, which corresponds to the maximum ambient ozone levels observed at the Kranzberg site. The results show that the trees can survive these moderate ozone levels, and there were no visible injuries nor significant effects on stem growth. Detailed investigations on the leaf and cell level and of the metabolism, enzymes and stress metabolites, carbon allocation, the root, and mycorrhiza system, however, showed a wealth of effects on how the beech and spruce trees reacted on the defined ozone stress. A summary of results is given in [79] and the references therein.

The influence of ozone on humans is difficult to study given the fact that experiments with exposition chambers are restricted to modest ozone concentrations. Furthermore, humans react very differently, so that responses found in one particular group do not necessarily hold for the whole mankind. This should be borne in mind when air quality standards are established.

In one aspect all humans are alike: The human skin is well protected and cannot be damaged by ozone, at least for the ranges observed at the Earth's surface. The mucous membranes, however, are very sensitive, thus being subject to irritations in nose and throat. Since ozone is hardly soluble in water, respiration can carry it well into the lungs where it can inflame the bronchia. Ozone can cause coughing and sore or scratchy throat and aggravate lung diseases such as asthma, emphysema, and chronic bronchitis. It makes lungs more susceptible to infections. Thus it is the respiratory tract where humans are vulnerable to ozone exposure, and thus measurements of the pulmonary function have been used to study the ozone impact.

It has been shown that the pulmonary function is not significantly affected at ambient ozone levels up to about 100 ppb falling off towards higher ozone levels [80]. This fall-off is strongest for hardworking people whose pulmonary function at 200 ppb and 300 ppb is reduced to 80 % and 55 %, respectively, this deterioration being much less for people without stress.

Given the fact that humans react very differently to ambient ozone exposure it is difficult to define threshold values beyond which ozone is considered hazardous to human health. The state of California defines standards of 90 ppb and 70 ppb for exposure of 1 hour and 8 hour respectively. The US national standard is 75 ppb for 8 hour exposure. In the European Union the maximum daily 8 hour mean is even set as low as 120 $\mu g/m^3$ which is about 60 ppb. Clearly these standards are exceeded on many days, especially during summer months. They must be considered goals which governments may hope to achieve in the future.


**Fig. 5.17** Aerial view of the Kranzberg ozone fumigation experiment (KROFEX). A group of five beech and five spruce trees are continuously fumigated with ozone such that the $O_3$ level in the canopies doubles the ambient $O_3$ monitored outside the fumigated area on the left tower. Ozone is produced from oxygen by a commercial ozone generator and fed to a mixing tank (not shown). From there the ozone/air mixture controlled by the reference monitor is dispersed in the fumigation volume by a system of teflon tubes with defined outlets hanging vertically under a scaffolding above the canopies. Other parts of the scaffolding allow experimenters to work in the fumigated and non-fumigated canopies. After [62]

## 5.3 Surface UV and Ozone Layer Changes

Peter Fabian

In Sect. 3.3, UV radiation, its biological effects, and its relationship to ozone layer thickness have been discussed. Changes in ozone layer thickness, long-term decreasing trends as a result of atmospheric pollution by man, by long-lived chlorine- and bromine-bearing substances, have been discussed in Sect. 5.1. Long-term trends of surface UV radiation related to ozone layer thicknesses, annual means, as well as short seasonal effects caused by the polar ozone holes have been documented. Main papers dealing with the Northern and Southern Hemispheres and seasonal effects related to polar ozone holes are discussed in this chapter.

### *5.3.1 Long-Term Trends*

UV-B increases from total ozone decreases for the years 1979–1992, based on NIMBUS-7/TOMS satellite data, are documented by Herman et al. [81]. Hereby the UV increases are computed by a model incorporating improved in-flight instrument

calibration. The linear-fit slopes (percent per decade) of the action spectra-weighted UV-flux exposure integral for the whole period 1979–1992 including cloud effects (see Sect. 3.3) are highest at high latitudes of both hemispheres, amounting to 15 %, 10 %, and 5 %, for DNA damage, plant growth, and erythema, respectively. For tropical latitudes no significant radiation changes are found. Erythemally weighted UV trends over northern latitudes are shown for central Europe, the Mediterranean region, North Atlantic, and eastern Russia [82].

Local effects are documented for St. Petersburg/Russia [83] and Athens [84]. In both cases total ozone reductions of 3 % and 2.5 %, respectively, per decade during summer time, and 11 % and 7 %, respectively, during winter time, causing increases of erythematically active UV of 7 % and 22 % and 5 % and 14 %, respectively, during summer and winter times. This results in Radiation Amplification Factors (RAF) of about 2 for both stations, in winter as well summer.

In Italy [85] and Bavaria [86] ozone trends have been shown to be anticorrelated with UV-B radiation which was measured by means of ground-based Brewer spectrophotometers (see Sect. 3.6) at Rome, Ispra, and Hohenpeissenberg. Long-term and seasonal variations are clearly shown from the available data.

Hemispheric differences of UV radiation at midlatitude stations have been worked out by Seckmeyer and McKenzie [87]. By means of a combination of spectral measurements made in Germany and New Zealand, with the same spectroradiometer, together with model calculations, they show that biologically weighted UV during New Zealand (45°S) summer months is about a factor 2 larger than those found during summer months in Germany (48°N).

These differences are larger than expected and are due to decreased stratospheric ozone over New Zealand and increased levels of tropospheric ozone over Germany.

### *5.3.2 Effects of the Ozone Hole and Its Breakdown*

The ozone hole was first discovered over Antarctica because the stratospheric wind system and related low temperatures are stable during winter and symmetrical around the South Pole [88]. Polar stratospheric clouds are formed, and in heterogeneous reactions the active halogen radicals are produced which, at the end of the polar night (October), immediately destroy ozone (see Sects. 3.1.4, 5.1.3). Low ozone levels inside the polar vortex remain until, when summer comes (December), the vortex gets deformed and moves air depleted in ozone, out to lower latitudes. This ‘end of the ozone hole’ brings ozone-depleted air to South America, Australia, and New Zealand.

The effect of the 1990 ozone hole was intensively studied at Mc Murdo/Antarctica [78]. UV radiation values at 305 nm in October exceeded by a factor 3–6 ‘normal values’ expected for undepleted ozone levels.

Roy et al. [89] show comparisons of solar UV-B irradiances for the Australian/New Zealand sector with total ozone during December 1987 and January 1988, the breakdown of the 1987 ozone hole (Fig. 5.18). A long series of summer

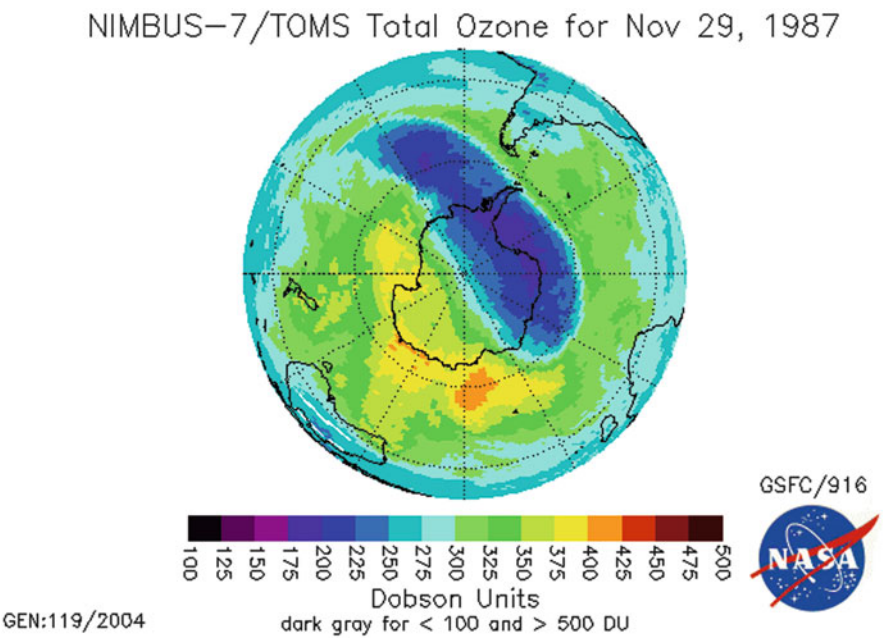


**Fig. 5.18** Breakdown of the 1987 Antarctic ozone hole, after [78]

(December–February) total ozone and UV Index data for Lauder/New Zealand, 1979–1999, documenting the previous ozone holes, is shown in Fig. 5.19 (from McKenzie et al. [90]).

Interesting UV-B enhancements are documented for Punta Arenas in Chile [91]. Here, at 53°S, when the ozone hole breaks down, the UV-B is up to about ten times the 'normal values', the erytheme-weighted integrated flux has increased to 180 mW/m$^2$ from undisturbed 70 mW/m$^2$.

On the Northern Hemisphere, the situation with respect to polar ozone holes is less clear than on the Southern Hemisphere. This is because the stratospheric winter circulation around the pole is less symmetrical. Thus the ozone hole is asymmetrical and weaker; effects of the ozone hole can be observed even at midlatitudes driven by the variable polar vortex.

On the Southern Hemisphere, as long as the ozone hole is stable, ozone depletion and UV-B increases are confined to the centre of the vortex, which is the polar region. A shift to lower latitudes as described above happens when the vortex breaks down at the beginning of summer.

On the Northern Hemisphere, however, due to the asymmetry of the vortex, all kinds of variations can occur. Depending on how the vortex behaves, ozone-depleted air can get to lower latitudes long before the 'final' breakdown of the vortex. An impressive example is shown in Fig. 6.2 (Chap. 6): During January/February of 1992 the Arctic vortex was deformed over the European sector towards midlatitudes. Thus, TOMS measured massive ozone reductions over large parts of

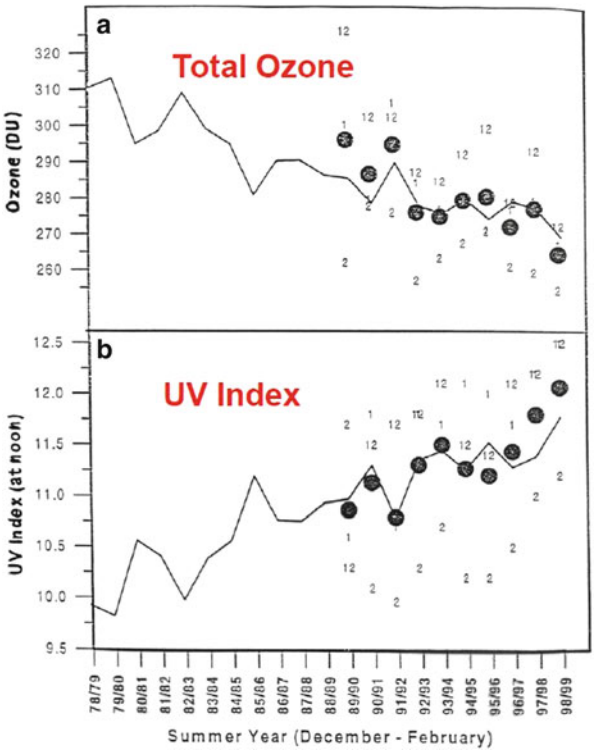


**Fig. 5.19** Total ozone (**a**) and UV Index (**b**) for Lauder/New Zealand 1979–1999 [90]

Europe. On January 18, for instance, about 300 DU instead of regular 400 DU were measured over central to northwestern Europe and the adjacent Atlantic Ocean. This event gave the negotiators of the Copenhagen amendments of the Montreal Protocol (see Chap. 6), taking place soon thereafter, arguments to come up with an amendment aimed at speeding up the phaseout schedule for already controlled substances.

## 5.4 Ozone and Climate Change

Martin Dameris

This section relates how the development of the stratospheric ozone layer to date and in the future is connected to that of the climate.

Solar radiation is partially reflected and absorbed in the Earth's atmosphere. The remainder penetrates the atmosphere and warms up the Earth's surface. The heated planet emits infrared (IR) radiation (heat radiation) back into the atmosphere. Radiatively active molecules in the atmosphere, so-called greenhouse gases like carbon dioxide ($CO_2$), methane ($CH_4$), nitrous oxide ($N_2O$), water vapour ($H_2O$), or ozone ($O_3$), cause the troposphere to warm up, because they absorb the heat

radiation from the Earth; this is the greenhouse effect. Overall, the result is a mean global air temperature of about 288 K (15 °C) close to the Earth's surface. Without this natural greenhouse effect, the mean global temperature would be only about 255 K (−18 °C). But greenhouse gases also emit IR radiation themselves. The emission depends on the local atmospheric temperature. In the stratosphere, greenhouse gases generally emit more IR radiation than they absorb, which leads to a cooling of the stratosphere. As the temperature of the stratosphere increases with altitude, IR emissions also increase with altitude and are highest near the stratopause, i.e. an altitude of about 50 km. This cooling effect caused by greenhouse gases varies with latitude, as it depends on the balance between IR absorption (principally from below) and local IR emissions.

Changes in the concentration of greenhouse gases in the atmosphere have an immediate effect on the temperature structure, as the balance between the effect of the incident solar (short-wave) radiation and the terrestrial radiation (IR) emitted into the atmosphere is affected. The mean global temperature near the Earth's surface has risen by 0.74 °C in the last century owing to the greatly increased concentrations of greenhouse gases [16]. Data analyses have shown that the stratosphere, on the other hand, has clearly cooled down more or less constantly in recent decades. As expected, the observed trends indicate an altitude dependency with a more severe cooling trend in the upper than in the lower stratosphere. For example, the global mean lower stratosphere is cooled by 1–2 K and the upper stratosphere is cooled by 4–6 K from 1980 to about 1995 (see Chap. 4 in [1]). The cooling of the lower stratosphere during the 1980s and the first half of the 1990s was intensified by the significant decrease in stratospheric ozone content during that time. Moreover, the negative stratospheric temperature trend is modified by a series of natural processes in the atmosphere, such as the 11-year solar-activity cycle and strong volcanic eruptions. Therefore, the cooling in the past did not occur linearly. Since the mid-1990s, slowing loss of stratospheric ozone has significantly reduced the cooling rate of the lower stratosphere.

Temperature changes affect physical, dynamical, and chemical processes influencing the ozone content in the atmosphere in different ways. Moreover, the chemical state of the atmosphere changes as the concentration of trace species and ozone-depleting substances changes. This in turn alters the sensitivity of the stratospheric chemical system to temperature changes. The sensitivity of ozone chemistry in the middle and upper part of the stratosphere to changes in temperature is well explained. There, the chemical system is under photochemical control and is constrained by gas-phase reaction cycles that are well known. The most important ozone loss cycles in the stratosphere (via the catalysts $NO_x$, $ClO_x$, and $HO_x$) are slowing as temperatures decrease [92], leading to higher ozone concentrations.

The situation is more complicated in the polar lower stratosphere in late winter and spring where heterogeneous processes on surfaces of polar stratospheric cloud (PSC) and cold aerosol particles lead to markedly increased concentrations of $ClO_x$ and $BrO_x$. This in turn yields significant ozone losses via $ClO_x$ and $BrO_x$ catalytic cycles in the presence of sunlight. The rate of chlorine and bromine activation is strongly dependent on stratospheric temperatures, increasing significantly below

approximately 195 K. In a polar lower stratosphere with enhanced (over natural levels) concentrations of ozone-depleting substances, as it is currently observed, chlorine and bromine activation and consequent ozone losses at lower temperatures counteract any ozone increase through temperature-driven reduction in $NO_x$ and $HO_x$ gas-phase ozone loss.

The distribution of atmospheric trace gases, so the local concentrations are also affected by dynamic processes; in comparison to chemical processes they play an equally important role. In addition to that dynamic and chemical processes in the atmosphere interact with each other in to some extent highly complex ways. Understanding all of these processes and their feedback is a key to both comprehending short-term fluctuations in the thickness of the ozone layer and to be able to explain long-term trends.

Climate change modifies processes that drive the circulation systems. This results in modifications of air mass transport and the transportation routes, with consequences for the atmospheric distribution of climate-influencing trace gases, including ozone. This, in turn, can affect the Earth's climate. Although the dynamic processes controlling stratospheric circulation are understood quite well, significant uncertainties still remain regarding the variability of these processes and their effects in a changing climate. So far, analyses of observation data have not given any clear, conclusive indication of how climate change affects stratospheric circulation. An intensification of meridional circulation would, for example, result in the extratropical atmosphere heating up (adiabatic downwelling) and the tropical atmosphere cooling down (adiabatic upwelling). This would directly impact transport into the stratosphere of tropospheric source gases (that is, those originally emitted in the troposphere that then rise up into the stratosphere, where they are chemically changed), so-called product gases (intermediates and products generated in the troposphere) and water vapour, which are present in much higher concentrations in the troposphere than in the stratosphere. But stratospheric air masses with high ozone concentrations (or low water vapour concentrations) could also be increasingly transported into the troposphere, where ozone (water vapour) concentrations are normally significantly lower (higher). These redistributions would in turn affect the radiation balance and chemical processes of the atmosphere. Therefore, the assessment of the sensitivity of ozone-related chemistry to climate changes is rather complicated (see Chap. 5 in [2]).

As a result of the international agreements on protecting the stratospheric ozone layer (Montreal Protocol and amendments), it is expected that the strong chemical ozone depletion observed over the past decades will decrease in the near future. The ozone layer's thickness should start to build up again and the ozone hole over Antarctica should close up (see Chap. 3 in [1]). However, the speed at which the ozone layer will re-form and its future development also depend on the consequences of progressive climate change. The recovery of the ozone layer thus takes place under atmospheric conditions different to those prevailing during the ozone-depletion processes of recent decades. Consequently, it is highly unlikely that the ozone layer will return to exactly the state it had before the time of enhanced concentrations of ozone-depleting substances. For this reason, current future

assessments of the stratospheric ozone layer, which are mostly based on results obtained from numerical atmospheric models, still in part yield largely varying results.

However, based on our current understanding of atmospheric processes and expected variations owing to climate change, some robust predictions for the development of the stratospheric ozone layer can be made. Owing to further increasing greenhouse gas concentrations, global atmospheric temperatures will continue to change over the coming decades; it is expected that the stratosphere will cool down further owing to radiation effects. Exact predictions on the extent of the expected trend are difficult to make, as future greenhouse gas emissions are uncertain [16]. Furthermore, it must be considered that, because of the expected recovery of the ozone layer, stratospheric ozone heating rates will increase again, to some extent counteracting the increased cooling from rising greenhouse gas concentrations. However, as the ozone concentration depends largely on the background temperature, there will be some feedback. As climate change also involves a change in stratospheric dynamics, 'dynamic' heating of the stratosphere can also occur, depending on the time of year and place. Owing to the interactions described above, a further cooling of the lower polar stratosphere could lead to a delay in the ozone hole closing up above Antarctica, whilst the ozone layer could rebuild faster in other areas of the stratosphere.

Future predictions based on numerical simulations with Chemistry-Climate Models (CCMs; see [17]) indicate that the regeneration of the ozone layer will be faster in some stratospheric regions than in others, where it is quite possible that regeneration will be delayed. A continued increase in greenhouse gas concentrations will cause the stratosphere to cool further, on the one hand resulting in faster recovery of ozone in the middle and upper stratosphere and, on the other hand, slowing down the rebuilding of the ozone layer in the polar lower stratosphere during the spring months. There, lower temperatures lead to an increased formation of PSCs.

The ozone layer, including the polar regions, is expected to make a full recovery by the middle of the century [1]. Owing to climate change, it seems plausible that the thickness of the ozone layer will actually exceed that of earlier years from then on. The results of many CCM simulations are in agreement in this conclusion.

## References

1. WMO (2011) World Meteorological Organization, scientific assessment of ozone depletion: 2010. Global ozone research and monitoring project, Report No. 52, Geneva, Switzerland
2. WMO (2007) World Meteorological Organization, scientific assessment of ozone depletion: 2006. Global ozone research and monitoring project, Report No. 50, Geneva, Switzerland
3. Crutzen PJ (1971) Ozone production rates in an oxygen-hydrogen-nitrogen oxide atmosphere. J Geophys Res 76(30):7311–7327. doi:10.1029/JC076i030p07311
4. Molina MJ, Rowland FS (1974) Stratospheric sink for chlorofluoromethanes: chlorine atom-catalysed destruction of ozone. Nature 249:810–812. doi:10.1038/249810a0

5. Steinbrecht W, Claude H, Schönenborn F, McDermid IS, Leblanc T, Godin-Beekmann S, Keckhut P, Hauchecorne A, Van Gijsel JAE, Swart DPJ, Bodeker GE, Parrish A, Boyd IS, Kämpfer N, Hocke K, Stolarski RS, Frith SM, Thomason LW, Remsberg EE, von Savigny C, Rozanov A, Burrows JP (2009) Ozone and temperature trends in the upper stratosphere at five stations of the network for the detection of atmospheric composition change. Int J Remote Sens 30:3875–3886
6. Chipperfield MP, Fioletov VE (Lead Authors), Bregman B, Burrows J, Connor BJ, Haigh JD, Harris NRP, Hauchecorne A, Hood LL, Kawa SR, Krzyścin JW, Logan JA, Muthama NJ, Polvani L, Randel WJ, Sasaki T, Stähelin J, Stolarski RS, Thomason LW, Zawodny JM (2007) Chapter 3: Global ozone: past and present. In: Scientific assessment of ozone depletion: 2006, Global ozone research and monitoring project-Report No. 50, World Meteorological Organization, Geneva, 572 pp
7. Steinbrecht W, Haßler B, Brühl C, Dameris M, Giorgetta MA, Grewe V, Manzini E, Matthes S, Schnadt C, Steil B, Winkler P (2006) Interannual variation patterns of total ozone and temperature in observations and model simulations. Atmos Chem Phys 6:349–374
8. Dameris M, Peter T, Schmidt U, Zellner R (2007) Das Ozonloch und seine Ursachen. Chem Unserer Zeit 41:152–168. doi:10.1002/ciuz.200700418
9. Solomon S, Garcia RR, Rowland FS, Wuebbles DJ (1986) On the depletion of Antarctic ozone. Nature 321:755–758. doi:10.1038/321755a0
10. Solomon S (1999) Stratospheric ozone depletion: a review of concepts and history. Rev Geophys 37:275–316
11. Labitzke K (1980) Climatology of the stratosphere and mesosphere. Philos Trans R Soc Lond A296:7–18
12. Molina LT, Molina MJ (1987) Production of $Cl_2O_2$ from the self-reaction of the ClO radical. J Phys Chem 91:433–436
13. Farman JC, Gardiner BG, Shanklin JD (1985) Large losses of total ozone in Antarctica reveal seasonal ClOx/NOx interaction. Nature 315:207–210
14. Newman PA, Gleason JF, McPeters RD, Stolarski RS (1997) Anomalously low ozone over the Arctic. Geophys Res Lett 24:2689–2692
15. Dameris M, Loyola D (2012) Chapter 45: Recent and future evolution of the stratospheric ozone layer. In: Schumann U (ed) Atmospheric physics, background-methods-trends. Springer, Heidelberg, pp 747–761. doi:10.1007/978-3-642-30183-4. ISBN 978-3-642-30182-7
16. IPCC, Intergovernmental Panel on Climate Change (2007) In: Solomon S, Qin D, Manning M, Chen Z, Marquis M, Averyt KB, Tignor M, Miller HL (eds) Climate change 2007: the physical science basis: contribution of working group I to the fourth assessment report of the intergovernmental panel on climate change, Cambridge University Press, Cambridge, 996 p
17. SPARC CCMVal (2010) In: Eyring V, Shepherd TG, Waugh DW (eds) SPARC CCMVal report on the evaluation of chemistry-climate models, SPARC Report No. 5, WCRP-132, WMO/TD-No. 1526. http://www.atmosp.physics.utoronto.ca/SPARC/ccmval_final/index.php
18. Ravishankara AR, Daniel JS, Portman RW (2009) Nitrous oxide ($N_2O$): the dominant ozone-depleting substance emitted in the 21st century. Science 326:123–125. doi:10.1126/science.1176985
19. Wild O, Prather MJ, Akimoto H (2001) Indirect long-term global radiative cooling from $NO_x$ emissions. Geophys Res Lett 28(9):1719–1722
20. Dameris M, Grewe V, Köhler I, Sausen R, Brühl C, Grooß J-U, Steil B (1998) Impact of aircraft $NO_x$ emissions on tropospheric and stratospheric ozone. Part II: 3-D model results. Atmos Environ 32:3185–3199
21. Grewe V, Dameris M, Fichter C, Sausen R (2002) Impact of aircraft NOx emissions. Part 1: Interactively coupled climate-chemistry simulations and sensitivities to climate-chemistry feedback, lightning and model resolution. Meteorol Z 3:177–186
22. Lee DS, Pitari G, Grewe V, Gierens K, Penner JE, Petzold A, Prather MJ, Schumann U, Bais A, Berntsen T, Iachetti D, Lim LL, Sausen R (2010) Transport impacts on atmosphere and climate: aviation. Atmos Environ 44:4678–4734

23. Chameides WL, Lindsay RW, Richardson J, Kiang CS (1988) The role of biogenic hydrocarbons in urban photochemical smog-Atlanta as a case-study. Science 241:1473–1475
24. Starn TK, Shepson PB, Bertman SB, White JS, Splawn BG, Riemer DD, Zika RG, Olszyna K (1998) Observation of isoprene chemistry and its role in ozone production at a semi-rural site during the 1995 Southern oxidants study. J Geophys Res Atmos 103:22425–22435
25. Finnlayson-Pitts B, Pitts JN Jr (1999) Chemistry of the upper and lower atmosphere. Academic, San Diego, CA
26. Sillman S (1999) The relation between ozone, NOx and hydrocarbons in urban and polluted rural environments. Atmos Environ 33:1821–1845
27. Haagen-Smit AJ, Bradley CE, Fox MM (1953) Ozone formation in photochemical oxidation of organic substances. Ind Eng Chem 45:2086–2089
28. Leighton PA (1961) Te photochemistry of air pollution. Academic, New York
29. Kleinman LI, Peter H, Daum DG, Imre H, Lee Y-N, Nunnermacker LJ, Springston SR, Weinstein-Lloyd J, Newman L (2000) Ozone production in the New York City urban plume. J Geophys Res 105:14495–14511
30. Rappenglück B, Oyola P, Olaeta J, Fabian P (2000) The evolution of photochemical smog in the Metropolitan Area of Santiago de Chile. J Appl Meteorol 39:275–290
31. South Coast air quality management district, El Monte, CA, http://www.aqmd.gov
32. Ball DJ (1976) Photochemical ozone in the atmosphere of Greater London. Nature 263:580–582
33. Tulet P, Maalej A, Grassier V, Rosset R (1999) An episode of photooxidant plume pollution over the Paris region. Atmos Environ 33:1651–1662
34. Fabian P, Haustein C, Jakobi G, Rappenglück B, Suppan P, Steil P (1994) Photochemical smog in the Munich metropolitan area. Beitr Phys Atmos 67:39–56
35. Ziomas IC, Suppan P, Rappenglück B, Balis D, Tzoumake R, Melas D, Papayannis A, Fabian P, Zerefos C (1995) A contribution to the study of photochemical smog in the greater Athens area. Beitr Phys Atmos 68:191–203
36. Raga GB, Raga AC (2000) On the formation of an elevated ozone peak in Mexico City. Atmos Environ 34:4097–4102
37. Liu C-M, Liu SC (1990) A study of Taipei ozone problem. Atmos Environ 24A:1461–1472
38. Deutscher Bundestag (1990) Vorsorge zum Schutz der Erdatmosphäre zum Thema Schutz der tropischen Wälder. Drucksache 11/7220, Zweiter Bericht der Enquete-Kommission
39. Crutzen PJ, Heidt LE, Krasnec JP, Pollock WH, Seiler W (1979) Biomass burning as a source of atmospheric gases CO, H2, N2O, NO, CH3Cl, and COS. Nature 282:253–256
40. Ferek RJ, Reid JS, Hobbs PV, Blake DR, Liousse C (1998) Emission factors of hydrocarbons, halocarbons, trace gases and particles from biomass burning in Brazil. J Geophys Res Atmos 103:32107–32118
41. Koppmann R, Khedim A, Rudolph J, Poppe D, Andeae MO, Helas G, Welling M, Zenker T (1997) Emissions of organic trace gases from savanna fires in southern Africa during the 1992 Southern African Fire Atmospheric Research Initiative and their impact on the formation of tropospheric ozone. J Geophys Res Atmos 102:18879–18888
42. Delany AC, Haagensen P, Walters S, Wartburg AF, Crutzen PJ (1985) Photochemically produced ozone in the emission from large-scale tropical vegetation fires. J Geophys Res 90:2425–2429
43. Andrea MO (1997) Emission of trace gases and aerosols from savanna fires. In: van Wilgen BW, Andreae MO, Goldammer JG, Lindesay JA (eds) Fire in the Southern African Savanna, ecological and environmental perspectives. Witwatersrand University Press, Johannesburg, pp 161–183
44. Kim JH, Newchurch MJ (1996) Climatology and trends of tropospheric ozone over the eastern Pacific Ocean: the influences of biomass burning ad tropospheric dynamics. Geophys Res Lett 23:3723–3726
45. Diab RD, Thompson AM, Zunckel M, Coetzee GJR, Combrinck J, Bodeker GE, Fishman J, Sokolic F, McNamara DP, Archer CB, Nganga D (1996) Vertical ozone distribution over southern Africa and adjacent oceans during SAFARI-92. J Geophys Res 101:23823–23833

46. Olson JR, Fishman J, Kirchhoff VWJH, Nganga D, Cros B (1996) Analysis of the distribution over the southern Atlantic region. J Geophys Res 101:24083–24093
47. Friedli HR, Atlas E, Stroud VR, Giovanni L, Campos T, Radke LF (2001) Volatile organic trace gases emitted from North American wildfires. Global Biogeochem Cycles 15:435–452
48. Lobert JM, Keene WC, Logan JA, Yevich R (1999) Global chlorine emissions from biomass burning: Reactive chlorine emissions inventory. J Geophys Res Atmos 104:8373–8389
49. Hao WM, Scharffe D, Lobert JM, Crutzen P (1991) Emissions of N2O from the burning of biomass in an experimental system. Geophys Res Lett 18:18999–19002
50. Cofer WR, Levine JS, Winstead EL, Stocks BJ (1991) New estimates of nitrous oxide emissions from biomass burning. Nature 349:689–691
51. Nganga D, Minga A, Cros B, Biona CB, Fishman J, Grant WB (1996) The vertical distribution of ozone measured at Brazzaville, Congo during TRACE A. J Geophys Res Atmos 101:24095–24103
52. Kirchhoff VWJH, Rasmussen RA (1990) Time variations of CO and O3- concentrations in a region subject to biomass burning. J Geopys Res Atmos 95:7521–7532
53. Marufu L, Dentener F, Lelieveld J, Andeae MO, Helas G (2000) Photochemistry of the African troposphere: influence of biomass-burning emissions. J Geophys Res Atmos 105:14513–14530
54. Koe LCC, Arellano AF, McGregor JL (2001) Investigating the haze transport from 1997 biomass burning in Southeast Asia: its impact upon Singapore. Atmos Environ 35:2723–2734
55. Disselkamp RS, Carpenter MA, Cowin JP, Berkowitz CM, Chapmn EG, Zaveri RA, Laulainen NS (2000) Ozone loss in soot aerosols. J Geophys Res 105:9767–9771
56. Kita K, Fujiwara M, Kawakami S (2000) Total ozone increase associated with forest fires over the Indonesian region and its relation to the El Nino-Southern oscillation. Atmos Environ 34:2681–2690
57. Thompson AM, Witte JC, Hudson RD, Guo H, Herman JR, Fujiwara M (2001) Tropical tropospheric ozone and biomass burning. Science 291:2128–2131
58. Rinsland CP, Goldman A, Murcray FJ, Stephen TM, Pougatchev NS, Fishman J, David SJ, Blatherwick RD, Novelli PC, Jones NB, Connor BJ (1999) Infrared solar spectroscopic measurements of free tropospheric CO, C2H6, and HCN above Mauna Loa, Hawaii: seasonal variations and evidence for enhanced emissions from the Southeast Asian tropical fires of 1997-1998. J Geophys Res Atmos 104:18667–18680
59. Fabian P, Rollenbeck R, Spichtinger N, Brothers L, Dominguez G, Thiemens M (2009) Sahara dust, ocean spray, volcanoes, biomass burning: pathways of nutrients into Andean rainforests. Adv Geosci 22:85–94
60. Newell RE, Evans MJ (2000) Seasonal changes in pollutant transport to the North Pacific: the relative importance of Asian and European sources. Geophys Res Lett 27:209–2512
61. Tanimoto H, Kajii Y, Hirokawa J, Akimoto H, Minko NP (2000) The atmospheric impact of boreal forest fires in far eastern Siberia on the seasonal variation of carbon monoxide: observations at Rishiri, a northern remote island in Japan. Geophys Res Lett 27:4073–4076
62. Werner H, Fabian P (2002) Free-air fumigation of mature trees—a novel system for controlled enrichment in grown-up beech and sprucc canopies. Environ Sci Pollut Res 9:117–121
63. Jaffe D, Anderson T, Covert D, Kotchenruther R, Trost B, Danielson J, Simpson W, Berntsen T, Karlsdottir S, Blake D, Harris J, Carmichael G, Uno I (1999) Transport of Asian air pollution to North America. Geophys Res Lett 26:711–714
64. Spichtinger N, Wenig M, James P, Wagner T, Platt U, Stohl A (2001) Satellite detection of a continental-scale plume of nitrogen oxides from boreal forest fires. Eophys Res Lett 28:4579–4582
65. Damoah R, Spichtinger N, Forster C, James P, Mattis I, Wandinger U, Beirle S, Wagner T, Stohl A (2004) Around the world in 17 days- hemispheric-scale transport of forest fire smoke from Russia in May 2003. Atmos Chem Phys 4:1311–1321

66. Galbally IE (1971) Surface ozone observations at Aspen dale, Victoria, 1964-1970. Atmos Environ 5:15–25
67. Feister U, Warmbt W (1987) Long-term measurements of surface ozone in the German Democratic Republic. J Atmos Chem 5:1–21
68. Staehelin J, Thudium J, Buehler R, Volz-Thomas A, Graber W (1994) Trends of surface ozone concentrations at Arosa (Switzerland). Atmos Environ 28:75–87
69. Naja M, Akimoto H, Staehelin J (2003) Ozone in background and photochemically aged air over central Europe: analysis of long-term ozonesonde data from Hohenpeissenberg and Payerne. J Geophys Res 108(D2):4063. doi:10.1029/2002JD002477
70. Brönnimann S, Buchmann B, Wanner H (2002) Trends in near-surface ozone concentrations in Switzerland: the 1990s. Atmos Environ 36:2841–2852
71. Fiore AM, Jacob DF, Logan JA, Yin JH (1998) Long-term trends in ground level ozone over the contiguous United States, 1980-1995. J Geophys Res 103:1471–1480
72. Tarasick DW, Wardle DI, Kerr JH, Bellefleur JJ, Davies J (1995) Tropospheric ozone trends over Canada: 1980-1993. Geophys Res Lett 22:409–412
73. Jaffe D, Price H, Parrish D, Goldstein A, Harris J (2003) Increasing background ozone during spring on the west coast of North America. Geophys Res Lett 30:1613–1617
74. Guderian R, Tingay D, Rabe R (1985) Effects of photochemical oxidants on plants. In: Guderian R (ed) Air pollution by photochemical oxidants. Springer, Heidelberg, pp 129–133
75. Sandermann H (1996) Ozone on plant health. Annu Rev Phytopatol 14:347–366
76. Lefohn AS (ed) (1992) Surface level ozone exposures and their effects on vegetation. Lewis Publishers, Chelsea, MI, 306 p
77. Karnosky DF, Werner H, Holopainen T, Percy K, Oksanen T, Oksanen E, Heerdt C, Fabian P, Nagy J, Heilmann W, Cox R, Nelson N, Matyssek R (2007) Free-air exposure systems to scale up ozone research to mature trees. Plant Biol 9:181–190
78. NASA Goddard Space Flight Center. Data available under http://ozoneaq.gsfc.nasa.gov/nimbus7ozone.md
79. Matyssek R et al (2007) Ozone sensitivity of forest trees. Plant Biol 9(2):163–356
80. Hazucha MJ (1987) Relationship between ozone exposure and pulmonary function changes. J Appl Physiol 62:1671–1680
81. Herman JR, Bhartia PK, Ziemke J, Ahmad Z, Larko D (1996) UV-B increases (1979-1992) from decreases of total ozone. Geophys Res Lett 23:2117–2120
82. Ziemke JR, Chandra S, Herman J, Varotsos C (2000) Erythemally weighted UV trends over northern latitudes derived from NIMBUS 7 TOMS measurements. J Geophys Res 105:7373–7382
83. Varotsos C, Kondratyev KY, Katsikis S (1995) On the relationship between total ozone and solar ultraviolet radiation at St. Petersburg, Russia. Geophys Res Lett 22:3481–3484
84. Varotsos C (1994) Solar ultraviolet radiation and total ozone, as derived from satellite and ground-based instrumentation. Geophys Res Lett 21:1787–1790
85. Casale GR, Meloni D, Miano S, Palmieri S, Siani AM, Capellani F (2000) Solar UV-B irradiance and total ozone in Italy: fluctuations and trends. J Geophys Res 105:4895–4901
86. Gantner L, Winkler P, Köhler U (2000) A method to derive long-term time series and trends of UV-B radiation (1968-1997) from observations at Hohenpeissenberg (Bavaria). J Geophys Res 105:4879–4888
87. Seckmeyer G, McKenze RL (1992) Increased ultraviolet radiation in New Zealand (450S) relative to Germany (480N). Nature 359:135–137
88. Stamnes K, Jin Z, Slusser J, Booth C, Lucas T (1992) Several-fold enhancement of biologically effective ultraviolet radiation levels at MCMURDO Station Antarctica during the 1990 ozone hole. Geophys Res Lett 19:1013–1016
89. Roy CR, Gies HP, Elliot G (1990) Ozone depletion. Nature 347:235–236
90. McKenzie S, Connor B, Bodeker G (1999) Increased summertime UV radiation in New Zealand in response to zone loss. Science 285:1709–1711
91. Kirchhoff VWJH, Zamorano F, Casiccia C (1997) UV-B enhancements at Punta Arenas, Chile. J Photochem Photobiol B 38:174–177
92. Haigh J, Pyle J (1982) Ozone perturbation experiments in a two-dimensional circulation model. Q J R Meteorol Soc 108:551–574

# Chapter 6
# International Legislation: The Vienna Convention and the Montreal Protocol

In 1974 the world was alarmed by Molina and Rowland's famous paper (Ref. [21], of Chap. 3) predicting a severe depletion of the ozone layer caused by the continuous liberation of chlorofluorocarbons (CFCs) 11 and 12, $CCl_3F$ and $CCl_2F_2$, respectively. At that time about 700,000 t of these substances were released every year, as spray can propellant, refrigerants, solvents and foam blowing agents, with about 10 % annual emission increase. These CFCs were extremely useful: inert like noble gases, non-inflammable, non-toxic, without smell or taste. But just because of their inertness they are not decomposed in the troposphere, they accumulate and gradually get mixed to the higher layers of the atmosphere, where, by UV attack and reactions with excited oxygen atoms, Cl atoms are liberated which catalytically destroy ozone (see Sect. 3.1.3).

With the aim of sustaining the ozone layer, under strong pressure of the public, several countries (USA, Canada, Norway, Sweden) banned by law the "non-essential" use of CFCs as aerosol propellant. The European Union member states reluctantly agreed in 1977 not to increase the annual CFC production. The overall result was that the total amount of CFC-11 and CFC-12 globally emitted levelled off at about 700,000 t/year gradually growing to 800,000 during the 1980s.

Ground-based measurements showed that the abundances of CFC-11 and CFC-12 as well as other halocarbons were growing, in accordance with global emission rates, and measurements with balloon-borne instruments proved that these substances had been transported to the stratosphere as predicted [1]. The predicted ozone depletion, a few percent at that time, was so small that it could hardly be verified by measurements. Nevertheless the United Nations established, within their Environment Program (UNEP), an ad hoc expert group to work out a global framework for the protection of the ozone layer, which was signed in 1984 in Vienna by 28 nations and subsequently ratified by 166 states. With this Vienna Convention the signatories agreed to take "appropriate measures... to protect human health and the environment against adverse effects resulting or likely to result from human activities which modify or are likely to modify the ozone layer". These measures were unspecified and mostly aimed at encouraging research, international cooperation and exchange of information.

P. Fabian and M. Dameris, *Ozone in the Atmosphere*,
DOI 10.1007/978-3-642-54099-8_6, © Springer-Verlag Berlin Heidelberg 2014

The Vienna Convention set an important precedent: for the first time nations agreed in principle to tackle a global environmental problem before its effects were felt or even scientifically proven.

The discovery of the Antarctic Ozone Hole, a severe seasonal ozone depletion (see Sects. 5.1 and 7.1), was instrumental in promoting an international agreement on specific measures. Had it been difficult before to identify tiny ozone layer changes of a few percent, given the background of natural fluctuations, a seasonal depletion of 50 % and more was a big effect now. And it could be shown soon thereafter that halogen atoms released from anthropogenic halocarbons were the major cause of this large depletion. Thus, in September of 1987 the Montreal Protocol on "Substances that deplete the Ozone Layer" was signed by 24 countries; it has subsequently been ratified by 165 nations.

This protocol came into force on 1 January 1989 as a flexible instrument enabling modifications in the light a virtually continuous scientific review process reported to the Parties in subsequent years. That way regulations have evolved since 1989 as the scientifically driven requirements and the political and societal needs of countries have changed.

According to the original protocol, the growth of halogens in the atmosphere would have been only slightly less than without regulations (see Fig. 6.1). Clearly, reductions of production and usage were quite modest, 50 % until 1998 compared to 1986 figures, for CFCs 11, 12, 113, 114 and 115, while for halons 1211, 1301 and 2402 a freeze at the 1986 level was to occur from 1993 onwards. Thereby every substance was weighted by its specific ozone depletion potential (ODP). For Third World countries these reductions were foreseen to be enacted 10 years later. As Fig. 6.1 shows, the growth of ozone depleting substances in the atmosphere would have continued albeit slightly less rapidly.

It was at the follow-up conferences (London 1990, Copenhagen 1992, and Vienna 1995) that the original Montreal Protocol was amended such that a real phase-out of ozone depleting halogens could be achieved. The London amendment included methyl chloride and methyl chloroform in the reduction scheme, too, and it was decided to end production of all CFCs, halons and $CCl_4$ until 2000, that of $CH_3CCl_3$ until 2005. Again, for Third World countries a 10-year postponement was granted.

The real breakthrough was achieved in 1992 in Copenhagen: under the impression of massive ozone depletions that had been observed during January/February 1992 over large areas of Europe, the total phase-out date of CFCs and $CCl_4$ was shifted to 1996 and that of halons to 1994. Furthermore, methyl bromide was included in the Protocol with the aim to freeze its usage in the industrial countries by 1995. Thus, the occurrence of an ozone hole like feature over the Arctic, with massive ozone losses and corresponding UV increases over densely populated parts of Europe (see Fig. 6.2), led to a regulation which for the first time initiated a decrease of ozone depleters in the atmosphere.

Nevertheless, ozone depletion progressed further, and the extent of the Antarctic ozone hole and corresponding polar ozone losses on the Northern Hemisphere continued growing. During the Vienna Conference in 1995, the production and

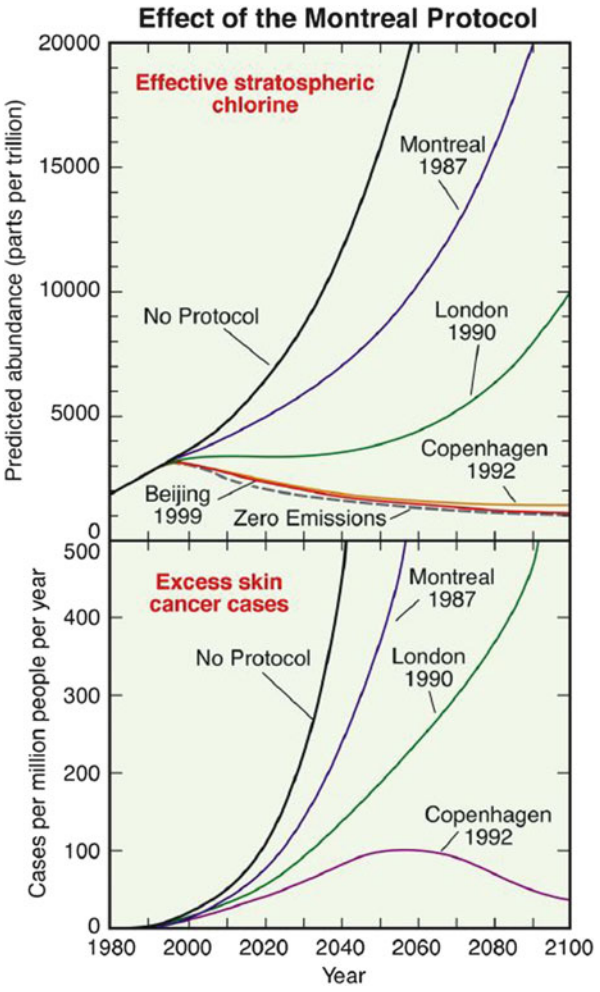


**Fig. 6.1** Effect of the Montreal Protocol and its later amendments on the atmospheric halogen level, after [2]

usage of CFCs and halons were reduced further and a complete phase-out of methyl bromide was fixed. When the parties met again in 1997 in Montreal, the effect of the regulations was clearly discernible in the field data. The maximum chlorine abundance in the troposphere had been reached by 1993, the maximum in the stratosphere by about 2000. Indeed, the reduction had been achieved even earlier than foreseen in the protocol.

While the Parties to the Montreal Protocol have been required to report their annual production and consumption figures of ozone depleting substances to UNEP's Ozone Secretariat, scientific assessments about the state of the ozone layer have been carried out in regular intervals within the Global Ozone Research and Monitoring Project. That way it has been possible to control the outcome of the

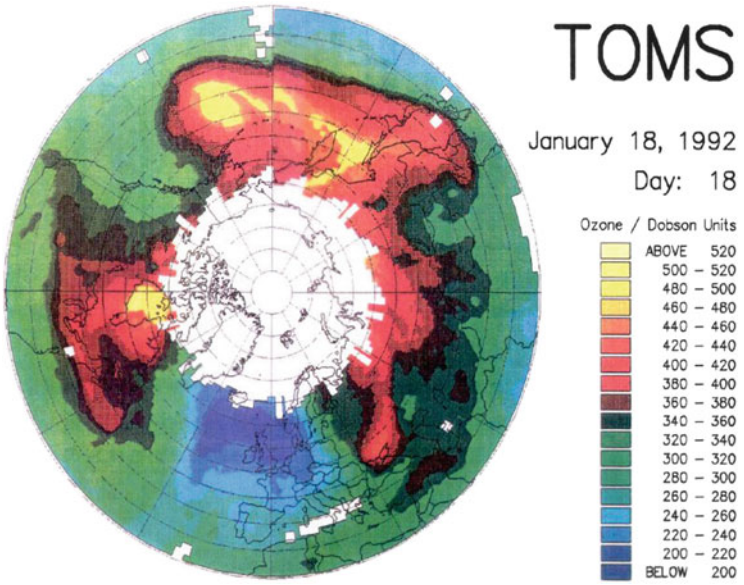


**Fig. 6.2** Ozone reduction over central Europe

legal actions. Figure 6.3 shows in the upper panel reported annual production rates of the major CFCs whose production had practically been terminated by 2000.

The lower panel shows reported production rates of hydro-halocarbons. These have been used as substitutes for the fully halogenated CFCs banned by the Montreal Protocol. With the exception of HCFC-22 which has been in usage for long, they are largely decomposed in the troposphere already by OH, hardly reach the upper atmospheric layers and thus have a much smaller ozone depletion potential than CFCs.

But even after 2000, emission rates of CFCs and halons were not zero: illegal trading, outgassing from foams, leaking from refrigerators, application of fire extinguishers were sources of halocarbons even when no fresh production took place. Production and usage of ozone depleters have been terminated thanks to the Montreal Protocol and its amendments, but, according to present view, the atmospheric halogen level will have fallen to the pre-ozone hole value not before sometime between 2060 and 2080. Thus, global ozone depletion and seasonal ozone losses in polar regions will even keep our children and grandchildren busy.

The impact of the Montreal Protocol and its amendments can be vividly observed and understood in the projection of the concentration of ozone depleting substances (Fig. 6.1). In the absence of the protocol, the concentration of chlorine/bromine would have increased fivefold by 2050 compared to its maximum value by 2000, i.e. from 3.5 ppb to 17 ppb, with the consequence of 50 % and 70 % ozone destruction over Northern and Southern midlatitudes, respectively, which in turn would double and quadruple surface UV-B levels in the two hemispheres. This no

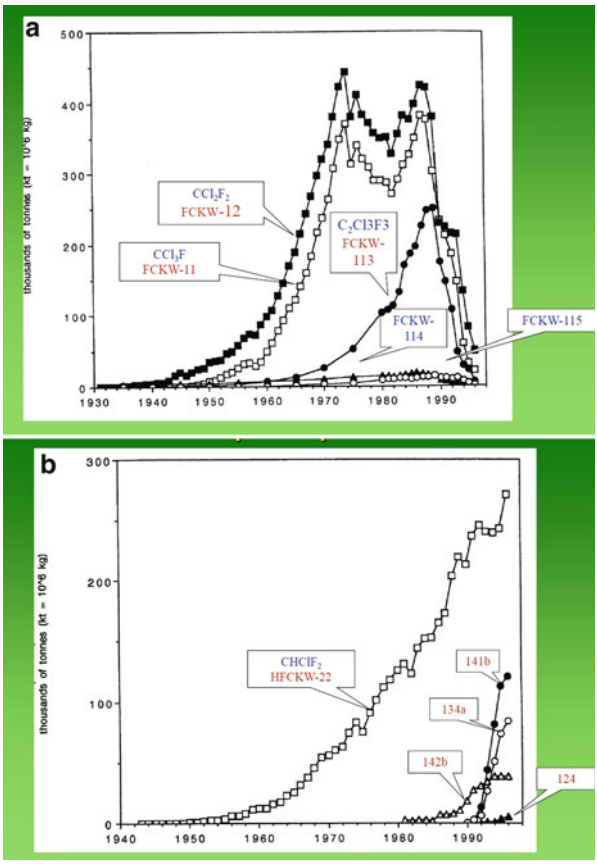


**Fig. 6.3** Annual production of major CFCs as reported by industry (**a**) and HCFCs (**b**), from the beginning of production until 1996, from [3]

doubt is a unique and spectacular example of halting a natural calamity through concerted global effort and understanding. Hopefully, a similar global consensus will evolve soon to abate climate change.

The Montreal Protocol is widely regarded as one of the most effective international environmental treaties in existence. It has proved to be flexible and robust, evolving over time in response to new developments in science and technology. In the mid 1980s, considerable doubt over the extent and causes of ozone depletion was expressed throughout the globe, and the feasibility of action was greatly debated. But just within 15 years, the phase-out schedule for ozone depleting substances was implemented worldwide.

The Protocol has been hailed as a model for future international agreements, and many of its features already have been incorporated into, or adopted for, other treaties. The progress of negotiations in many ways provides a model by involving participants from all key groups—governments, industry, scientists and NGOs. The flexibility built into the protocol in the form of its review process for targets and amendments allowed a continuous evolution to respond to changes in both

scientific evidence and technological developments. The limits on supply imposed by the control schedules have encouraged the rapid development of cost-effective alternatives, which in turn has helped to reduce demand.

An international agreement in the modern world can be effective only if it recognises the special needs of developing countries. Keeping this view, in the Montreal Protocol for developing countries, provisions of financial assistance and technology transfer, and a suitable grace period before the implementation of the phase-out schedule, have been made. The evolving phase-out schedules and the trade provisions have encouraged newly industrialising countries to move out of old technology and accelerate their own phase-out even if not required to do under the terms of agreements.

Perhaps the most important feature of the ozone regime is the way in which it has brought together an incredible number of participants from the different streams in the pursuit of a common end. Scientists have provided information with steadily increasing degree of precision on the causes and effects of ozone depletion. Industry, responding to the stimulus provided by the control measures, has developed alternatives more rapidly and less expensive than initially thought possible and has fully participated in the debates over further phase-out. NGOs and the media are the essential channels of communication and education, with the people of the world in whose name the measures have been taken and who were instrumental, particularly in the early years, in spurring decision makers to take firm action and later to help to sustain pressure to take further steps. Governments have meticulously worked together and were able to negotiate agreements acceptable to a range of countries with widely varying circumstances, aims and resources, and showed courage and foresight in putting precautionary principles into effect before the scientific evidence was entirely clear [4].

## References

1. Duscha H, Borchers R, Fabian P, Bischof W (1990) First results of RASMUS. Source gases in the mesosphere. Adv Space Sci 10(6):77–81
2. WMO (1999) Scientific assessment of ozone depletion 1998. Global Ozone Research and Monitoring Project-Report 44, WMO, Geneva
3. Midgley PM, McCulloch A (1999) Production, sales and emissions of halocarbons from industrial sources. In: Fabian P, Singh ON (eds) The handbook of environmental chemistry, vol 4E, Reactive halocarbons in the atmosphere. Springer, Berlin, pp 155–190
4. Action on ozone, 2000 edition (Produced by the secretariat for the Vienna Convention for the protection of the ozone layer and the Montreal protocol on Substances that Deplete the Ozone layer), p 22. ISBN: 92-807-1884-3

# Chapter 7
# Historical Highlights

## 7.1 The Discovery of the Antarctic Ozone Hole and Elucidation of Its Sources

The Antarctic Ozone Hole, a significant seasonal ozone depletion over wide areas of Antarctica during Austral spring, had not been predicted and thus was a big surprise for the entire ozone community.

During the 1984 Quadrennial Ozone Symposium held in a beach resort at the Halkidiki coast in Greece, a Japanese scientist, Shigeru Chubachi, presented a poster with 1982/1983 total ozone data measured at Syowa (75°S), one of the Japanese Dobson stations. While during January until August 1982, the ozone layer thickness had varied around 300–330 Dobson Units (DU); it dropped sharply at the beginning of September reaching a minimum of about 200 DU in October.

Hundreds of ozone scientists saw this poster including the three who received the 1995 Nobel Price of Chemistry (see Sect. 7.2). They all muttered: Chubachi should go back and recalibrate his Dobson, because the results he is presenting here cannot be correct: Total ozone is known to be minimal at the equator, where about 250 DU occur. From there total ozone increases towards higher latitudes. When only 200 DU are claimed to have been measured at polar latitudes, this is hard to accept. A discussion with Chubachi was impossible as this Japanese Scientist had severe problems with speaking English and defending his results.

When the poster session closed nobody of the scientific community had accepted Chubachi's measurement of an ozone hole. Hundreds of holiday makers returned from the beach, reddened and sunburnt, but completely unaware of the scientific activities in the conference hall of the hotel they stayed at, without any feeling for the importance of Chubachi's results if these could have been confirmed.

Chubachi's important results would have gone lost if they would have not been published in the Proceedings of this Quadrennial Ozone Symposium [1]. Half year later, the world got alarmed when J.C. Farman and other scientists of the British Antarctic Survey (BAS) published in Nature [2] large losses of total ozone measured at the BAS station Halley Bay, similar to those found by Chubachi at Syowa.

P. Fabian and M. Dameris, *Ozone in the Atmosphere*,
DOI 10.1007/978-3-642-54099-8_7, © Springer-Verlag Berlin Heidelberg 2014

Large was the surprise in the entire ozone world as nobody had predicted such an effect. There was no theory predicting such an effect to happen regularly doing September/October over the Antarctic region. Since the end of the 1970s, a well-designed ozone sensor was operating on NIMBUS-7 satellite (see Sect. 3.6). There was big surprise at the American space agency NASA who operated this sensor which had been developed for surveilling the ozone layer. The NASA scientists responsible for this satellite experiment had, however, not noticed any total ozone depletion over the south polar region. This was because the computer for the data evaluation was programmed such that these enormously low ozone values were characterised as faulty and thus were discarded. These raw data had fortunately been stored. Their after-analysis yielded now, although retarded, a wealth of information about extension and morphology of this phenomenon [3, 8].

The American Geophysical Union (AGU) invited ozone scientists from all over the world to work on theories related to the Antarctic ozone hole and submit their results for a special volume of the AGU journal Geophysical Research Letters planned to be printed within Volume 14, 1987. The international response was great, and thus this volume contains an impressive collection of papers with explanations of the formation of the Antarctic ozone hole [4].

The deepest ozone holes have been measured during October of the years 1987, 1989, 1990 and 1991, with total ozone as low as 120 DU. Direct measurements with balloon-born radiosondes showed that the ozone losses happened between 10 and 25 km altitude, where almost all ozone got lost during these episodes.

The fact that the Antarctic ozone hole was first measured by ground-based Dobson instruments operated by Japanese and British scientists [1, 2], but not by the sophisticated satellite instrument on NIMBUS-7, caused enormous alarm within the US American ozone research community. A large American expedition group was established under the leadership of Susan Solomon from the National Ocean and Atmosphere Agency (NOAA) to carry out ground-based measurements, special aircraft and balloon-sonde measurements, in order to find the causes of the recent ozone hole. Main results are reported by Solomon and other participants of these expeditions [5–7]. The most exciting and convincing experiment was flown aboard the ER-2 aircraft. ER-2 used to be used as spying aircraft; it can fly at almost 20 km altitude. During the Airborne Antarctic Ozone Expedition AAOE 1987, it was launched at Punta Arenas/Chile (at about 64°S) fuelled such that it could fly at 19 km altitude towards the South Pole, up to the point that remaining fuel would allow the return flight to Puntas Arenas.

The most important instrument capable of measuring $O_3$ and ClO had been developed by J.G. Anderson of Harvard University. Results of the two flights aboard the ER-2 between 64°S and 70°S, on August 23, 1987 and September 16, 1987, are published [7]. The first of these was done during polar night, the second one after the end of polar night. The boundary of the polar vortex was at about 68°S for both flights.

During the first flight, ozone showed almost no significant latitudinal variations; it was about 2.0 ppm at cruising altitude during the entire flight. ClO, on the contrary, rose from about 10 ppt to almost 80 ppt, after the polar vortex had been

crossed. It showed that at the end of the polar night, ClO had been formed which would, after the return of the sun, achieve the destruction of ozone (see Sect. 3.1.4).

During the second flight which happened after the end of the polar night, ozone showed a drastic decrease after the polar vortex had been crossed, due to ClO which had been formed during polar night. This experiment clearly proves what the heterogeneous reactions demand. The spatial and temporal evolution of the ClO–$O_3$ anticorrelation [6] was called after the experiment as "the smoking gun". This name reminds us of similar approaches in the criminal literature, where the smoking gun is the proof of the suspected relations.

The remarkable fact is that the Antarctic ozone hole was detected by ground-based long-time routine observations but not by high-tech satellite measurements. This happened during a time when long-time routine measurement series for the Earth's environment were not considered valuable. An example is the $CO_2$ measurement programme based on Mauna Loa, run by the University of California, San Diego. This programme and the annual measured $CO_2$ increases in surface air are extremely important in connection with climate research. The programme could be maintained, and we all have to be grateful for the continuation of financial support by various agencies.

During the 1984 Quadrennial Ozone Symposium in Greece when Chubachi presented his poster, almost nobody accepted it as a real measurement showing for the first time the Antarctic Ozone Hole. When about 6 months later the publication by Farman et al. appeared in Nature, the world was alarmed, and Farman, Gardiner and Shanklin were regarded as the discoverers of the Antarctic Ozone Hole.

During the years 1986–1988 the expeditions lead by Solomon [3–7] brought together measurement data confirming the mechanism of the ozone hole origin. Thus, during the Quadrennial Ozone Symposium which took place in August 4–13, 1988 in Göttingen/Germany (see Sect. 7.3), the ozone hole issues were thoroughly discussed, and Chubachi was accepted to be the discoverer.

## 7.2 The 1995 Nobel Prize of Chemistry Awarded to Three Pioneers of Ozone Research

The 1995 Nobel Prize in Chemistry was awarded jointly to Paul J. Crutzen, Mario J. Molina and F. Sherry Rowland "for their work concerning the formation and decomposition of ozone". This is the first Nobel Prize in atmospheric Chemistry in general and for ozone chemistry in particular. Quoted here is some excerpt taken from the congratulatory article by R.G. Prinn (1995), a colleague, coworker and long-time associate of the Nobel Laureates:

"The contemporary ozone depletion issues effectively began in the 1930s with the invention of an extremely useful class of nearly inert chemicals called chlorofluorocarbons (CFCs), and in the 1970s with proposals for a global fleet of

supersonic commercial aircraft which would fly in and exhaust gases in the lower stratosphere.

Crutzen, Molina and Rowland played leading roles in elucidating the way in which these natural and artificial emissions affect the ozone layer which protects the global biosphere from harmful UV radiation. Their initial proposal investigated a large international research programme on the ozone layer and also proved to be a catalyst for a much wider-ranging study of the complex chemical and biological connections which exist on Earth."

The first connections began to be made when Crutzen published two papers in 1970 and 1971 proposing that the catalytic reactions involving nitric oxide and nitrogen oxide are a major ozone destruction mechanism (see Sect. 3.1.3). In the natural stratosphere, the major source of these nitrogen oxides is the reaction of electronically excited oxygen atoms (themselves produced from ozone) with nitrous oxide. As pointed out by H. Johnston, supersonic aircraft currently deposit these catalytic nitrogen oxides directly into the stratosphere.

The second connection was made when in two papers in 1974 and 1975, M. Molina and F.S. Rowland proposed that the nearly inert chlorofluorocarbons (CFCs) and chlorocarbons (CCs) were dissociated by ultraviolet light in the stratosphere to produce chlorine atoms and chlorine monoxide. Only a short time before that, it had been recognised that these chlorine species catalytically destroy ozone (see Sect. 3.1.3). CFCs were widely used in the 1970s for refrigeration, air conditioning, aerosol can propellants, solvents, plastic foam puffing agents and a myriad of other applications. The major CC was trichloroethane (methyl chloroform), which was widely used as a cleaning agent in electronics and automobile industries.

These early proposals of ozone depletion led to a rapid expansion of research in stratospheric chemistry. For a variety of reasons, including potential ozone depletion by the Crutzen reactions, plans for large supersonic aircraft fleets were shelved in the mid-1970s. There was also enough early confidence in the Molina-Rowland theory that several countries in the mid-1970s phased out the use of CFCs in several trivial uses, particularly aerosol cans. Nevertheless, even as evidence for the Crutzen, Molina and Rowland theories mounted, the observational evidence for actual depletion of ozone was equivocal. Due to changing wind patterns, the thickness of the stratospheric ozone layer is highly variable in space and time, and therefore changes in its thickness are very difficult to detect. A series of international assessments were begun in order to periodically examine the validity of these ozone-depleting hypotheses. It was a watch- and-wait phase.

The situation changed dramatically with the publication of the discovery of the Antarctic Ozone Hole in 1984/1985 (see Sects. 5.1.3 and 7.1). A remarkable thinning of the ozone layer was occurring every spring over Antarctica, and the thinning was increasing with time. However, this very evident ozone depletion was not explained by the then-current ozone-depleting theories. These theories did not include the chemistry instigated by reactions involving the stratospheric ice clouds prevalent over Antarctica due to the extremely low temperatures occurring there. The scientific assessments accelerated and the first significant CFC regulatory policy negotiations began with the 1985 Vienna Convention leading to the 1987


**Fig. 7.1** The three Nobel Laureates (Chemistry 1995). F.S. Rowland, M. Molina, P.J. Crutzen (from *left* to *right*) (courtesy P.J. Crutzen)

Montreal Protocol (see Chap. 6). Simultaneously, several researchers were gathering evidence for unexpected chlorine, bromine, and nitrogen chemistry in the Antarctic spring atmosphere (see Sect. 7.1).

Theoretical and laboratory studies were establishing the facts that the reactions on ice particles can lead to release of chlorine monoxide. A new catalytic cycle was discovered by Molina and colleagues involving the dimer of chlorine monoxide which operates efficiently in the ozone hole (see Sect. 3.1.4) (Figs. 7.1 and 7.2).

The ozone depletion story is not ending, however, with the Nobel Awards and successful implementation of the Montreal Protocol. Removal of very long-lived CFCs from the atmosphere will still take many decades, so we shall be living with a perturbed ozone layer for several more decades.

There is still much work remaining. Nevertheless, the remarkable contributions by three members of our community are a great pleasure to acknowledge.

## 7.3 Gordon M.B. Dobson, the International Ozone Commission and Its Quadrennial Ozone Symposia

Dobson (1889–1976) had realised in the 1920s already that research related to ozone, an extremely important atmospheric constituent of immense variations in time and space, would require well-coordinated ground-based networks. He managed to provide an excellent instrument, the Dobson spectrophotometer [9], and established well-run and coordinated international networks, even reaching the Southern Hemisphere [10]. The ozone layer thickness is expressed in Dobson Units (DU), see Sect. 3.1, honouring a scientist of great excellence. One of his Assistants, C.D. Walshaw, wrote in 1976 in an obituary: "Dobson eschewed all the modern methods by which distinguished scientists waste their time—telephone, secretaries, meetings and committees. Instead he worked quietly and steadily at

**Fig. 7.2** P.J. Crutzen receiving The 1995 Nobel Chemistry Price from his Majesty Carl XVI Gustaf King of Sweden (courtesy P.J. Crutzen)

home, spending the afternoons cultivating his large and productive garden at Oxford. Many distinguished persons have enjoyed the hospitality of that home. . .”

Not being a hectic person, he contemplated which activities were important, and he acted successfully: He was the first to organise ozone discussion meetings, and the first of these was organised in Paris in 1929 and the second one in Oxford in 1936. Dobson founded the first International Ozone Commission (IOC), the first meeting of which took place in Oslo in 1948, where he was elected President of IOC. In 1951 he initiated the organisation of holding regular ozone symposia, which culminated into today’s famous Quadrennial Ozone Symposium. It may be pointed out that these symposia, which in the beginning were attended by the members of the select groups known to each other are now invaded by well over 500 scientists, of whom most are younger people from new groups. This clearly demonstrates that now there is a wide spread global keen interest in ozone research, which perhaps Dobson wished. His contributions to the overall growth of ozone research in general, and ozone monitoring in particular, is spectacular and unparalleled.

Rumen Bojkov, a former employee of the World Meteorological Organization (WMO) and long-year Secretary of the IOC, published a detailed book [11] on all 15 Quadrennial Ozone Symposia from No. 1 (Paris 1948) until No. 15 (Tromsö 2008). As many of the sessions were devoted to Dobson Measurements, calibration problems and results, partly receiving funding by WMO, the WMO-IOC-Secretary was extremeful helpful for research and progress of global ozone research.

It is interesting that the first presentation of the Antarctic Ozone Hole by Chubachi happened during the 9$^{th}$ Quadrennial Ozone Symposium at Halkidiki/Greece 1984, where almost nobody accepted Chubachi’s findings. When the Farman et al. Nature paper had appeared in 1985 and results of related research had been published, the 10$^{th}$ Quadrennial Ozone Symposium held in August 4–13 at Göttingen/Germany became the place where all attending scientists agreed in the new findings, that way making Göttingen the place where the Antarctic Ozone Hole

became a top environmental issue. The author of his book (PF), a member of IOC for several periods and organiser of the 10th Quadrennial Ozone Symposium at Göttingen, is looking back with great memories.

## References


1. Chubachi S (1985) A special ozone observation at Syowa station, Antarctica, from February 1982 to January 1983. In: Zerefos CS, Ghazi A (eds) Atmospheric ozone. Reidel, Dordrecht, p 285
2. Farman JC, Gardiner BG, Shanklin D (1985) Large losses of total ozone in Antarctica reveal seasonal ClOx/NOx interactions. Nature 315:207
3. Solomon S, Gracia RR, Ravishankara AR (1994) On the role of iodine in ozone depletion. J Geophys Res 99:20491–20499
4. American Geophysical Union (AGU) (1987) Geophys Res Lett 14(5)
5. Solomon S, Gracia RR, Rowland FS, Wuebbles DJ (1986) On the depletion of Antarctic ozone. Nature 321:755–758
6. Solomon S (1988) The mystery of Antarctic ozone hole. Rev Geophys 26:131–148
7. Anderson JG, Burne WH, Profitt MH (1989) Ozone destruction by chlorine radicals within the Antarctic vortex. The spatial and temporal evolution ClO-O3 anticorrelation based on in-situ ER-2 data. J Geophys Res 94:11465–11479
8. Stolarski RS, Krueger AJ, Schoeberl MR, McPeters RD, Newman PA, Alpart JC (1986) NIMBUS 7 SBUV/TOMS measurements of the springtime Antarctic ozone hole. Nature 322:808–814
9. Dobson GMB (1930) Observations of the amount of ozone in the Earth's atmosphere and its relations to other geophysical conditions. Proc R Soc Lond A 129:413
10. Dobson GMB (1968) Forty years of research on atmospheric ozone at Oxford: a history. Appl Opt 7:37–405
11. Bojkov RD (2012) International Ozone Commission: history and activities. International Association of Meteorology and Atmospheric Sciences (IAMAS), IAMAS Publication Series No. 2, Secretariat IAMAS at DLR, Oberpfaffenhofen